MDM2 as a chromatin modifier

Dissertation

for the award of the degree

“Doctor rerum naturalium” (Dr. rer. nat.)

of the Georg-August-Universität Göttingen

within the doctoral program

“Molecular Biology of Cells”

of the Georg-August University School of Science (GAUSS)

submitted by

Sabrina Gerber

from *Kaiserslautern, Germany*

Göttingen, 2020

Thesis Committee

Prof. Dr. Matthias Dobbelstein, Institute of Molecular Oncology, University Medical Center Göttingen (UMG)

Prof. Dr. Argyris Papantonis, Institute of Pathology, University Medical Center Göttingen (UMG)

PD Dr. Elisabeth Heßmann, Clinic for Gastroenterology and Gastrointestinal Oncology, University Medical Center Göttingen (UMG)

Members of the Examination Board

Referee: Prof. Dr. Matthias Dobbelstein, Institute of Molecular Oncology, University Medical Center Göttingen (UMG)

2nd Referee: PD Dr. Elisabeth Heßmann, Clinic for Gastroenterology and Gastrointestinal Oncology, University Medical Center Göttingen (UMG)

Further Members of the Examination Board

Prof. Dr. Argyris Papantonis, Institute of Pathology, University Medical Center Göttingen (UMG)

Prof. Dr. Heidi Hahn, Institute of Human Genetics, University Medical Center Göttingen (UMG)

Dr. Ufuk Günesdogan, Department of Developmental Biology, Göttingen Center of Molecular Biosciences, University of Göttingen

Dr. Nuno Raimundo, Institute of Cellular Biochemistry, University Medical Center Göttingen (UMG)

Date of oral examination: 22.06.2020

Affidavit

Herewith I declare that the PhD Thesis entitled “MDM2 as a chromatin modifier” was written independently and with no other sources and aids than quoted.

Göttingen, 11th May 2020

(Sabrina Gerber)

Acknowledgements

I would like to thank Prof. Dr. Matthias Dobbelstein for introducing me into the world of cancer research and for giving me the opportunity to work with him and his group on this fascinating project. I really enjoyed and appreciate the helpful scientific discussions we had during the last couple of years. Furthermore, I am very grateful for his continuous support and his encouragement to follow-up my own ideas about this project which enabled me to gain most of my scientific and professional skills and to develop personally.

I would also like to thank the past and present members of my thesis advisory committee, Prof. Dr. Argyris Papantonis, Dr. Elisabeth Heßmann and Prof. Dr. Steven Johnsen for their helpful and constructive input. Furthermore, I would like to thank Prof. Dr. Heidi Hahn, Dr. Ufuk Günesdogan and Dr. Nuno Raimundo for agreeing on joining my extended thesis committee.

Additionally, I would like to thank the Göttingen Graduate School for Neurosciences, Biophysics, and Molecular Biosciences (GGNB) and the Ph.D. program “Molecular Biology of Cells” for accepting me as a graduate student.

I would also like to thank the ENCODE consortium and all collaborating institutes for providing their sequencing data. Also, special thanks go to all my collaborators who contributed to this work. Especially, I would like to thank Antje Dickmanns, who has worked with me on this project from the beginning of my Ph.D. Thank you for your continuous support and friendship - within the lab, during our scientific discussions and mentally in the time of scientific crisis. Furthermore, I would like to thank Ana P. Kutschat, Xin Wang and Dr. Feda Hamdan for our helpful and constructive scientific discussions as well as their support and patience in teaching me how to run bioinformatic analyses. Additional thanks for bioinformatic consulting go to Prof. Dr. Steven Johnsen, Dr. Michael Lidschreiber and Dr. Zeynab Najafova. At last, I would like to thank my previous lab rotation student, Kester Henningsen, for contributing to this work.

I would also like to thank all past and present members of the Molecular Oncology and Tumor Epigenetics department, in particular Antje, Sabine, Cathrin, Anna, Nadine, Claudia, Ana, Feda and Xin. Thank you all for creating such a wonderful working atmosphere and for making me enjoy coming to work every day.

Special thanks go to Ana P. Kutschat for proofreading this thesis.

Finally, I would like to thank my family for their unrestricted love and support. Especially, I would like to thank my parents for enabling me to follow my passion and my husband for his patience and never-endling support during all ups and downs during my Ph.D.

This thesis is dedicated to Sabine, Markus, and Alex.

Table of Contents

List of Figures

List of Tables

Abbreviations

5mC	5-methylcytosine
aa	Amino acid
Ac	Acetylation
APS	Ammonium peroxodisulfate
BCA	Bicinchroninic acid
Bp	Base pair
BSA	Bovine serum albumin
Caspase	Cysteine-aspartic protease
CBX	Chromodomain protein
cDNA	Complementary DNA
CGI	CpG island
ChIP	Chromatin-immunoprecipitation
CHX	Cycloheximide
Co-IP	Complex-immunoprecipitation
CTD	C-terminal domain
DBD	DNA binding domain
DMEM	Dulbecco's Modified Eagle's Medium
DMSO	Dimethyl sulfoxide
DNA	Deoxyribonucleic acid
DSIF	DRB sensitivity-inducing factor
DTT	Dithiotreit
E. coli	Escherichia coli
EDTA	Ethylene diamine tetraacetic acid
EED	Embryonic ectoderm development
EGS	Ethylene glycol bis(succinimidyl succinate)
EGTA	Ethylene glycol tetraacetic acid
EMT	Epithelial-mesenchymal transition
EtOH	Ethanol
EZH2	Enhancer of zeste homolog 2
FBS	Fetal bovine serum
GSEA	Gene set enrichment analysis
GO	Gene ontology

H2AK119	Histone 2A lysine 199
H3K27	Histone 3 lysine 27
H3K36	Histone 3 lysine 36
H3K4	Histone 3 lysine 4
H3K9	Histone 3 lysine 9
HCC	Hepatocellular carcinoma
HEPES	4-(2-hydroxyethyl)-1-piperazineethanesulfonic acid
HP1	Heterochromatin protein 1
HRP	Horseradish peroxidase
IP	Immunoprecipitation
KDM2A/B	Lysine demethylase 2 A/B
LPF	Lipofectamine
MDM2	Murine double minute 2
Me	Methylation
MEF	Mouse embryonic fibroblast
MetOH	Methanol
mRNA	Messenger RNA
NELF	Negative elongation factor
NP-40	Nonidet^{TM} P-40 substitute
OvCar	Ovarian cancer
P53RE	P53 recognition element
PAS	Polyadenylation signal
PBS	Phosphate-buffered saline
PcG	Polycomb group
PCGF	Polycomb group RING finger protein
PCL1-3	Polycomblike protein 1-3
PDAC	Pancreatic ductal adenocarcinoma
PFA	Paraformaldehyde
PHC	Ph homolog
PIC	Pre-initiation complex
Pol II	RNA Polymerase II
PRC1/2	Polycomb repressor complex 1/2
pSer2	Phosphorylation at serine 2 of the Pol II CTD
pSer5	Phosphorylation at serine 5 of the Pol II CTD

P-TEFb	Positive transcription elongation factor b
qRT-PCR	Quantitative reverse-transcription polymerase chain reaction
RING	Really interesting new gene
RNA	Ribonucleic acid
RNF2	E3 ubiquitin-protein ligase RING2
ROS	Reactive oxygen species
RT	Room temperature *or* reverse transcription (context dependent)
RYBP	RING/YY1-binding protein
SCM	Sex comb on midleg homolog
SDS	Sodium dodecyl sulfate
SDS-PAGE	SDS-polyacrylamide gel electrophoresis
siRNA	Small interfering RNA
st.f.	Sterile filtrate
SUZ12	Suppressor of zeste 12
TAD	Transactivation domain
TBS	Tris-buffered saline
TEMED	Tetramethylethylenediamine
TNFα	Tumor necrosis factor alpha
TRAIL	TNF-related apoptosis-inducing ligand
TSS	Transcriptional start site
Ub	Ubiquitination
w/v	weight to volume
wt	wild-type
ZF	Zinc finger

1. Abstract

Since its discovery about 40 years ago, the transcription factor p53 has turned into the most extensively studied protein in the context of human cancers due to its essential role in promoting tumor suppression. P53 regulates central processes such as the induction of cell cycle arrest, senescence, or apoptosis in response to cellular stresses, thus preventing tumorigenesis in mammals. Being the major negative regulator of p53, the E3 ubiquitin ligase MDM2 is as much of interest to cancer researchers as p53 itself. Down to the present day, its major function is assigned to antagonizing p53. However, evidence of additional, p53-independent, functions is accumulating.

One of these functions is the role of MDM2 as a p53-independent regulator of transcription. Previous studies have proven that MDM2 can interact with the general transcription machinery. Additionally, it acts as a chromatin-modifying co-factor promoting the formation of the repressive histone modifications H3K27me3 and H2AK119ub1 by Polycomb repressor complexes. However, since most of these studies were either conducted *in vitro* or in the absence of p53 *in vivo*, a comprehensive analysis of the MDM2 chromatin association in the presence of its major interaction partner p53 is still missing.

In this thesis, we have investigated the global chromatin-binding pattern of endogenous MDM2 protein in various cell systems with diverse p53 status. Strikingly, comparative analyses of MDM2 binding sites identified in p53 wild-type, deleted and mutated systems revealed that MDM2 associates with more than 50 % of all CpG islands identified in human cells. This targeted binding of MDM2 to CpG islands is mediated through its direct interaction with the histone demethylase and CpG island-binding protein KDM2B, a known component of a variant Polycomb repressor complex.

Preliminary results addressing the function of this KDM2B-directed chromatin recruitment of MDM2 indicate that both proteins cooperate in the repression of CpG island-associated genes, potentially through affecting the recruitment of RNA Polymerase II to those sites. This hypothesis is further strengthened by gene expression studies conducted in p53 mutated cells. In these studies, we found that MDM2 and Polycomb repressor complexes cooperatively repress target genes of the inducible TNF signaling pathway.

Since CpG islands associate with the transcriptional start sites of about 50-60 % of all human genes, it is highly possible that this newly identified MDM2-KDM2B axis is central to the regulation of a multitude of physiological processes in the cell.

2. Introduction

2.1. Transcription as a determinant of a cell's fate

The transcription of genes is a central process shaping a cell's phenotype and an ability to respond to external stimuli. Transcriptional changes due to mutations within signaling cascades or components of the basal transcription machinery are characteristic in cancer (Bradner et al., 2017). Therefore, understanding the mechanisms underlying transcriptional regulation is key to comprehend carcinogenesis.

2.1.1. RNA Polymerase II-mediated transcription

2.1.1.1. RNA Polymerase II – structure and function

In eukaryotic cells, RNA Polymerase II (Pol II) synthesizes protein-coding messenger RNAs (mRNA) and regulatory non-coding RNAs (Proudfoot, 2016). It consists of a 10-subunit Pol II core, a peripheral heterodimer, and a flexibly linked C-terminal domain (CTD). The latter belongs to the Pol II subunit Rpb1 and consists of 52 YSPTSPS heptapeptide repeats in humans (Cramer et al., 2008; Kireeva et al., 2013). During the transcription cycle, the Pol II CTD is subjected to extensive phosphorylation, regulating the Pol II machinery and transcription in general (Phatnani and Greenleaf, 2006).

2.1.1.2. The transcription cycle – Initiation, elongation and termination

The transcription cycle can be subdivided into three distinct steps: transcription initiation, elongation and termination (Fig. 2.1).

2.1.1.2.1. Transcription initiation

During transcription initiation, inactive Pol II is recruited to the transcriptional start site (TSS) of genes to start transcript synthesis (Fig. 2.1 A). For this purpose, a pre-initiation complex (PIC) is formed at the core promoters of genes, starting with the sequence-specific binding of the general transcription factor TFIID followed by the sequential recruitment of TFIIA, TFIIB, the Pol II-TFIIF complex, TFIIE and TFIIH (Haberle and Stark, 2018; Sainsbury et al., 2015). PIC assembly is supported through transcriptional co-factors such as the Mediator, a multi-subunit complex recruited to enhancer sites by transcription factors upon binding to their consensus sites (Allen and Taatjes, 2015; Baek et al., 2006; Esnault et al., 2008). The Mediator facilitates PIC assembly by interacting with general transcription factors. Furthermore, it binds to the unphosphorylated CTD of promoter-bound Pol II, thus contributing to the formation of enhancer-promoter gene loops (Allen and Taatjes, 2015).

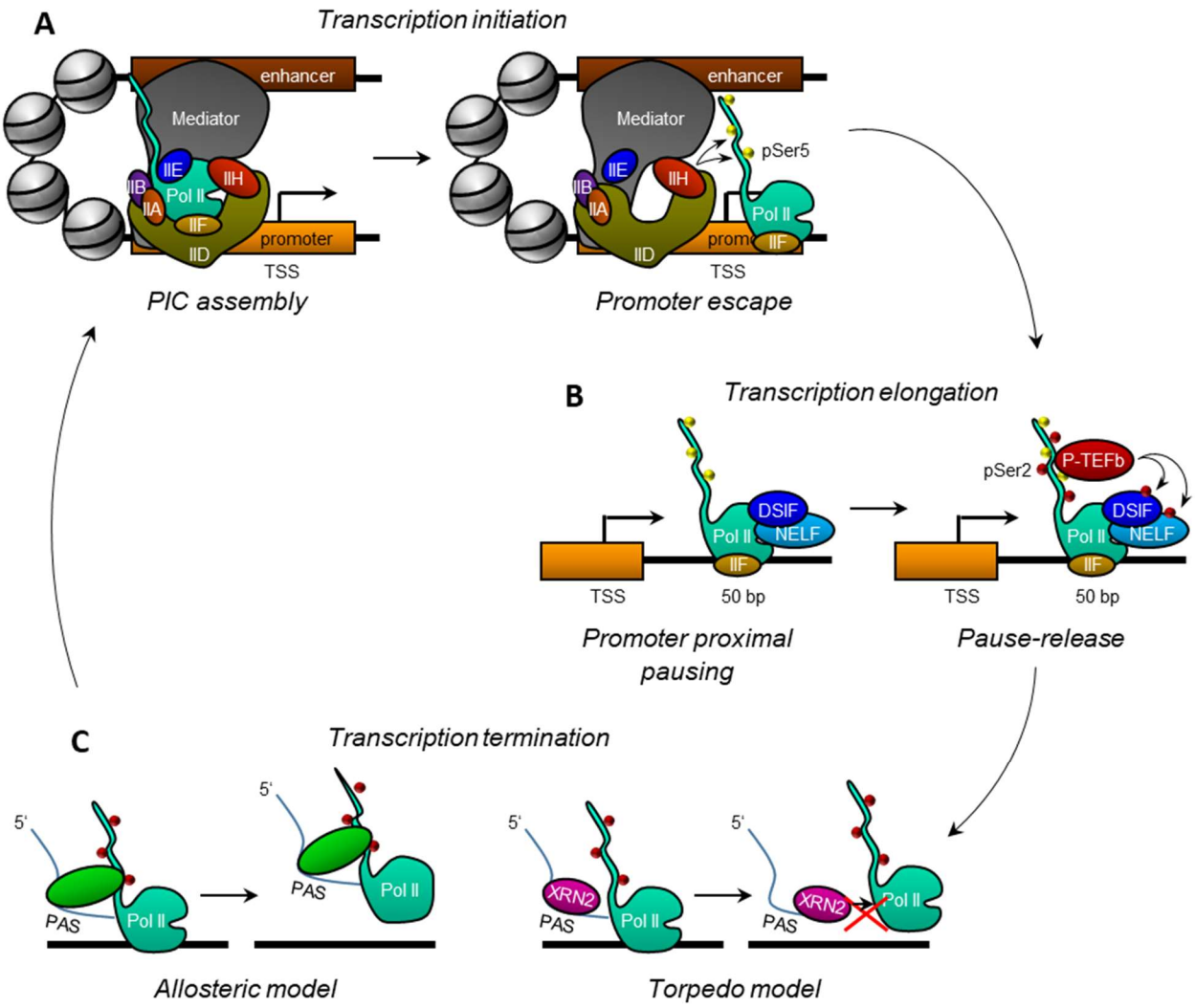

Fig. 2.1: The transcriptional cycle (simplified; partially adapted from Allen and Taatjes, 2015). (A) Transcription is initated upon the assembly of a pre-initation complex (PIC, left). Promoter escape of recruited Pol II is achieved through serine 5 phosphorylation (pSer5) of the Pol II CTD by TFIIH (right). (B) Early elongating Pol II complex pauses due to binding of the pausing factors DSIF and NELF (left). Binding of P-TEFb and subsequent phosphorylation of the Pol II CTD at serine 2 (pSer2), DSIF and NELF triggers the Pol II pause-release (right). (C) Upon synthesis of the polyadenylation signal (PAS) within the 3' end of nascent transcripts, transcription is terminated through PAS-binding factors. The alosteric model (left) and the torpedo model (right) of transcription termination are shown.

Upon PIC assembly, the TFIIH subunit XPB melts the promoter DNA, resulting in the formation of a transcription bubble to start transcript synthesis (Haberle and Stark, 2018; Sainsbury et al., 2015). Meanwhile the CDK7-cyclin H-MAT1 module of TFIIH phosphorylates serine 5 (pSer5) of the Pol II CTD (Liu et al., 2004; Sainsbury et al., 2015). This modification initiates the recruitment of co-factors, such as 5'-end RNA capping enzymes or chromatin modifiers (Ebmeier et al., 2017; Ho et al., 1998; Komarnitsky et al., 2000), and induces the dissociation

of Pol II from the Mediator and PIC (Nechaev and Adelman, 2012; Søgaard and Svejstrup, 2007; Wong et al., 2014). Upon promoter escape, TFIIF stays associated with the elongating Pol II complex while TFIID, TFIIA, TFIIE, TFIIH and the Mediator remain at the promoter forming a scaffold complex to re-initiate another round of transcription (Cojocaru et al., 2008; Yudkovsky et al., 2000).

2.1.1.2.2. Transcription elongation

Shortly after promoter escape, the DRB sensitivity-inducing factor (DSIF) binds to the nascent transcript emerging from the Pol II complex and to the Pol II CTD. Following, the negative elongation factor (NELF) is recruited (Missra and Gilmour, 2010; Yamaguchi et al., 1999a). This causes a Pol II pausing at 30 to 50 bp downstream of the TSS (Fig. 2.1 B left; Rasmussen and Lis, 1993; Yamaguchi et al., 1999b), permitting an accumulation of Pol II at the 5' end of genes to synchronize their expression (Haberle and Stark, 2018). The release of paused Pol II is mediated through the positive transcription elongation factor b (P-TEFb) that phosphorylates both, the CTD of Pol II at serine 2 (pSer2) as well as DSIF and NELF through its CDK9 subunit (Kim and Sharp, 2001; Liu et al., 2015; Marshall et al., 1996). Phosphorylation of DSIF and NELF leads to the dissociation of NELF and the conversion of DSIF into an elongation-stimulating factor, resulting in the pause-release of Pol II and the resumption of transcription (Fig. 2.1 B right; Liu et al., 2015).

2.1.1.2.3. Transcription termination

In contrast to initiation and elongation, transcription termination is less well studied. Currently, there are two models on how transcription termination of protein-coding genes may occur: the allosteric model and the torpedo model (Proudfoot, 2016). In both models, the polyadenylation signal (PAS) within the 3'-end of nascent transcripts serves as the origin of transcription termination. In the allosteric model, transcription of the PAS initiates the recruitment of cleavage and polyadenylation factors binding to the 3'-end of the nascent transcript and to pSer2 of the Pol II CTD (Ahn et al., 2004; Kuehner et al., 2011). This primarily induces Pol II pausing, followed by conformational changes within the Pol II complex and subsequent dissociation of Pol II from the DNA template (Fig. 2.1 C left; Orozco et al., 2002; Proudfoot, 2016; Zhang et al., 2015). The torpedo model complements this PAS-driven termination process. Beside 3'-end processing factors, a complex containing the 5' – 3' exoribonuclease XRN2 interacts with the Pol II CTD. Transcript cleavage downstream of the PAS allows XRN2 to digest the remaining transcript behind Pol II, eventually colliding with Pol II and leading to the dissociation of Pol II from the DNA (Fig. 2.1 C right; Kuehner et al., 2011; Proudfoot, 2016; West et al., 2004). The released Pol II enzymes may then recycle to the TSS to re-initiate another round of transcription (Kuehner et al., 2011).

2.1.2. Transcriptional regulation through epigenetic mechanisms

In addition to the depicted events directly targeting the transcriptional machinery, epigenetics provides multiple mechanisms to regulate gene expression. Epigenetics refers to heritable changes to gene expression without changing the underlying DNA sequence (Bird, 2002) and comprises DNA methylation, post-translational modifications of histones as well as gene regulation by long non-coding RNAs (Yan et al., 2018). Since the regulation through non-coding RNAs is not relevant to this work, this mechanism is excluded from further introduction.

2.1.2.1. DNA methylation and CpG islands

Methylation of cytosine at the fifth carbon of its pyrimidine ring represents a permanent and heritable mechanism to impact transcription (Fig. 2.2). In differentiated tissues, it is established at cytosines within CpG dinucleotides (Lister et al., 2009) and maintained during replication (Bird, 2002; Greenberg and Bourc'his, 2019). DNA methylation can diminish transcription factor binding to its consensus sites and affect target gene transcription by masking the binding and recognition sequence (Fig. 2.2 A; Campanero et al., 2000; Yin et al., 2017). Furthermore, DNA methylation promotes nucleosome compaction (Fig. 2.2 B) and recruits methyl CpG-binding proteins, which interact with chromatin remodeling factors to antagonize transcription (Fig. 2.2 C; Choy et al., 2010; Jones et al., 1998; Ng et al., 1999). However, recent studies indicate that DNA methylation within gene bodies may also favor ongoing transcription by marking exons for co-transcriptional splicing (Gelfman et al., 2013) and inhibiting transcription initiation at intragenic promoters (Fig. 2.2 D; Greenberg and Bourc'his, 2019; Neri et al., 2017). Hence, DNA methylation is a double-edged sword in transcriptional regulation.

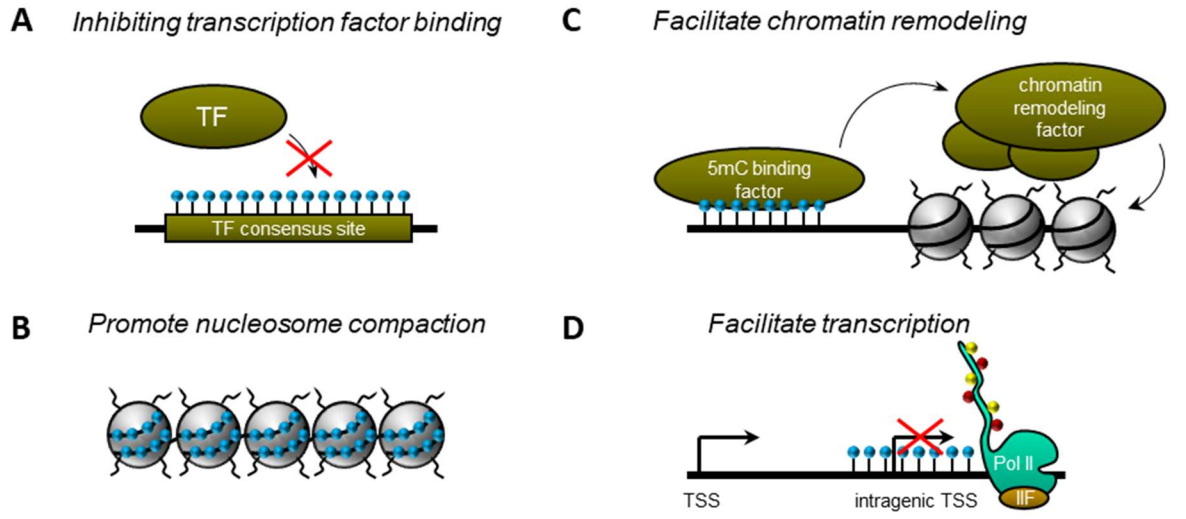

Fig. 2.2: Transcriptional regulation through DNA methylation. (A) DNA methylation (blue dots) inhibits transcription factor binding to consensus sites. (B) Promotion of nucleosome compaction though DNA methylation. (C) 5mC-binding factors recruit chromatin remodeling factors affecting the adjacent chromatin landscape. (D) DNA methylation inhibits sporadic transcription initiation from intragenic TSSs during ongoing transcription.

Although about 70 % of all CpG dinucleotides within the genome of human differentiated cells undergo DNA methylation (Lister et al., 2009), CpG located in CpG islands (CGIs) are an exception. CGIs are interspersed DNA regions characterized by elevated GC-content and a high frequency of CpG dinucleotides lacking DNA methylation (Bird et al., 1985). They are associated with about 70 % of all human gene promoters (Saxonov et al., 2006) and implicated in gene expression. During embryogenesis, the methylation of CGIs is a key regulatory step to persistently silence genes resulting in X-chromosome inactivation, silencing of germline-specific genes and the imprinting of genes to ensure their mono-allelic expression (Bird, 2002; Greenberg and Bourc'his, 2019).

In contrast, the role of CGIs in transcriptional regulation in differentiated cells remains partially elusive, hence being subject of ongoing research. The majority of CGIs are considered to mark transcription initiation sites, regardless of whether they are located at annotated TSSs or more distal sites (Deaton and Bird, 2011; Illingworth et al., 2010). At least in part, transcription initiation is achieved by transcription factor binding at consensus sites within CGIs and by establishing a permissive chromatin state (Fig. 2.3 A). This process is mediated by proteins expressing a zinc finger (ZF)-CxxC-domain that specifically binds to unmethylated CpG dinucleotides (Blackledge and Klose, 2011; Deaton and Bird, 2011). Upon binding, ZF-CxxC proteins such as CFP1 or KDM2A alter histone modifications around the CGI to define an open chromatin structure (Fig. 2.3 B; Blackledge et al., 2010; Thomson et al., 2010), facilitating the recruitment of the transcription machinery (Blackledge and Klose, 2011; Illingworth et al., 2010; Vermeulen et al., 2007). Furthermore, the KDM2A paralogue KDM2B was recently shown to regulate gene expression through direct interference with Pol II occupancy and pausing at genes with CGI-associated TSSs (Turberfield et al., 2019). Taken together, DNA methylation and CGIs provide two striking layers of epigenetic gene regulation that, nevertheless, still need to be further investigated to entirely resolve their mode of action.

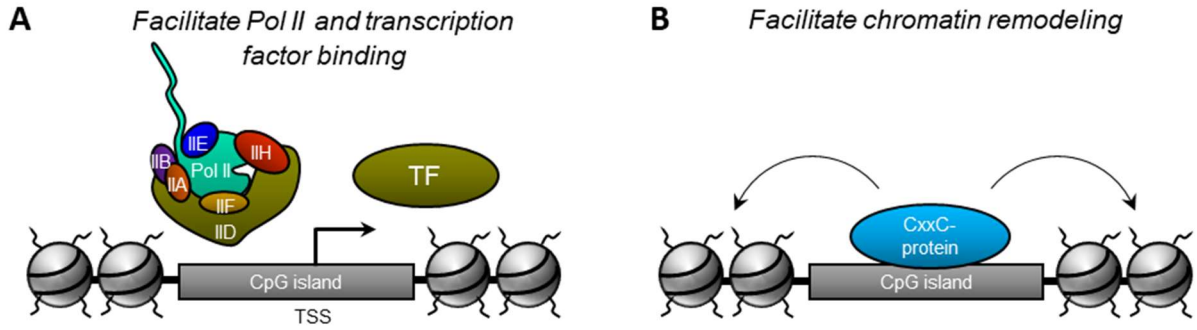

Fig. 2.3: Impact of CpG islands on transcription. (A) CGIs establish an open and permissive chromatin environment around the TSS, thus facilitating the binding of the transcriptional machinery and transcription factors. (B) Proteins expressing a ZF-CxxC-domain can bind to unmethylated CGIs and induce the remodeling of surrounding chromatin.

2.1.2.2. *Affecting the chromatin state – nucleosome positioning and histone modifications*

As previously mentioned, changing the chromatin state (e.g. from ‘open’ referring to accessible DNA to ‘closed’ describing tightly packed, inaccessible DNA) is another multifaceted way to regulate transcription. In eukaryotic cells, 147 bp of DNA are wrapped around an octamer of two H2A, H2B, H3 and H4 histones (Kouzarides, 2007) and stabilized by a linker histone H1, which binds to DNA and connects consecutive nucleosomes (Hergeth and Schneider, 2015). This leads to the formation of a nucleosome, the core subunit of chromatin.

The chromatin state may be altered by the re-positioning of nucleosomes through chromatin-remodeling factors and by transient post-translational modifications of histones (Cosgrove et al., 2004; Petty and Pillus, 2013). The latter fulfills different functions depending on the site of action. Modifications of histone domains exposed to the lateral surface of nucleosomes are involved in various DNA-based processes, such as DNA repair or transcription, and directly affect histone-DNA interactions (Cosgrove et al., 2004; Lawrence et al., 2016). Additionally, histones are post-translationally modified at their extruding N-terminal tails. There is a large variety of chemical groups that can be added at numerous potential modification sites within histone tails (Zhao and Garcia, 2015). The high complexity of this epigenetic system, resulting from innumerable different combinations of histone modifications within a genomic region, facilitates the regulation of a large variety of DNA-associated processes. This principle is also described by the “histone code” hypothesis (Fig. 2.4; Strahl and Allis, 2000).

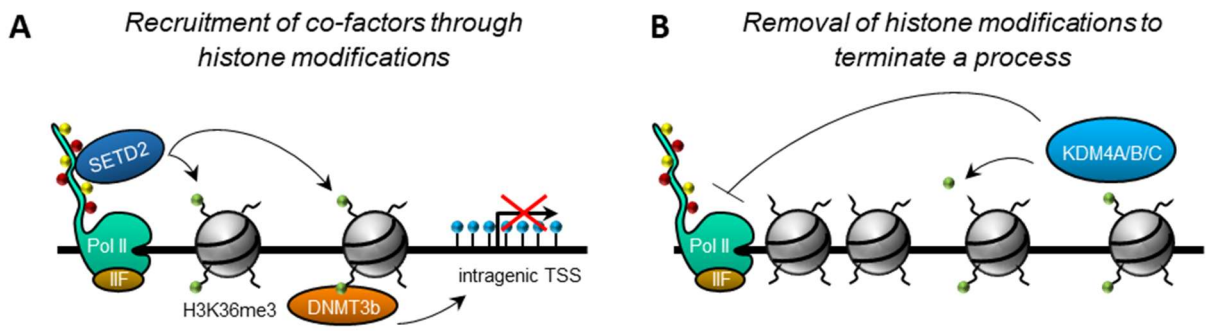

Fig. 2.4: Example illustrating the principles of the “histone code” hypothesis. (A) The formation of histone modifications initiates the recruitment of co-factors supporting ongoing processes. In this example, the histone methyltransferase SETD2 binds to the phosphorylated CTD of Pol II and catalyzes H3K36me3 (green dots) at adjacent histone tails (SETD2 = “writer”). Established H3K36me3 is further bound by the DNA methyltransferase 3b (DNMT3B = “reader”), facilitating DNA methylation to silence intragenic TSS. (B) The removal of histone modifications can initiate the termination of DNA-based processes. H3K36me3 established by SETD2 can be removed by KDM4 histone demethylases (KDM4A/B/C = “erasers”), thus compacting chromatin and inhibiting another round of transcription of the same locus.

Post-translational modifications are established in a context-specific manner by specific enzymes, the so called “writers”. These modifications are recognized by “reader” proteins which bind to their specific cognate modification and trigger further processes like the recruitment of specific co-factors or the catalysis of other histone modifications in the adjacent area. Furthermore, another context-dependent response is the specific removal of present histone modifications through “eraser” proteins (Mohammad et al., 2019; Soshnev et al., 2016). Based on the tight interplay of these three processes, specific combinations of histone modifications are accounted to specific DNA-based processes, hence serving as recognition marks of these processes as well as potential therapeutic targets (Mohammad et al., 2019).

Acetylation and methylation of histone tails are the most abundant histone modifications (Mohammad et al., 2019) and key marks reflecting a gene’s activity. Histone acetylation is frequently associated with transcriptional activation (Zhao and Garcia, 2015 and references therein) and facilitates transcription by promoting the binding of bromo-domain containing proteins to recruit important transcriptional co-factors (Shi and Vakoc, 2014). The acetylation of histone 3 at lysine 27 (H3K27ac) is a key mark of actively transcribed genes. Since it associates with active promoters, enhancers and super-enhancer sites (Creyghton et al., 2010; Hilton et al., 2015; Pott and Lieb, 2015), H3K27ac is frequently used to define transcriptional regulatory elements based on sequencing data. In addition to co-factor recruitment, histone acetylation is supposed to facilitate transcription by weakening the DNA-histone interaction (Hong et al., 1993). However, this effect remains debatable considering that recent publications demonstrated that histone acetylation can also be involved in transcriptional repression under specific conditions (Kaimori et al., 2016; Mehrotra et al., 2014).

In contrast to acetylation, the methylation of histone tails plays a dual role in transcriptional regulation. On the one hand, the tri-methylation of histone 3 at lysine 4 (H3K4me3) and di- and tri-methylation at lysine 36 (H3K36me2/3) associate with promoters and gene bodies of actively transcribed genes respectively, hence supporting transcription (Barski et al., 2007; Bernstein et al., 2005; Huang and Zhu, 2018; Neri et al., 2017). Notably, the CGI-binding lysine demethylases KDM2A and KDM2B remove H3K36me2 and H3K4me3 from promoters of CGI-associated genes (D’Oto et al., 2016). Hence, these modifications are not only crucial for general transcription, but also of particular interest to the regulation of CGI-associated genes.

On the other hand, the tri-methylation of histone 3 at lysine 9 (H3K9me3) and 27 (H3K27me3) are global marks for transcriptional repression (Barski et al., 2007). Worth noticing, multiple additional histone modifications have been observed next to acetylation and methylation such as phosphorylation, ubiquitination, biotinylation, ADP-ribosylation, SUMOylation and others (Zhao and Garcia, 2015). Hence the depicted histone modifications and related functions are just a small insight into this large and complex gene regulatory system.

2.2. The p53-MDM2 system as a determinant of transcriptional regulation

2.2.1. The tumor suppressor p53

Changes in cellular gene expression patterns are induced through the triggering of signaling pathways that in turn result in the activation of signaling-specific transcription factors. In the context of cancers, the tumor suppressor p53 is one of the best studied transcription factors. P53 is a 393 aa nuclear protein encoded by the *TP53* gene on chromosome 17p13.1 (Joerger and Fersht, 2010; Integrative Genomics Viewer v2.3). Initially identified in 1979 as a 53 kDa host protein binding to the SV40-encoded large T antigen in transformed cells (Lane and Crawford, 1979; Linzer and Levine, 1979), p53 has turned into a major focus of cancer research due to its frequent genetic alterations in human cancers (cBioportal).

Non-mutated “wild-type” p53 has been shown to fulfill major tumor-suppressive functions in response to a large variety of cellular stresses of which genotoxic stress is probably the most prominent context (Horn and Vousden, 2007). Upon DNA damage, kinases of the DNA damage response pathway mediate the initial phosphorylation of p53 at serine 15, thus triggering further modifications at multiple residues within its N- and C-terminal domains. This renders p53 resistant towards suppression, leading to its activation and subsequent oligomerization with other p53 proteins (Gu and Zhu, 2012; Meek and Anderson, 2009). P53 homo-tetramers bind to the so called p53 recognition elements (P53REs), within p53 target gene promoters to facilitate their expression, which consists of tandem repeats of the sequence 5’ - PuPuPuCA/TA/TGPyPyPy - 3’ (Pu refers to the purine bases A and G, Py to the pyrimidine bases C and T; Laptenko and Prives, 2006). To date, more than 340 high-confidence p53 target genes have been identified that are involved in central processes such as the induction of cell cycle arrest, DNA repair, metabolic functions, cellular senescence, and apoptosis (Fischer, 2017; Kastenhuber and Lowe, 2017). Therefore, wild-type p53 is a key factor preventing tumorigenesis through maintaining DNA integrity and eliminating cells with irreparable genomic injuries, why it is also called the “guardian of the genome” (Lane, 1992).

In normal unstressed cells, p53 is kept at low basal levels to ensure cell cycle progression and to prevent apoptosis in the absence of DNA damage (Giaccia and Kastan, 1998). For this purpose, a tight regulation of p53 protein levels and activity are required to maintain cells in a non-transformed and viable state. One major factor establishing this tailored regulation of p53 is its antagonist murine double minute 2 or MDM2.

2.2.2. The E3 ubiquitin ligase MDM2 - antagonist of p53

MDM2 is encoded by the *MDM2* gene located on chromosome 12q15. Its murine homolog *mdm2* has been discovered more than 30 years ago as a one of two highly amplified genes present in paired acentromeric extrachromosomal bodies, so called double minutes, in spontaneously transformed murine cells (Cahilly-Snyder 1987). Originally identified as a factor promoting tumorigenesis upon expression (Fakharzadeh et al., 1991), MDM2 has evolved into one of the most studied proteins in cancer research due to its fundamental role in antagonizing p53 (Karni-Schmidt et al., 2016).

2.2.2.1. MDM2 proteins - structure, homologs, and isoforms

The *MDM2* gene gives rise to multiple MDM2 protein isoforms that are generated based on two different internal start codons and alternative mRNA splicing. The full-length p90 MDM2 protein is induced through the translational start site located within exon 3 of the *MDM2* gene and is a 491 aa E3 ubiquitin ligase that is primarily located in the nucleoplasm of cells (Iwakuma and Lozano, 2003). It comprises multiple functional domains defining its physiological roles (Fig. 2.5).

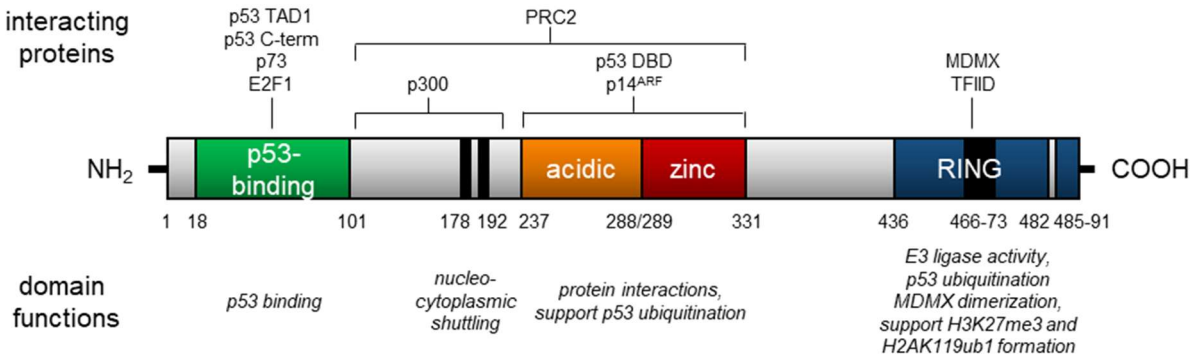

Fig. 2.5: MDM2 protein structure with selected interaction partners and functions (partially adapted from Karni-Schmidt et al., 2016). Scheme of functional domains within the MDM2 protein. Localization of functional domains is indicated by amino acid numbers underneath the protein structure. A selection of interaction partners and functions of the depicted domains involved in MDM2-mediated transcriptional regulation is indicated. For references, please refer to sections 2.2.2.1-4.

A p53-binding domain spanning from aa 18-101 is located at the amino-terminal part of full-length MDM2 (Iwakuma and Lozano, 2003). It is a hydrophobic pocket that can bind to three residues, namely Phe19, Trp23 and Leu26, within the first N-terminal transactivation domain (TAD) of p53 to facilitate the MDM2-p53 interaction (Kussie et al., 1996). Additionally, the p53-binding domain interacts with the C-terminal part of p53, thus supporting the MDM2-p53

complex formation and p53 antagonism (Poyurovsky et al., 2010). Despite its clearly defined role in p53 binding, this region may also facilitate the interaction with other proteins, such as the p53 family member p73α or the transcription factor E2F1, hence fulfilling additional functions next to p53 binding (Bálint et al., 1999; Fåhraeus and Olivares-Illana, 2014; Martin et al., 1995; Riley and Lozano, 2012).

Next to the p53-binding domain, a nuclear localization signal and a nuclear export signal are located at aa 178 and 192, respectively (Karni-Schmidt et al., 2016), enabling the nucleo-cytoplasmic shuttling of MDM2 (Roth et al., 1998).

An acidic domain ranging from aa 237-288 connected to a zinc finger domain spanning aa 289-331 represent the central functional domains of MDM2 (Karni-Schmidt et al., 2016). In collaboration with the region from aa 102-236, these central domains serve as a binding platform for a variety of MDM2 interaction partners, such as its negative regulator $p14^{ARF}$, the transcriptional co-factor p300 or the chromatin-modifying Polycomb repressor complex 2 (Fåhraeus and Olivares-Illana, 2014; Grossman et al., 1998; Riley and Lozano, 2012; Wienken et al., 2016). Furthermore, the acidic domain of MDM2 supports its antagonism towards p53 by promoting p53 ubiquitination and inhibiting its binding to DNA (Cross et al., 2011; Kawai et al., 2003; Ma et al., 2006).

The carboxy-terminal part of MDM2 is formed by its RING (Really Interesting New Gene) domain ranging from aa 436-482. The MDM2 RING finger exhibits an E3 ubiquitin ligase activity that is required for the ubiquitination of MDM2 itself and of its substrates such as p53 (Fang et al., 2000; Karni-Schmidt et al., 2016; Ranaweera and Yang, 2013). Furthermore, MDM2 oligomerizes with its structural homolog MDMX. MDMX comprises a N-terminal p53-binding domain and a C-terminal RING domain similar to the ones of MDM2, while its central acidic and zinc finger domains are less conserved (Shvarts et al., 1996). Heterodimerization of MDM2 and MDMX occurs through interaction of their RING domains that is supported by the last C-terminal residues of MDM2 (Leslie et al., 2015). In those complexes, MDMX buffers the auto-ubiquitination of MDM2, thus promoting its stability. Furthermore, the enlargement of the MDM2 RING domain due to dimerization increases its enzymatic activity although the MDMX RING domain itself lacks E3 function (Linke et al., 2008). Therefore, MDMX has turned out to be a valuable partner to sustain MDM2 function. In addition to its function in oligomerization, the MDM2 RING domain has been shown to facilitate the interaction of MDM2 with the TFIID complex (Léveillard and Wasylyk, 1997). Furthermore, the MDM2 RING finger possesses an intrinsic nucleolar localization signal facilitating its shuttling into the nucleolar compartment (Karni-Schmidt et al., 2016).

Next to full-length MDM2, its truncated p76 version is the most abundant isoform present in cells. It is translationally induced by an intrinsic start codon present in exon 4 and lacks the N-terminal p53-binding domain (Iwakuma and Lozano, 2003; Perry et al., 2000). Therefore, it does not antagonize p53 but has been shown to be a dominant negative regulator of full-length MDM2, promoting p53 stabilization instead (Perry et al., 2000). Additionally, various MDM2 mRNA splice variants have been identified that fulfill both, tumorigenic as well as tumor suppressive functions (Karni-Schmidt et al., 2016). Hence, the products of the *MDM2* gene may be considered as central components regulating tumor development.

2.2.2.2. MDM2 regulation

2.2.2.2.1. Transcriptional regulation of MDM2

Due to its high impact on p53 activity, a tight regulation of MDM2 protein levels is a prerequisite to prevent tumorigenesis in cells. On the transcriptional level, *MDM2* gene expression is controlled through two distinct promoters, called P1 and P2 (Fig. 2.6 left). The constitutive P1 promoter is located upstream of exon 1 of the *MDM2* gene and maintains basal MDM2 expression in the absence of p53, e.g. through NF-κB binding (Barak et al., 1994; Busuttil et al., 2010; Iwakuma and Lozano, 2003; Wade et al., 2013). In contrast, the intrinsic P2 promoter located within the first intron is required for inducible *MDM2* gene expression. It contains two p53 consensus sites that supposedly need to be bound both in order to fully activate *MDM2* transcription (Zauberman et al., 1995). Based on this principle, active p53 induces the expression of its own major antagonist, thus establishing a negative p53-MDM2 feedback loop. However, *MDM2* transcription from the P2 promoter may also be induced by a series of additional transcription factors such as AP-1, ETS, Smad2/3, SP1 or MYCN (Manfredi, 2010; Wade et al., 2013; Zhao et al., 2014).

Since the first translational start codon is located within exon 3 of the *MDM2* gene, the transcripts from both promoters may give rise to the full-length MDM2 protein (Iwakuma and Lozano, 2003; Manfredi, 2010). However, transcripts derived from P1-initiated transcription contain a longer 5' untranslated region derived from the non-coding exon 2 which may favor the use of the alternative in-frame translational start sites downstream of the initial one. Hence, P1-initiated transcription facilitates the generation of N-truncated MDM2 isoforms while P2-derived transcripts are preferably translated from the first start codon, thus generating a full-length MDM2 protein (Barak et al., 1994).

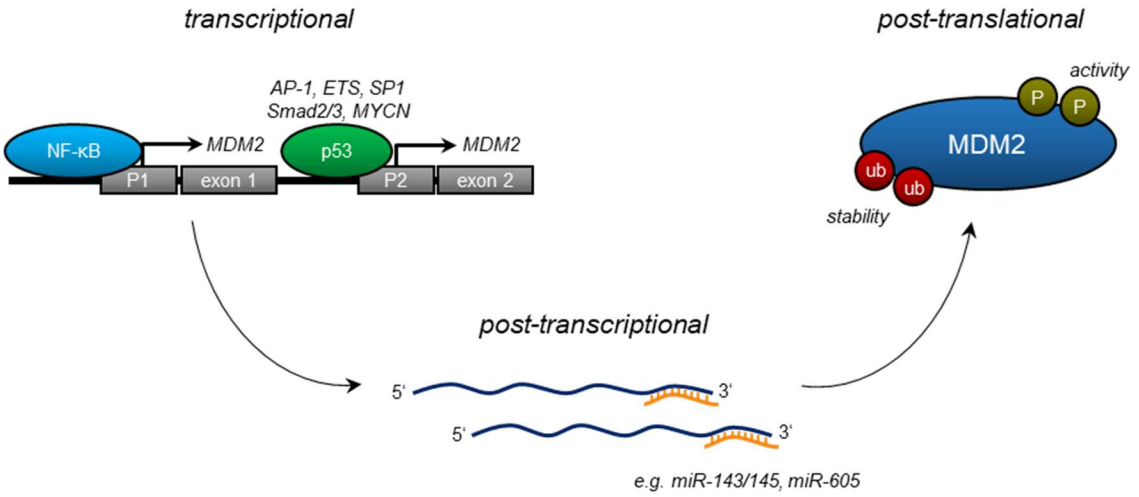

Fig. 2.6: Mechanisms of MDM2 regulation (simplified). MDM2 can be regulated on the transcriptional level through two distinct promoters P1 and P2 (left). While P1 induces basal MDM2 expression, transcription from P2 can be induced by multiple transcription factors including p53. Regulation on the post-transcriptional level occurs through microRNA-mediated RNA interference (middle). Upon protein translation, MDM2 regulation relies on its interaction with partner proteins affecting its stability through changing its ubiquitination status and on further chemical modifications such as phosphorylation, modulating MDM2 activity (right).

2.2.2.2.2. Post-transcriptional regulation of MDM2

In addition to transcriptional control, MDM2 expression is also regulated post-transcriptionally through RNA interference (Fig. 2.6 middle). RNA interference relies on the binding of a small RNA, e.g. microRNA, to a complementary mRNA, thus either facilitating its degradation or inhibiting its translation (O'Brien et al., 2018). MDM2-encoding mRNA can be targeted by a large series of microRNAs, thus inhibiting MDM2 protein expression and activating p53. Some of these microRNAs are direct transcriptional targets of p53 themselves, such as miR-143/154 or miR-605 (Karni-Schmidt et al., 2016; Wade et al., 2013; Zhao et al., 2014). Therefore, RNA interference partially represents a second regulatory feedback loop between p53 and MDM2 that, unlike the transcriptional one (cf. section 2.2.2.2.1), promotes p53 function.

2.2.2.2.3. Post-translational regulation of MDM2

Upon translation, MDM2 is still highly regulated through post-translational mechanisms (Fig. 2.6 right). As depicted previously, ubiquitination is a critical determinant of MDM2 protein stability. In addition to its dimerization with MDMX (cf. section 2.2.2.1), interaction with the deubiquitinating enzyme HAUSP stabilizes MDM2 protein levels while ubiquitination through the E3 ligases NAT10 or PCAF diminishes them (Brooks et al., 2007; Linares et al., 2007; Liu et al., 2016). Another way to regulate MDM2 is through its antagonist $p14^{ARF}$. $P14^{ARF}$ binds to the central domain of MDM2, leading to its destabilization, inhibiting its nucleo-cytoplasmic

shuttling, and facilitating its nucleolar accumulation. Through these mechanisms, $p14^{ARF}$ contributes to tumor suppression via p53 activation (Tao and Levine, 1999; Zhang et al., 1998). In addition to protein-protein interactions affecting MDM2 protein stability and localization, MDM2 can also be subjected to a multitude of post-translational modifications regulating its activity, of which phosphorylation is the most abundant one (Fåhraeus and Olivares-Illana, 2014; Wade et al., 2013; Zhao et al., 2014). Worth noticing, the mechanisms depicted here only represent examples highlighting the complexity of this intracellular network regulating MDM2 to sustain the tumor-suppressive functions of p53.

2.2.2.3. MDM2 as an antagonist of the tumor suppressor p53

As already indicated previously, the tailored regulation of p53 protein levels and activity through MDM2 is crucial to keep the non-transformed and viable cell state. One way by which MDM2 interferes with the transcriptional activity of p53 is by inhibiting its interaction with other proteins (Fig. 2.7). P53 possesses two N-terminal transactivation domains, TAD1 and TAD2, which are crucial for the recruitment of transcriptional co-factors such as the histone acetyl transferases p300/CBP, the Mediator complex or general transcription factors (Sullivan et al., 2018). The hydrophobic pocket within its p53-binding domain enables MDM2 to bind to the TAD1 of p53 (cf. 2.2.2.1; Kussie et al., 1996), thus blocking its interactions with other proteins (Momand et al., 1992; Oliner et al., 1993; Shi and Gu, 2012). This function is supported by its heterodimerization partner MDMX that binds to p53 TADs independently via its own p53-binding domain to prevent protein-protein interactions (Popowicz et al., 2008; Raj and Attardi, 2017). Notably, blocking the recruitment of p300/CBP by MDM2/MDMX complexes drives multiple inhibitory mechanisms. On the one hand, it inhibits the establishment of an accessible chromatin state around p53 binding sites through the loss of p300-mediated H3K27ac formation, thus affecting the binding of the transcription machinery (Espinosa and Emerson, 2001). On the other hand, it blocks p300-mediated acetylation of the p53 C-terminal regulatory domain, thus facilitating MDM2-driven ubiquitination of this region (Meek and Anderson, 2009).

Ubiquitination through the MDM2 RING finger antagonizes p53 in two different ways. On the one hand, MDM2 mono-ubiquitinates p53, preferably under conditions exhibiting low MDM2 levels (Biderman et al., 2012; Carter et al., 2007; Li et al., 2003). Mono-ubiquitination of p53 exposes its nuclear export signal and induces the recruitment of ubiquitin binding enzymes which modify p53, e.g. via SUMOylation and NEDDylation. These modifications interrupt the p53-MDM2 interaction and promote the nuclear-cytoplasmic shuttling of p53 (Fig. 2.7; Carter et al., 2007). This sequestration prevents p53 from binding to P53REs within target gene promoters, thus inhibiting p53-mediated transcription. Additionally, interaction of the MDM2 acidic domain with the p53 DBD induces a conformational change within this region, thus reducing DNA binding capacities of nuclear p53 proteins (Fig. 2.7; Cross et al., 2011).

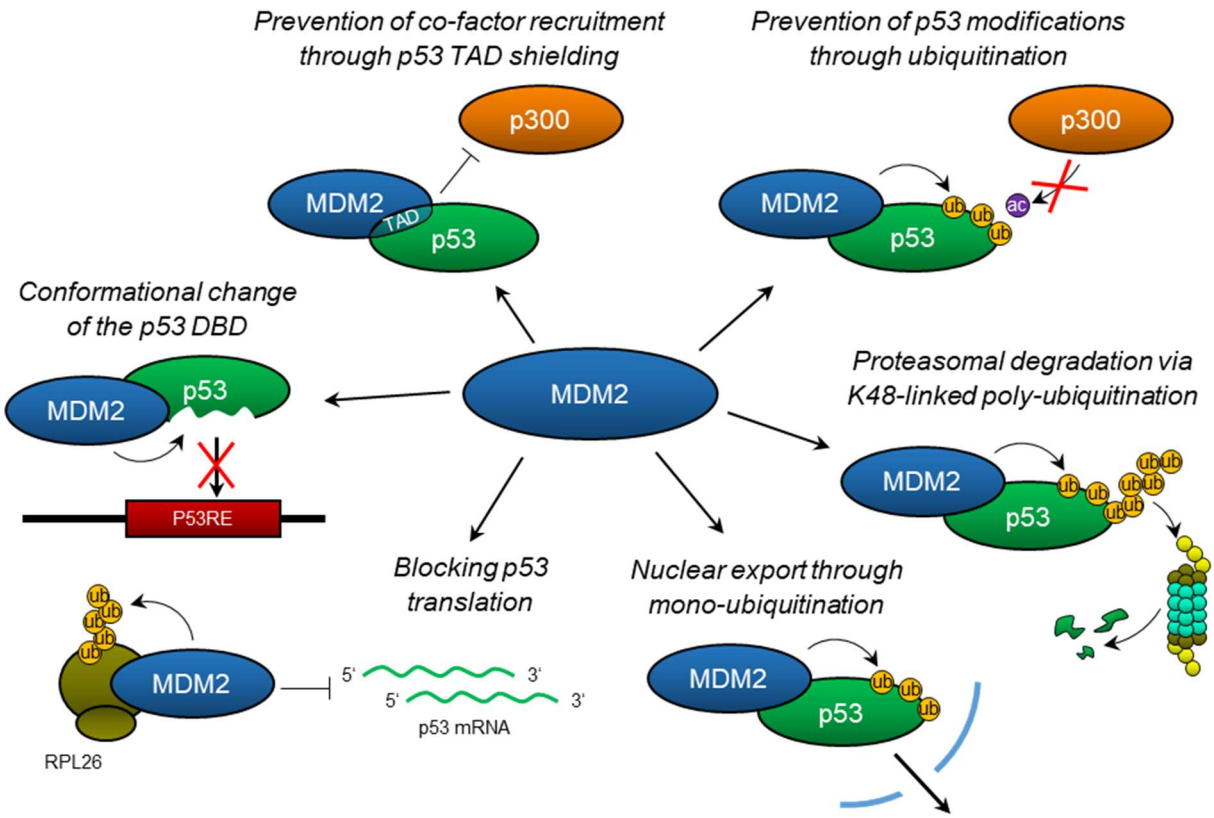

Fig. 2.7: MDM2-mediated mechanisms of p53 antagonism. MDM2 antagonizes p53 through mechanisms affecting both, p53 activity and protein stability. For further information on the respective mechanisms, please refer to section 2.2.2.3. Abbreviations: TAD: transactivation domain, DBD: DNA binding domain, P53RE: p53 recognition element, ub: ubiquitination, ac: acetylation.

On the other hand, MDM2 poly-ubiquitinates p53 at its lysine residues K370, K372, K373, K381, K382 and K386 (Fang et al., 2000; Rodriguez et al., 2000), thus inducing its degradation by the 26S proteasome (Fig. 2.7; Haupt et al., 1997; Kubbutat et al., 1997; Shi and Gu, 2012). Notably, this regulatory function is again supported through the heterodimerization of MDM2 with MDMX and is further prompted through its acidic domain (Kawai et al., 2003; Wang et al., 2011b). In addition to the induction of p53 proteasomal degradation, MDM2 interferes with p53 mRNA translation through interacting with the ribosomal protein L26. Upon binding, MDM2 blocks the association of L26 with p53 mRNA and induces the proteasomal degradation of a small proportion of L26 proteins through poly-ubiquitination (Fig. 2.7; Ofir-Rosenfeld et al., 2008).

Taken together, MDM2 antagonizes the tumor-suppressive functions of p53 through blocking its transactivation function and regulating its protein levels and activity in close collaboration with MDMX. Hence, MDM2 and MDMX are considered to be major oncogenes in cells affecting p53-induced transcription.

2.2.2.4. MDM2 as a p53-independent transcriptional regulator

Although the regulation of p53-mediated transcription through the depicted mechanisms is supposedly the most important and most prominent function of MDM2, p53-independent functions of MDM2 have been reported as well. In this regard, several publications show that MDM2 also works as a transcriptional regulator independently of its interaction with p53 (Fig. 2.8; Biderman et al., 2012).

Next to p53, MDM2 has been shown to interact with a multitude of other transcription factors, such as the p53 family member p73, HBP1, Smad4, FOXO1/3a, ATF3/4 or E2F1 (Fig. 2.8 A). The mechanisms by which MDM2 affects their transcriptional capabilities varies. While MDM2 binding induces the proteasomal degradation of some transcription factors including HBP1 and FOXO1/3a (Cao et al., 2019; Fu et al., 2009), it inhibits the activity of other transcription factors such as p73 without affecting their protein levels (Bálint et al., 1999; Dobbelstein et al., 1999; Wu and Leng, 2015). However, MDM2 has also been shown to promote the activity of transcription factors. For instance, direct MDM2 binding stabilizes the transcription factor E2F1 and supports its oncogenic functions by promoting its transcriptional activities (Martin et al., 1995; Zhang et al., 2005). Collectively, MDM2 initiates changes in in gene expression in cells by affecting transcription factor functions.

In addition to transcription factor-dependent gene expression, MDM2 has also been shown to work as a transcriptional repressor in a more global fashion. First indications of this global regulatory role were found in *in vitro* studies about 20 years ago showing that MDM2 interacts with components of the transcriptional PIC, thus repressing basal transcription (Fig. 2.8 B; Léveillard and Wasylyk, 1997; Thut et al., 1997). This picture of MDM2 as a global transcriptional regulator was further expanded in 2004 by Minsky and Oren showing that MDM2 is also involved in epigenetic transcriptional control. Using *in vitro* ubiquitination assays, they demonstrated that MDM2 can mediate the ubiquitination of H2A and H2B based on its C-terminal RING domain. This *in vitro* function was partially confirmed in subsequent expression studies in HEK293 cells showing that MDM2 promotes the ubiquitination of H2B, but not of H2A *in vivo* (Minsky and Oren, 2004). However, recent studies performed by our group drew a slightly different picture. Experiments investigating the role of MDM2 in the formation of endogenous histone modifications in murine embryonic fibroblasts (MEFs) revealed that MDM2 supports the catalysis of H3K27me3 as well as the mono-ubiquitination of H2A at lysine 119 (H2AK119ub1). Mechanistically, this effect depends on the MDM2 RING domain and is mediated through its physical interaction with the chromatin-modifying Polycomb repressor complexes, which install the H3K27me3 and H2AK119ub1 marks (Fig. 2.8 C; Wienken et al., 2016).

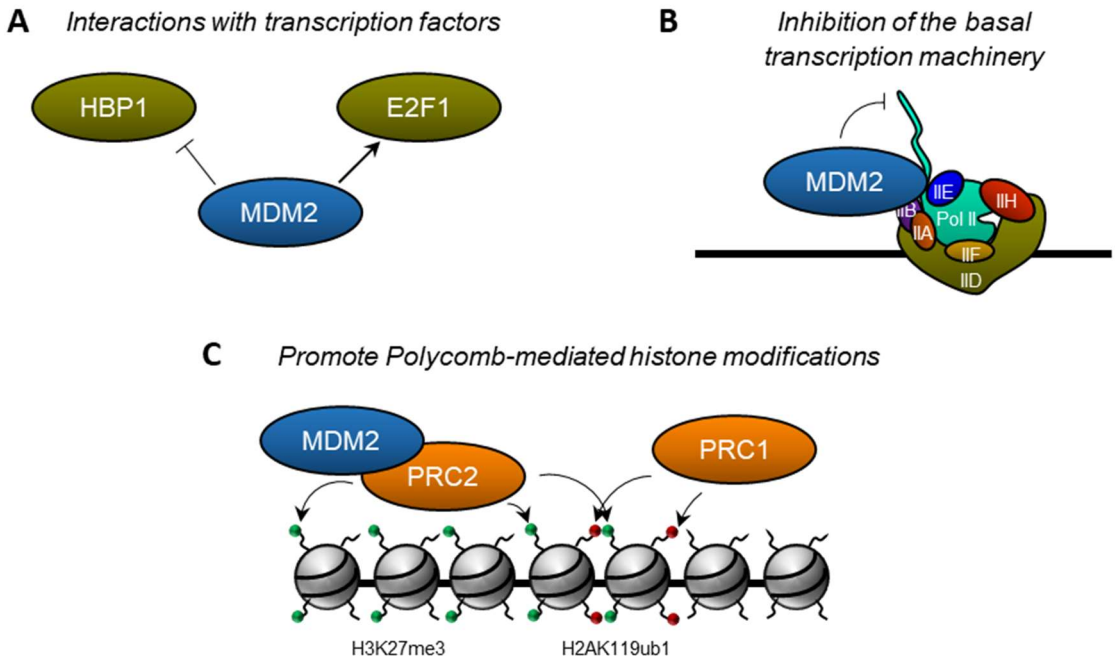

Fig. 2.8: P53-independent mechanisms of transcriptional regulation by MDM2.
(A) MDM2 can regulate gene expression through interaction with a large variety of transcription factors others than p53. (B) MDM2 inhibits the basal transcriptional machinery, potentially through direct interaction with general transcription factors required for the assembly of the transcriptional PIC. (C) MDM2 supports the formation of H3K27me3 (green dots) and H2AK119ub1 (red dots) mediated by Polycomb repressor complex 2 and 1, respectively.

2.3. Polycomb repressor complexes

Polycomb repressor complexes belong to the family of Polycomb group (PcG) proteins. Members of this protein family may form a large variety of chromatin-modifying complexes with distinct functions that can be subdivided into Polycomb repressor complex 1 (PRC1) and 2 (PRC2) and Polycomb repressive deubiquitinase (Chittock et al., 2017). Since deubiquitinating Polycomb complexes are not essential to this work, the following paragraphs will focus on the structural and functional features of PRC1 and PRC2 complexes.

2.3.1. Polycomb repressor complexes - subtypes and structures

PRC2 complexes describe the subgroup of PcG protein complexes that mediate the formation of mono-, di- or tri-methlyation of H3 at lysine 27 (H3K27me1, H3K27me2, H3K27me3) (Laugesen et al., 2019). They consist of a PRC2 core composed of the SET-domain dependent methyltransferase enhancer of zeste homolog 2 (EZH2), suppressor of zeste 12 homolog (SUZ12) and embryonic ectoderm development (EED), joined by additional interacting

proteins. Depending on the proteins associated with this PRC2 core, two subtypes of PRC2 complexes can be defined. In PRC2.1, the PRC2 core interacts either with polycomblike (PCL) proteins 1-3 or with c17orf96/c10orf12. In contrast, PRC2 core proteins in PRC2.2 associate either with the DNA-binding protein JARID2 or the Zinc finger protein AEBP2 (Fig. 2.9 A; Chittock et al., 2017).

In comparison to PRC2 complexes, the composition of PRC1 complexes is even more diverse. All PRC1 complexes consist of a PRC1 core comprising of a heterodimer of a RING1 molecule (either RING1A or RING1B; RING1B is referred to as RNF2 from now on) and a Polycomb group RING finger (PCGF) protein. In turn the N-terminal RING domains of the heterodimer mediate the mono-ubiquitination of histone 2A at lysine 119 (H2AK119ub1; Chittock et al., 2017). To date, six different PCGF proteins have been identified to dimerize with RING1 molecules to form PRC1 core subunits. Accordingly, six major PRC1 complexes are known so far (PRC1.1 - PRC1.6) that build the base for further complex variations depending on the additional co-factors associated with these PRC1 cores (Gao et al., 2012).

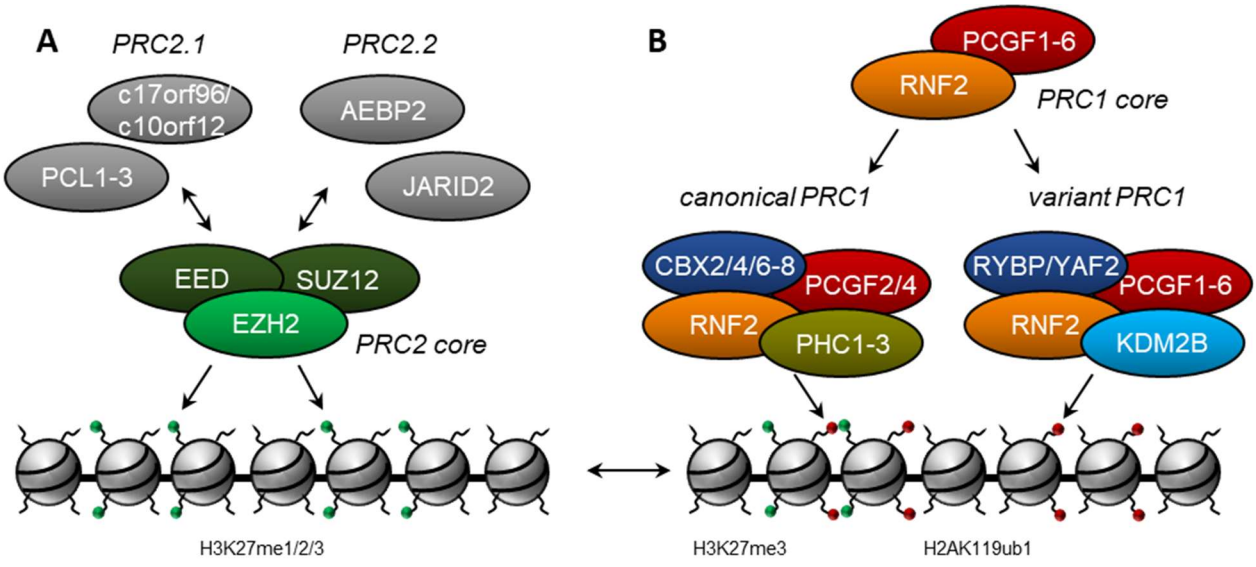

Fig. 2.9: Structure and function of Polycomb repressor complexes (simplified; partially adapted from Chittock et al., 2017). (A) PRC2 complexes consist of a PRC2 core containing EZH2, EED and SUZ12 subunits. Depending on the interacting proteins, they can form the PRC2.1 and PRC2.2 subgroups mediating the formation of mono-, di-, and tri-methylation of H3K27 (green dots). (B) The core subunit of PRC1 complexes consists of a heterodimer formed by a RING1 molecule (RING1A/B; RING1B referred to RNF2 here) and one out of six PCGF molecules (PCGF1-6). This core forms a multitude of subvariants which are classified into canonical and variant PRC1 complexes. Canonical PRC1 are characterized by a CBX subunit and mediate H2AK119ub1 (red dots) formation upon binding to H3K27me3. In contrast, variant PRC1 complexes contain RYBP/YAF2 instead of a CBX subunit and catalyze H2AK119ub1 independently of H3K27me3. The depicted PRC1 complexes are simplified versions highlighting the main characteristics of both subclasses.

PRC1 complexes can be classified into two functional subgroups, the canonical and the variant PRC1. Canonical PRC1 complexes are characterized by a core subunit composed of a heterodimer of RING1 and either PCGF2 or PCGF4. Additionally, they contain canonical complex components such as chromodomain proteins (CBXs), Ph homologs (PHCs) and Sex Comb on Midleg homologs (SCMs) (Fig. 2.9 B, left; Gao et al., 2012). In contrast, the core subunit of variant PRC1 complexes can be formed by heterodimerization of RING1 with any of the known PCGF1-6 proteins. These six variant PRC1 core subunits interact with a multitude of core-specific co-factors, thus giving rise to a large variety of variant PRC1 complexes (Fig. 2.9 B, right; Chittock et al., 2017). Due to this high diversity, variant PRC1 complexes are the predominant PRC1 subgroup and catalyze the vast majority of H2AK119ub1. In particular, the variant PRC1.1 complex that is characterized by PCGF1 and the CpG island-binding CxxC-protein KDM2B seems to be an important driver of H2AK119ub1 formation by synergistically acting with other variant PRC1 complexes (Fursova et al., 2019). In addition to their core subunits and associated co-factors, variant PRC1 complexes are mainly characterized by the presence of the RING/YY1-binding protein (RYBP) or its homolog YAF2. Since RYBP/YAF2 of variant PRC1 complexes are mutually exclusive to CBX/PHC/SMC of canonical PRC1, these co-factors are reliable markers to distinguish canonical from variant PRC1 complexes (Gao et al., 2012).

2.3.2. Polycomb repressor complexes in transcriptional repression

Initially identified as a gene controlling the sequential development of *Drosophila melanogaster*, PRC complexes have turned into major transcriptional regulators maintaining a cell's epigenetic memory (Duncan, 1982; Lewis, 1978; Schuettengruber et al., 2017). There are multiple ways by which PRCs may facilitate gene repression. For instance, PRC1 and PRC2 regulate gene expression through the catalysis of transcriptionally repressive histone modifications based on their enzymatic core subunits. While PRC2 complexes mediate the formation of mono-, di- and tri-methylation of H3K27 through the SET domain of their EZH2 component, PRC1 complexes promote the mono-ubiquitination of H2AK119 via its RING1 molecule (Chittock et al., 2017; Schuettengruber et al., 2017). Notably, both complexes closely cooperate in gene repression by facilitating their reciprocal recruitment. On the one hand, canonical PRC1 may bind to pre-existing H3K27me3 modifications via its CBX subunit and fortify the pre-existing gene repression through the additional catalysis of H2AK119ub1 (Gao et al., 2012; Schuettengruber et al., 2017). On the other hand, variant PRC1s can be recruited to sites lacking previous H3K27me3 to establish H2AK119ub1 that may promote subsequent PRC2 recruitment and H3K27me3 (Fursova et al., 2019). CpG islands are prominent examples of such sites. The variant PRC1.1 complex can be recruited to CGIs via its subcomponent

KDM2B which is capable of binding to CGIs via its CxxC-domain. Through this mechanism, variant PRC1.1 establishes a broad pattern of H2AK119ub1 in synergy with other variant PRC1 complexes, irrespectively of pre-existing H3K27me3 to prime genomic regions for further Polycomb-mediated transcriptional repression (Blackledge et al., 2014; Farcas et al., 2012; Fursova et al., 2019; Wu et al., 2013).

Furthermore, PRC1 complexes facilitate chromatin compaction (Francis et al., 2004; Schuettengruber et al., 2017; Shao et al., 1999). In contrast to H2AK119ub1 formation, that is primarily established by variant PRC1 due to the supportive function of the RYBP/YAF2 subunits (Fursova et al., 2019; Gao et al., 2012), chromatin compaction is mainly mediated by canonical PRC1. Interactions between the canonical PRC1 components CBX2 and PHC facilitate both, the compaction of adjacent chromatin as well as the formation of long-distance chromatin looping. This contributes not only to the repression of Polycomb target genes, but also to the establishment of a three-dimensional chromatin architecture within the nucleus (Illingworth, 2019).

2.4. Scope of the thesis

In this study, we sought to further elucidate the role of the p53-antagonist MDM2 in transcriptional control. Next to its pivotal role in regulating p53-mediated transcription, previous studies have already proven that MDM2 also functions as a transcriptional regulator in a p53-independent fashion. This is achieved through its interaction with and regulation of different transcription factors as well as its impairment of transcription by interacting with the basal transcription machinery and promoting the catalysis of repressive histone modifications (for further reference please refer to section 2.2.2.4). However, especially the latter effects were mainly observed in artificial *in vitro* and p53-deleted *in vivo* systems. Therefore, our current knowledge about MDM2 in transcriptional regulation in the presence of p53 *in vivo* is still very limited.

To shed some more light on this hypothesized p53-independent function of MDM2, the following questions should be addressed in this study.

1) Does the presence of p53 affect the association of MDM2 with chromatin?

Previous studies highlighted different aspects of the association of MDM2 with chromatin, depending on the respective system that was used. Studies conducted in p53-deficient systems reported the association of MDM2 with other transcription factors or epigenetic remodelers such as PRC complexes (Riscal et al., 2016; Wienken et al., 2016). In contrast, targeted chromatin binding studies carried out in the presence of p53 have shown that p53 can

recruit MDM2 to p53 target sites (Minsky and Oren, 2004). These aspects raise the question whether p53 can sequester MDM2 from “p53-independent” sites to p53 target genes, resulting in an entirely p53-dependent MDM2 chromatin-binding in p53-proficient systems. For this purpose, comprehensive global MDM2 chromatin-binding studies should be conducted in various cell systems with different p53 status to investigate the impact of p53 on MDM2 chromatin recruitment to both, p53 target and non-target sites. Down to the present day, there is only one data set available describing the global chromatin binding of endogenous and overexpressed MDM2 (Riscal et al., 2016). However, since this study was conducted in a p53 null system and only identified a limited number of MDM2 binding sites, this data set is not suitable to answer this major question of the dependency of global MDM2 chromatin-binding on p53.

2) If MDM2 chromatin recruitment is p53-independent, is there any underlying pattern explaining MDM2 chromatin-binding instead?

Assuming that MDM2 associates with chromatin in a p53-independent fashion even in p53-proficient systems, the mechanism driving this chromatin recruitment should be further investigated. For this purpose, it should be tested whether MDM2 can bind independently to DNA via a yet unknown DNA binding domain or whether its chromatin association is mediated through its interaction with chromatin-binding proteins. To answer these questions, targeted chromatin-binding studies should be performed using chromatin-immunoprecipitation. Furthermore, the identified MDM2 binding sites should be compared to publicly available data sets to identify potentially underlying pattern associated with MDM2 binding sites.

3) Does MDM2 chromatin-binding affect basal or inducible transcription, even in the presence of p53?

As a last point, the consequences of MDM2 chromatin recruitment should be further elucidated. Previous publications already reported a repressive function of MDM2 on transcription by both, the establishment of repressive histone modifications as well as its interaction with the basal transcriptional machinery (Léveillard and Wasylyk, 1997; Thut et al., 1997; Wienken et al., 2016). Hence it should be tested whether the site-specific recruitment of MDM2 represses transcription at those sites as well. Furthermore, it should be tested whether a potential impact on transcription is restricted to basal transcription or whether this is also applicable in the context of induced transcription.

3. Material and Methods

3.1. Material

3.1.1. Chemicals and reagents

Table 3.1.1: Chemicals and reagents used.

Reagent	Catalogue no.	Supplier
0.05 % Trypsin/EDTA	25300054	Invitrogen
Acetic acid, 100 % Ph. Eur., water-free	6755.1	Roth
Agar-Agar	5210.2	Roth
Ammonium sulfate $(NH_4)_2SO_4$	9218.1	Roth
Ammonium peroxodisulfate (APS)	9592.2	Roth
Ampicillin, sodium salt	A0839	AppliChem
Bovine serum albumin (BSA)	8076.3	Roth
Bromphenol blue	B0126	Sigma
Ciprofloxacin (200 mg/100 ml)	-	Fresenius Kabi GmbH
Chloroform	3313.1	Roth
cOmpleteTM Protease Inhibitor Cocktail, EDTA-free	5056489001	Roche
dATP, stock solution (100 mM)	1202.4	Primetech
dCTP, stock solution (100 mM)	1203.4	Primetech
dGTP, stock solution (100 mM)	1204.4	Primetech
dTTP, stock solution (100 mM)	1205.4	Primetech
Dimethyl sulfoxide (DMSO) for cell culture	A3672,0100	AppliChem
Disodium phosphate dihydrate ($Na_2HPO_4 \cdot 2\ H_2O$)	3580.1	Roth
Dithiotreit (DTT), > 99 % p.a.	6908.4	Roth
D-(+)-Trehalose dihydrate	5151.3	Roth
Dulbecco's Modified Eagle's Medium (DMEM), powder, low glucose, pyruvate	31600-091	Life Technologies
Ethanol (EtOH) absolute, 99.9 %	2246.2500	ChemSolute / Th. Geyer
Ethylene diamine tetraacetic acid (EDTA)	8040.1	Roth
Ethylene glycol bis(succinimidyl succinate) (EGS)	21565	Thermo Scientific
Ethylene glycol tetraacetic acid (EGTA)	3054.2	Roth
Fetal bovine serum (FBS) superior	S0615	Merck
Formaldehyde solution, 37 % (PFA)	F1635-500ML-D	Sigma
Glycine	3908.3	Roth
HEPES	9105.4	Roth
Hydrochloric acid, 25 %	825.2511	Th Geyer
Immobilon Western HRP Substrate	WBKLS0500	Merck Millipore
Isopropanol / 2-Propanol	6752.4	Roth

Kanamycin sulfate	A1493	AppliChem
Leupeptin hemisulfate	A2183.0010	AppliChem
L-glutamine, 200 mM solution	25030123	Life technologies
Lipofectamine 2000 (LPF 2000)	11668019	Life technologies
Lipofectamine 3000 (LPF 3000)	L3000015	Invitrogen
Lithium chloride solution, 8 M, > 99 %	L7026	Sigma
Magnesium chloride (MgCl2) solution, 1 M	M1028	Sigma
Maxima SYBR Green Master Mix (2x), separate ROX-vial	K0252	Thermo Scientific
Mc Coy's 5A (Modified) Medium	26600080	Gibco
Methanol (MetOH), 99 %	8388.6	Roth
Milk powder, blotting grade	T145.4	Roth
Nonidet™ P-40 substitute (NP-40)	74385	Sigma
Nuclease-free water	AM9939	Ambion
PageRuler prestained protein ladder	26617	Thermo Scientific
Pefabloc® SC-Protease-Inhibitor	A154.2	Roth
Penicilin/streptomycin	15140130	Gibco
Pepstatin A	A2205.0010	Th Geyer
Phosphate-buffered saline (PBS) tablets	18912014	Gibco
Ponceau-S	5938.1	Roth
Potassium chloride (KCl)	P017.1	Roth
Potassium dihydrogen orthophosphate (KH2PO4)	3904.1	Roth
Protein-A/G Plus agarose beads	sc-2003	Santa Cruz
Protein-G Sepharose™ 4 Fast Flow Media	17061805	GE Healthcare
Rotiphorese® Gel 30 (37,5:1) acrylamide stock solution	3029.1	Roth
Sodium bicarbonate ($NaHCO_3$)	6885.1	Roth
Sodium chloride (NaCl)	3957.2	Roth
Sodium deoxycholate (NaDOC)	30970-100G	Sigma
Sodium dodecyl sulfate (SDS) pellets	CN30.3	Roth
SpectraTM Multicolor High Range Protein Ladder	26625	Thermo Scientific
SuperSignal West Femto Maximum Sensitivity Substrate	34095	Thermo Scientific
SYBR Green	S7567	Life Technologies
TEMED	A1148,0025	AppliChem
Tetracyclin hydrochloride	A39246	Gibco
Tris Pufferan, ≥ 99.9 %, p.a.	4855.3	Roth
Triton X-100	A1388	AppliChem
TRIzolTM reagent	15596018	Life technologies
Tryptone/Peptone	8952.2	Roth
Tween-20	A4974,0500	AppliChem
Urea, ≥ 99.5 %, p.a.	3941.1	Roth
Tween® 20	A4974,0500	AppliChem
Yeast extract	2363.2	Roth

3.1.2. Consumables

Table 3.1.2: Consumables used.

Consumable	Catalogue no.	Supplier
BD Microlance 3 26G*1/2", 0.45 mm x 13 mm	303800	BD
Bioruptor® Pico Microtubes with Caps, 1.5 ml	C30010016	Diagenode
Cell scraper, 16 cm	83.1832	Sarstedt
Cell scraper, 25 cm	83.1830	Sarstedt
CELLSTAR tissue culture dish, 145 x 20 mm	639160	Greiner Bio-One
CELLSTAR tissue culture dish, 100 x 20 mm	664160	Greiner Bio-One
Corning® 150 ml Bottle Top Vacuum Filter, 0.22 µm pore 13.6 cm^2 PES Membrane, sterile	431161	Corning
Corning® 500 ml Bottle Top Vacuum Filter, 0.22 µm pore 33.2 cm^2 PES Membrane, sterile	431118	Corning
Corning® 50 mm Diameter Syringe Filters, 0.2 µm Pore	431227	Corning
Cyrotube vials, 1.8 ml	377267	Nunc
Reaction tubes, 2 ml	72.695.500	Sarstedt
Reaction tubes, 1.5 ml	0030120.086	Eppendorf
Falcon ®96-well Black/Clear Flat Bottom TC-treated Imaging Microplate with Lid	353219	BD Falcon
Falcon tube, 50 ml	227261	Greiner
Falcon tube, 15 ml	188271	Greiner
Filtertips (1000 µl)	70.762.211	Sarstedt
Filtertips (200 µl)	70.760.211	Sarstedt
Filtertips (20 µl)	70.760.213	Sarstedt
Filtertips (10 µl)	S1180-3810	Starlab
FrameStar® 96 Well Skirted PCR Plate	4ti-0961	4titude
Gelloader4 pipette tips	70.1190.100	Sarstedt
Hemocytometer (*Neubauer chamber*)	717820	Brand
HSW HENKE-JECT® 1 ml Syringe, single use	5010.200V0	Henke Sass Wolf
Hybond-P PVDF membrane	10600023	GE Healthcare Life Science
Low Binding tubes, clear, 1.6 ml	710176	Biozym
Multiply PCR tubes, 200 µ	72.737.002	Sarstedt
Neubauer chamber cover glass (20 x 26 x 0.4 mm)	2026H-001	Thermo Scientific
Nitrocellulose membrane, Protran BA83 (300 mm x 4m), 0.2 µm	10600001	GE Healthcare Life Science
Pasteur pipettes, 230 mm	64171020	Heinemann
Pasteur pipettes, 150 mm	7691060	Th Geyer
PCR mirocentrifuge tube, 0.5 ml	04-102-1150	Nerbe Plus
PCR tubes, 0.2 ml	72.737.002	Sarstedt
Pipette tips, 1000 µl	70.762.211	Sarstedt
Pipette tips, 200 µl	70.760.502	Sarstedt

Pipette tips, 10 µl	701130600	Sarstedt
QPCR adhesive clear seals	4ti-0560	4titude
Serological pipette, 25 ml	86.1685.020	Sarstedt
Serological pipette, 10 ml	86.1254.025	Sarstedt
Serological pipette, 5 ml	86.1253.025	Sarstedt
Syringes with Luer Lock, 50 ml, single use	I3 0506	Mediware
TC Plate 6 Well Standard F	83.3920.	Sarstedt
Tubular film, 0.1 mm thick, 300 mm x 25 m	160422	Heinemann Labortechnik
Whatman paper / blotting paper B002, 580 x 600 mm	GB58	Heinemann Labortechnik

3.1.3. Solutions

Table 3.1.3: Composition of the solutions used.

Solution	Composition
Solutions for Immunoblot analyses	
10x PBS, pH 7.4	24 mM NaCl 0.27 mM KCl 0.81 mM Na_2HPO_4 0.15 mM KH_2PO_4 in H_2O
10x TBS, pH 7.4	0.5 M Tris 1.54 M NaCl in H_2O
10x SDS running buffer	250 mM Tris 1.92 M glycine 34.7 mM SDS
10x Western salt buffer, pH 8.3	250 mM Tris 1.92 M glycine 0.02 % SDS in H_2O
6x Laemmli buffer	0.35 M Tris, pH 6.8 30 % Glycine 10 % SDS (w/v) 9.3 % DTT (w/v) 0.02 % Bromphenol blue (w/v)
Cell lysis buffer for protein harvest	66 % RIPA lysis buffer 33% 8 M urea Protease inhibitors: 10 µM Pefabloc 1 µg/ml Pepstatin A 1 µg/ml Leupeptin
Low range protein transfer buffer	10 % 10x Western salt buffer 20 % MetOH in H_2O

High range protein transfer buffer	10 % 10x Western salt buffer 10 % MetOH 0.01 % SDS in H_2O
Ponceau-S solution	0.5 % Ponceau-S (w/v) 1 % Acetic acid in H_2O
RIPA lysis buffer	1 % Triton X-100 1% sodium deoxycholate (w/v) 0.1 % SDS (w/v) 150 mM NaCl 10 mM EDTA 20 mM Tris-HCl, pH 7.5 in H_2O
1x TBS-T	10 % 10x TBS, pH 7.4 1 % Tween-20 in H_2O
Solutions for quantitative reverse-transcription PCRs	
dNTP mix, 2.5 mM	2.5 mM dATP 2.5 mM dCTP 2.5 mM dGTP 2.5 mM dTTP in nuclease-free H_2O
Mixed primer	50 µM oligo dT primer 15 µM random nonamers in nuclease-free H_2O
Self-made 10x qPCR mix	750 mM Tris-HCl, pH 8.8 200 mM $(NH_4)_2SO_4$ 0.1 % Tween-20 in H_2O, sterile filtrate (0.2 µm)
Self-made 2x qPCR Master Mix	1.727x self-made 10x qPCR mix 5.18 mM $MgCl_2$ 518 mM Trehalose in 10 mM Tris, pH 8.0 0.43 % Triton X-100 1:22,400 SYBR Green 0.345 mM dNTPs 34.54 U/ml Taq Polymerase
Solutions for chromatin-immunoprecipitations	
Buffer A	0.1 M NaCl 1 mM EDTA, pH 8.0 0.5 mM EGTA, pH 8.0 50 mM HEPES, pH 7.6 in H_2O
Buffer B	0.25 % Triton X-100 10 mM EDTA, pH 8.0 0.5 mM EGTA, pH 8.0 20 mM HEPES, pH 7.6 in H_2O

Buffer C	0.15 M NaCl 1 mM EDTA, pH 8.0 0.5 mM EGTA, pH 8.0 50 mM HEPES, pH 7.6 in H_2O
2x Decrosslinking buffer, pH 8.0	100 mM Tris-HCl, pH 8.0 20 mM EDTA, pH 8.0 2 % SDS in H_2O
Elution buffer	1 % SDS 0.1 M $NaHCO_3$ in H_2O
5x Incubation buffer with SDS	0.75 % SDS 5 % Triton X-100 0.75 M NaCl 5 mM EDTA, pH 8.0 2.5 mM EGTA, pH 8.0 100 mM HEPES, pH 7.6 in H_2O
5x Incubation buffer without SDS	5 % Triton X-100 0.75 M NaCl 5 mM EDTA, pH 8.0 2.5 mM EGTA, pH 8.0 100 mM HEPES, pH 7.6 in H_2O
Protein-protein crosslinking buffer	2 mM EGS (dissolved in DMSO) 6.93 % Buffer A in 1x PBS
Protein-DNA crosslinking buffer	1.1% PFA 7 % Buffer A in 1x PBS
Washbuffer 1	0.1 % SDS 0.1 % NaDOC 1 % Triton X-100 0.15 M NaCl 1 mM EDTA, pH 8.0 0.5 mM EGTA, pH 8.0 20 mM HEPES, pH 7.6 in H_2O
Washbuffer 2	0.1 % SDS 0.1 % NaDOC 1 % Triton X-100 0.5 M NaCl 1 mM EDTA, pH 8.0 0.5 mM EGTA, pH 8.0 20 mM HEPES, pH 7.6 in H_2O

Washbuffer 3	0.25 M LiCl 0.5 % NaDOC 0.5 % NP-40 1 mM EDTA, pH 8.0 0.5 mM EGTA, pH 8.0 20 mM HEPES, pH 7.6 in H_2O
10x Washbuffer 4	10 mM EDTA, pH 8.0 5 mM EGTA, pH 8.0 200 mM HEPES, pH 7.6 in H_2O
Solutions for complex-immunoprecipitations	
Co-IP buffer	300 mM NaCl 50 mM Tris-HCl, pH 7.5 1 % NP-40 in H_2O

3.1.4. Cell lines

Table 3.1.4: Cell lines used for experiments.

Cell line	Species	Entity	P53/MDM2 status
H1299	Human	Non-small cell lung carcinoma	P53 deletion
HCT 116	human	Colorectal carcinoma	P53 wt
PANC-1	human	Pancreatic adenocarcinoma	P53 mutant (R273H)
SJSA-1	human	Osteosarcoma	P53 wt MDM2 amplification

3.1.5. Cell culture media

Table 3.1.5: Media used for cell culture.

Medium	Supplements	Cell lines cultured with
Dulbecco's Modified Eagle's Medium (DMEM) with supplements	10% FBS 200 µM L-glutamine 100 U/ml penicillin/streptomycin 10 µg/ml ciprofloxacin 2 µg/ml tetracyclin	H1299 PANC-1 SJSA-1
Mc Coy's 5A (Modified) Medium with supplements	10% FBS 200 µM L-glutamine 100 U/ml penicillin/streptomycin	HCT116

3.1.6. Pharmacological inhibitors and cytokines

Table 3.1.6: Pharmacological inhibitors and cytokines used for cell treatment.

Inhibitor	Usage	Catalogue no.	Supplier
Cycloheximide (CHX), ≥ 95 %	Eukaryotic ribosomes, protein translation inhibitor	C7698	Sigma
Human recombinant TNFα	Stimulation of NF-κB signaling, induction extrinsic apoptosis	210-TA-020	R&D Systems
Human recombinant TRAIL	Induction extrinsic apoptosis	375-TL-010	R&D Systems
Idasanutlin (RG-7388)	Inhibition of the P53-binding domain of MDM2	S7205	Selleckchem
MG-132	Proteasome inhibitor, Increasing protein levels	474791-5MG	Millipore
Nutlin-3a	Inhibition of the P53-binding domain of MDM2	direct order	BOC Sciences

3.1.7. Small interfering RNA

Table 3.1.7: Small interfering RNAs from Ambion used for experiments.

Target	siRNA ID	Sequence
Negative control (mixed in equal ratios to get a pool)	SSC1	undisclosed
	SSC2	
MDM2 (mixed in equal ratios to get a pool)	Customer select	sense: 5‘ - GCCAUUGCUUUUGAAGUUAtt - 3‘ antisense: UAACUUCAAAAGCAAUGGCtt - 3‘
	S8629	sense: 5‘ - AGUCUGUUGGUGCACAAAAtt - 3‘ antisense: 5‘ - UUUUGUGCACCAACAGACUtt -3‘
	S224037	sense: 5‘ - AGACCCUGGUUAGACCAAAtt - 3‘ antisense: 5‘ - UUUGGUCUAACCAGGGUCUct - 3‘
RNF2 (mixed in equal ratios to get a pool)	S12067	sense: 5‘ - GGCUAGAGCUUGAUAAUAAtt - 3‘ antisense: 5‘ - UUAUUAUCAAGCUCUAGCCca - 3‘
	S12068	sense: 5‘ - CAAACGGACCAAAACAUCUtt - 3‘ antisense: 5‘ - AGAUGUUUUGGUCCGUUUGtt - 3‘
	S12069	sense: 5‘ - GGAGUGUUUACAUCGUUUUtt - 3‘ antisense: 5‘ - AAAACGAUGUAAACACUCCtt - 3‘
P53 (mixed in equal ratios to get a pool)	S605	sense: 5‘ - GUAAUCUACUGGGACGGAAtt - 3‘ antisense: 5‘ - UUCCGUCCCAGUAGAUUACca - 3‘
	S606	sense: 5‘ - GAAAUUUGCGUGUGGAGUAtt - 3‘ antisense: 5‘ - UACUCCACACGCAAAUUUCct - 3‘
	S607	sense: 5‘ - GGUGAACCUUAGUACCUAAtt - 3‘ antisense: 5‘ - UUAGGUACUAAGGUUCACCaa - 3‘

3.1.8. Plasmids

Table 3.1.8: Expression plasmids used for experiments.

Plasmid	Origin
pcDNA3	Invitrogen
pCMV-MDM2 wt	B. Vogelstein (Oliner et al., 1992)
pcHDM2 Δ58-90	A. J. Levine (Chen et al., 1993)
pcHDM2 Δ222-325	
pCMV-MDM2 RING mutant C464A	T. Jacks (Addgene plasmid #12086; Boyd et al., 2000)
pCMV-P53 wt	C. Prives
pTY-EF1a-mKDM2B wt -Flag	Y. Zhang (He et al., 2013)
pTY-EF1a-mKDM2B ΔCxxC-Flag	

3.1.9. Bacteria

Table 3.1.9: Bacterial strains used for plasmid expansion.

Strain	Supplier
DH10B^{TM}	Thermo Fisher Scientific

3.1.10. Bacterial growth media

Table 3.1.10: Bacterial strains used for plasmid expansion.

Medium	Composition
2x YT medium, pH 7.0	1.6 % Tryptone (w/v) 1 % yeast extract (w/v) 0.5 % NaCl (w/v)
LB medium, pH 7.0	1 % Tryptone (w/v) 0.5 % yeast extract (w/v) 1 % NaCl (w/v)
LB agar	1.2 % agar (w/v) in 1x LB medium

3.1.11. Antibodies

Table 3.1.11: Antibodies used.

Antibody	Species	Dilution/Amount	Catalogue no.	Supplier
Primary antibodies for Immuoblotting, ChIP and Co-IP				
β-actin	Mouse	WB: 1:40,000	ab6276-100	Abcam
β-Gal isotype control	Mouse	Co-IP: 3 µg	Z378B	Promega
Caspase 3 (1C12)	Mouse	WB: 1:500	9746	Cell Signaling
Cleaved caspase 3	Rabbit	WB: 1:500	9664	Cell Signaling
Flag® M2-Peroxidase (HRP) coupled	Mouse	WB: 1:2000	A8592	Sigma
HSC70	Mouse	WB: 1:40,000	sc-7298	Santa Cruz
H2AK119ub1 (D27C4) XP	Rabbit	ChIP: 2 µg	8240	Cell Signaling
H3K27ac	Rabbit	ChIP: 2 µg / 5 µg	C15410196	Diagenode
H3K27me3	Rabbit	ChIP: 2 µg	pAb-069-050	Diagenode
H2Av spike-in antibody	undisclosed	ChIP: 2 µg	61686	Active Motif
IgG isotype control	Rabbit	ChIP: 2 µg / 5 µg Co-IP: 3 µg	ab171870	Abcam
KDM2B (JHDM1B)	Rabbit	WB: 1:500 ChIP: 2 µg Co-IP: 3 µg	09-864	Millipore
MDM2 ChIP grade	Rabbit	WB: 1:500 ChIP: 2 µg	ab226939	Abcam
MDM2 IF2	Mouse	WB: 1:200 - 1:300 ChIP: 2 µg Co-IP: 3 µg	OP46-100UG	CalBiochem
P21 Waf1/Cip1 (12D1)	Rabbit	WB: 1:1000	2947	Cell Signaling
P53 DO-1	Mouse	WB: 1:1000 ChIP: 2 µg	SC126	Santa Cruz
PARP	Rabbit	WB: 1:1000	9542	Cell Signaling
Pol II CTD	Mouse	WB: 1:500 ChIP: 2 µg	C15200004	Diagenode
Rbp1 NTD (D8L4Y)	Rabbit	ChIP: 2 µg	14958	Cell Signaling
RNF2	Rabbit	WB: 1:500	5694	Cell Signaling
TBP	Mouse	ChIP: 2 µg	C15200002	Diagenode
TFIIE alpha/GTF2E1	Rabbit	ChIP: 2 µg	ab28177	Abcam

Antibody	Species	Dilution/Amount	Catalogue no.	Supplier
Secondary antibodies used for immunoblotting				
α-mouse HRP-conjugated IgG	Donkey	1:10,000	715-036-150	Jackson Immuno Research
α-rabbit HRP-conjugated IgG	Donkey	1:10,000	711-036-152	Jackson Immuno Research

3.1.12. Primer

Table 3.1.12: Primer used for quantitative PCRs.

Target	Sequence	Acknowledgement
Primer for reverse transfection		
Oligo dT	5' – TTTTTTTTTTTTTTTTTTTTTTTVN – 3'	
Random nonamer	5' – NNNNNNNNN – 3'	
Primer for human gene expression analysis (qRT-PCR)		
β-actin forward β-actin reverse	5' - CGACAGGCTGCAGAAGGAG - 3' 5' - GTACTTGCGCTCAAGAGGAG - 3'	Daniela Kramer
A20 forward A20 reverse	5' - TACTCGGAACTGGAATGATGAATGG - 3' 5' - GGGGCGAAATTGGAACCTGA - 3'	Robyn Kosinsky
CXCL8 forward CXCL8 reverse	5' – CCGGAAGGAACCATCTCACTG – 3' 5' – TGGCAAAACTGCACCTTCACAC – 3'	
EBI3 forward EBI3 reverse	5' – TCTCCATGGCTCCCTACGTG – 3' 5' – GGGTCGGGCTTGATGATGTG – 3'	
IL6 forward IL6 reverse	5' - CATCCTCGACGGCATCTCAG - 3' 5' - TCACCAGGCAAGTCTCCTCA - 3'	Ramona Schulz-Heddergott
IRF1 forward IRF1 reverse	5' – CCTCCACCTCTGAAGCTACAAC – 3' 5' – CCATCCACGTTTGTTGGCTG – 3'	
TNFAIP2 forward TNFAIP2 reverse	5' - CTACATGCTGCTGCTCTGGG - 3' 5' - CGCCTCACTGGACAGGAAT - 3'	Robyn Kosinsky
TRAF1 forward TRAF1 reverse	5' – CTTCTCCCCAGCCTTCTACACTG – 3' 5' – AAGAGCGACAGATGGGTTCTC – 3'	
Primer for human chromatin binding analysis (ChIP-qPCR)		
ATR forward ATR reverse	5' - GGAATCAGCGGAGGAGGATG - 3' 5' - GAGCTGGCTTCCATGATCCC - 3'	
BARD1 forward BARD1 reverse	5' - CGATTATCCGGCATCGTCCC - 3' 5' - CTTCCCTGTGGTTTCCCGAG - 3'	
BBC3 forward BBC3 reverse	5' - CCCTGCTCTGGTTTGGTGAG - 3' 5' - AGTCACTCTGGTGAGGCGAT - 3'	Anusha Sriraman
BNIP1 forward BNIP1 reverse	5' - ACACGTGTCAGGGAAAGTCC - 3' 5' - CAGGACCCAAGTTCAAACGC - 3'	
FBXL3 forward FBXL3 reverse	5' - ATGTGACTCCCGCTTGAAGG - 3' 5' - CTGCTCCACCTCCCTAAACC - 3'	
GSPT2 forward GSPT2 reverse	5' - TCGCTCTTGCTGCCTTAACC - 3' 5' - TCCATGGTCTCGGAACTTGC - 3'	

IFNGR1 forward IFNGR1 reverse	5' - ATGGCTGATCAGGATGTGGG - 3' 5' - ACAAATAAGCACAGTCCCGC - 3'	
ITIH3 forward ITIH3 reverse	5' - CTTGGAAAACACCAGGCTTGCTC - 3' 5' - GACAGGGCCACCATGCAAATG - 3'	
MB forward MB reverse	5' - CTCATGATGCCCCTTCTTCT - 3' 5' - GAAGGCGTCTGAGGACTTAAA - 3'	Anusha Sriraman
MDM2 forward MDM2 reverse	5' - TTCAGTGGGCAGGTTGACTC - 3' 5' - CCAGCTGGAGACAAGTCAGG - 3'	Anusha Sriraman
MIR34AHG forward MIR34AHG reverse	5' - ATTCTTCCCCTTACGGAGGC - 3' 5' - GAAGGAGGCGGGAACTAGAC - 3'	
Neg. Ctrl forward Neg. Ctrl reverse	5' - TGGAGCCACCTTTACTCCAC - 3' 5' - GTAGTCATCATGGCCACCCC - 3'	
NFATC2 forward NFATC2 reverse	5' - TCCCAAAGCAAGGAGGTCTG - 3' 5' - CAGTTTGGCAGCTCAGTGAC - 3'	
P21 forward P21 reverse	5' - CTTTCTGGCCGTCAGGAACA - 3' 5' - CTTCTATGCCAGAGCTCAACATGT - 3'	Anusha Sriraman
PSMB6 forward PSMB6 reverse	5' - GGCGGCTACCTTACTAGCTG - 3' 5' - TGTGCACGTCCTATGAACCC - 3'	
SAMD11 forward SAMD22 reverse	5' - CTCTACGTGCGCAAACTCTG - 3' 5' - ACGAACTGGAACTCGTTGGG - 3'	
VAMP4 forward VAMP4 reverse	5' - AATCGAGGAAGTCGATCCGC - 3' 5' - TTCCTCCCCTAAAGCACAGC - 3'	

3.1.13. Enzymes

Table 3.1.13: Enzymes used.

Enzyme	Catalogue no.	Supplier
M-MuLV reverse transcriptase, buffer provided	M0253	Biolabs/NEB
Proteinase K, RNA grade	25530-049	Invitrogen
Rnase A (17,500 U)	19101	Qiagen
Taq-Polymerase (5,000 U)	1x00.4	Primetech

3.1.14. Kits

Table 3.1.14: Kits used.

Kit	Catalogue no.	Supplier
Bioanalyzer High Sensitivity DNA Analysis Kit	5067-4626	Agilent Technologies
Spike-in chromatin Spike-in Antibody Drosophila positive control primer set Pbgs Drosophila negative control primer set 1	53083 61686 71037 71028	Active Motif

KAPA Hyper Prep Kit (24 rxn) KAPA SI Adapter Kit Set A 30 µM 12 adapters x 40 µl KAPA SI Adapter Kit Set B 30 µM 12 adapters x 40 µl KAPA Pure Beads (30 ml)	07 962 347 001 08 005 702 001 08 005 729 001 07 983 280 001	Roche
MinElute PCR Purification Kit	28006	Qiagen
PierceTM BCA Protein Assay Kit	23227	Thermo Scientific
PureYieldTM Plasmid Midiprep System	A2393	Promega
QubitTM dsDNA High Sensitivity Assay Kit	Q32854	Thermo Scientific
ViaStain™ Live Caspase-3/7 Detection Kit for 2D/3D Cultures	CSK-V0003-1	Nexcelom

3.1.15. Devices

Tabe 3.1.15: Devices used.

Device	Supplier
Autoclave *DX-200*	Systec GmbH
Bioanalyzer 2100	Agilet Technologies
Blotting chamber	Biozym
Centrifuge *5810R*	Eppendorf
Centrifuge *5415D*	Eppendorf
Centrifuge *Heraeus Megafuge 1.0R*	Heraeus, Thermo Scientific
Chemiluminescence imager *ChemiDoc XRS+*	Bio-Rad
Chemiluminescence imager *Chemocam HR 16 3200*	Intas Science Imaging Instruments
DNA gel chamber	Biotech Service Blu
DynaMag™ -96 Side Magnet	Thermo Scientific
Electrophoresis chamber for SDS-PAGE	Amersham Biosciences
Freezer, -20 °C	Liebherr
Freezer, -80 °C	Heraeus, Thermo Scientific
Fridge, 4 °C	Liebherr
Heating block	HLC
Heating cabinet	Memmert
Hemocytometer, *Neubauer improved*	Brand
Ice machine B100	Ziegra
Imaging cytometer *Celigo*	Nexcelom
Incubator for bacterial culture *Minitron*	Infors HT
Incubator for cell culture *Hera Cell 150*	Heraeus, Thermo Scientific
Laminar flow *Hera safe*	Heraeus, Thermo Scientific
Liquid nitrogen tank *LS 4800*	Taylor-Wharton
Magnetic stirrer *MR 3001*	Heidolph
Microscope *Axiovert 40 C*	Zeiss
Microwave	Cinex

Pipette Aid portable *#4XXX-200*	Drummond Scientific
Pipettes *Eppendorf Research*, 100-1000 µl, 20-200 µl, 2-20 µl, 0.1-2.5 µl)	Eppendorf
Pipette, Multipipet	Eppendorf
Pipette, 8-channel	Eppendorf
pH meter *WTW-720*	WTW
Power Supply	Biometra
Qubit 2.0 Fluorometer	Invitrogen
Real-Time PCR Detection System *CFX96*	Bio-Rad
Rotator *PTR 300*	Grant Instruments
Roller *RM5-30V*	CAT
Scales *Acculab ALC-6100.1*	Sartorius
Scales *LE623S*	Sartorius
Scanner CanoScan *8600F*	Canon
Shaker *PROMAX 2020*	Heidolph
Sonicator *Bioruptor®*	Diagenode
Sonicator *Bioruptor® Pico*	Diagenode
Spectrophotometer *DS-11*	DeNovix
Spectrophotometer *NanoDrop ND-1000*	PeqLab
Table centrifuge	Biozym
Thermal cycler *T100™*	Bio-Rad
Thermocycler *Biometra T-personal*	Biometra
Thermomixer *ThermoMixer® comfort*	Eppendorf
UV-transilluminator *Intas UV-System Gel Jet*	Intas Science Imaging Instruments
Vacuum pump	IBS Integra Biosciences
Vortex *Vortex-Genie 2*	Scientific Industries
Water bath	Memmert

3.1.16. Databases

Table 3.1.16: Databases used.

Database	Weblink	Utilization
cBioportal for cancer genomics	https://www.cbioportal.org/ (Cerami et al., 2012; Gao et al., 2013)	Database of genetic alterations in cancers
DNA Data Bank of Japan	https://www.ddbj.nig.ac.jp/index-e.html (Mashima et al., 2017)	Download of publicly available sequencing data
Enrichr	https://amp.pharm.mssm.edu/Enrichr/ (Chen et al., 2013; Kuleshov et al., 2016)	Identification of factors associated with submitted genomic regions
The Human Protein Atlas	https://www.proteinatlas.org/ENSG00000135679-MDM2/cell	Identification of protein localizations in cells
iGenomes by Illumina	https://emea.support.illumina.com/sequencing/sequencing_software/igenome.html	Download of the hg38 and dm6 reference genomes

Molecular Signature Database v7.0	https://www.gsea-msigdb.org/gsea/msigdb/index.jsp (Liberzon et al., 2011)	Usage of gene sets and gene ontology sets for GSEA analysis
NCBI	https://www.ncbi.nlm.nih.gov/	Literature search (PubMed), Primer design (Primer-BLAST), Protein sequence homology studies (Blastp)
NCBI's Gene Expression Omnibus (GEO)	https://www.ncbi.nlm.nih.gov/geo/query/acc.cgi	Download of publicly available sequencing data
SRA (NCBI)	https://www.ncbi.nlm.nih.gov/sra/	Download of publicly available sequencing data

3.1.17. Software

Table 3.1.17: Software used for data analysis.

Software	Supplier / Source
Adobe Photoshop CS	Adobe
BEDTOOLS/2.24	Quinlan and Hall, 2010
BOWTIE2/2.3.4.1	Langmead and Salzberg, 2012
Celigo Image Cytometer Software	Nexcelom
CFX Manager Software for qPCR cycler	Bio-Rad
DEEPTOOLS/3.0.1	Ramírez et al., 2016
DESeq2/1.26.0	Love et al., 2014
EnhancedVolcano/1.4.0	Blighe et al., 2019
FASTQC/0.11.4	Andrews et al., 2015
FASTX/0.0.4	Hannon, 2010
ggplots/3.3.0	Wickham, 2016
goseq/1.38.0	Young et al., 2010
gplots/3.0.3	Warnes et al., 2020
GraphPad Prism v5.04	GraphPad Software Inc.
GSEA/4.0.3	Subramanian et al., 2005
HTSEQ/0.6.1	Anders et al., 2015
Hypergeometric Optimization of Motif EnRichment (HOMER) v4.11.1	Heinz et al., 2010
Integrative Genomics Viewer (IGV) v2.3	Broad Institute of MIT and Harvard (Robinson et al., 2011, 2017; Thorvaldsdóttir et al., 2013)
ImageLab v5.2.1	Bio-Rad
INTAS lab ID	Intas Science Imaging Instruments
MACS2/2.1.2	Feng et al., 2012; Zhang et al., 2008
Microsoft® Office 2016	Microsoft
Miniconda3	Anaconda Inc.
NanoDrop Software	Peqlab
Ranking Of Super Enhancer (ROSE)	Lovén et al., 2013; Whyte et al., 2013

RColorBrewer/1.1.2	Neuwirth, 2014
R environment	https://cran.r-project.org/bin/windows/base/ (R Development Core Team 3.0.1., 2013)
R Studio Package Manager	https://rstudio.com/products/rstudio/download/ R Studio Team (RStudio Inc., Boston, 2019)
SAMTOOLS/1.9	Li et al., 2009
SRATOOLKIT/2.9.2	Leinonen et al., 2011; NCBI SRA Toolkit Development Team, 2020
STAR/2.7.3a	Dobin et al., 2013
UV imager software	Intas Science Imaging Instruments
Xshell® 6 for Home/School	https://www.filehorse.com/download-xshell-free/ NetSarang Computer Inc.

3.1.18. External sequencing data

Table 3.1.18: Sources of external sequencing data sets used.

Publication	Accession no. (GEO or DDBJ)	Condition
The ENCODE Project Consortium (Davis et al., 2018; Dunham et al., 2012)	GSM945853	ChIP-seq: H3K27ac, HCT116
	GSE86662	ChIP-seq: Input, HCT116
	GSM818826	ChIP-seq: H3K27ac, PANC-1
	GSM818828	ChIP-seq: Input, PANC-1
Illingworth et al., 2010	GSE21442	CAP-seq: CGI, hBlood CAP-seq: CGI, hCerebellum CAP-seq: CGI, hSperm
Sriraman et al., 2018	GSE113369	RNA-seq: 6 h Nutlin-3a, SJSA-1
Su et al., 2019	GSE131830	ChIP-seq: KDM2B, PC3 ChIP-seq: RNF2, PC3 ChIP-seq: Input, PC3
Suzuki et al., 2014	DRR016956	ChIP-seq: H3K27ac, H1299
	DRR016957	ChIP-seq: Input, H1299

3.2. Methods

3.2.1. Human tissue culture

Human adherent cancer cell lines were cultured under sterile conditions using the laminar flow *Hera Safe* (Heraeus) and kept in a humidified atmosphere at 37 °C and 5 % CO_2. Cells were passaged thrice a week, depending on their confluency. For this purpose, cells were washed with pre-warmed PBS before detaching them from culture dishes using 0.05 % trypsin (w/v) dissolved in 0.53 mM EDTA (0.05 % trypsin/EDTA, Invitrogen), incubated for 3-5 min at 37 °C. Detachment of cells was quenched by adding the respective cell culture medium to split them into new cell culture dishes. All cell lines were used until passage number 15 to 20.

3.2.2. Freezing and thawing of cells

For long-term storage, the cell lines were preserved in liquid nitrogen and thawed to replace cells that have reached the maximum passage number. For freezing, the cells were detached from culture dishes as previously described (section 3.2.1) and pelleted by centrifugation for 5 min, 600 rpm at RT. The cell pellet was resuspended in pre-cooled FBS containing 10 % DMSO and distributed into cyro tubes. The aliquots were stored at -80 °C for 24 h before transferring them to liquid nitrogen tanks. For thawing, the frozen cell aliquot was resolved in the respective pre-warmed medium and the medium was changed the next day to liberate cells from remaining DMSO.

3.2.3. Treatment of cells with inhibitors and cytokines

Pharmacological inhibitors used in this work were all dissolved in DMSO while sterile filtered 0.2 % BSA served as solvent for human recombinant cytokines. All dissolved components were aliquoted and stored according to manufacturer's instructions. Due to their low half-life and fast degradation, thawed cytokine aliquots were only used once, and remaining solution was discarded after use.

Cells were seeded at least 24 h prior to treatment. A stock solution of the desired concentration (table 3.2.1) was prepared by dissolving the respective component in pre-warmed cell culture media and distributed equally on cells. An equal dilution of the respective solvent served as treatment control in each experiment.

Table 3.2.1: Drug concentrations used for experiments.

Inhibitor	Concentration used	Solvent
CHX	2.5 µg/ml	water, st. f.
Human recombinant TNFα	10 ng/ml	0.2 % BSA, st. f.
Human recombinant TRAIL	20 ng/ml	0.2 % BSA, st. f.
Idasanutlin	1 µM	DMSO
MG-132	20 µM	DMSO
Nutlin-3a	20 µM	DMSO

3.2.4. Preparation of plasmid DNA from *E. coli*

3.2.4.1. Bacterial transformation

To expand expression plasmids (table 3.1.8) in the chemically competent *Escherichia coli (E. coli)* strain DH10B^{TM}, 50 µl *E. coli* were incubated with 1 µl vector DNA for 30 min at 4°C, followed by a heat pulse for 10 min at 37°C and another cool down for 10 min at 4°C. *E. coli* subsequently recovered in 200 µl 2x YT medium for 1 h at 37°C and agitation. Successfully transformed bacteria were selected by plating on LB agar containing either 100 µg/ml Ampicillin or 50 µg/ml Kanamycin, depending on the antibiotic resistance inserted into the plasmid. The next day, one bacterial clone was picked and expanded overnight in 2xYT medium containing the respective antibiotic.

3.2.4.2. Isolation of vector DNA from E. coli

Isolation of plasmid DNA from cultured *E. coli* was achieved by using the *PureYield Plasmid Midiprep System* (Promega) according to manufacturer's instructions. Isolated vector DNA was eluted in 500 µl nuclease-free water and its concentration was determined using the spectrophotometer *NanoDrop ND-1000*.

3.2.4.3. Transient transfection of human cancer cells with plasmid DNA

Transient, exogenous expression of proteins was achieved by forward transfection of human cancer cells with plasmid DNA using Lipofectamine (LPF) transfectants. Cells were seeded the day before transfection according to the instructions below (table 3.2.2).

Table 3.2.2: Cell numbers seeded for forward transfection.

Cell line	Transfectant	Plate format	Cells seeded
H1299	LPF 2000	10 cm dish	500,000 – 600,000
		6-well plate	160,000 – 300,000

The transfection mix was composed of two pre-solutions (A and B) that were prepared in DMEM without supplements (DMEM (-), table 3.2.3). After 5 min incubation at RT, solution A and B were mixed in a 1:1 ratio and incubated for 20 min at RT to form lipid-DNA-vesicles. This transfection mix was then added to pre-seeded cells and incubated for 4-6 h at 37 °C before medium change. The cells were harvested 24 h or 48 h post transfection respectively and subjected to further analyses.

Table 3.2.3: Composition of transfection mixes for plasmid transfection.

Plate format	Solution A	Solution B	Final volume in plate
10 cm dish	12 µg DNA + 5 µl P3000 (for transfection with LPF3000) add 1000 µl using DMEM (-)	1000 µl DMEM (-) + 30 µl LPF 2000/ LPF3000	12 ml
6-well plate	2.4 µg DNA + 5 µl P3000 (for transfection with LFP3000) add 200 µl using DMEM (-)	200 µl DMEM (-) + 6 µl LPF 2000/ LPF3000	2.4 ml

3.2.5. Transient knockdown of proteins using small interfering RNA

Transient depletion of proteins was achieved by insertion of small interfering RNA (siRNA) into cells, targeting the mRNA of the protein of interest and inducing its degradation (Dana et al., 2017). An siRNA pool was used for protein knockdown prepared by mixing equal volumes of the 50 µM stock solutions of each siRNA targeting the same protein (table 3.1.7). In order for cells to take them up, a transfection mix was prepared as previously described using the following composition of solutions A and B (table 3.2.4).

Table 3.2.4: Composition of transfection mixes for reverse siRNA transfection.

Solution A	Solution B	Transfection composition	Final siRNA conc in well
249 µl DMEM (-) 0.5 µl pool 1 0.5 µl pool 2	245 µl DMEM (-) 5 µl LPF3000	per 6-well: 500 µl sol. A+B mix, total volume (including cells): 2.5 ml	10 nM
		per 96-well: 50 µl sol. A+B mix, total volume (including cells): 150 µl	16.6 nM

For reverse transfection, the cells were detached as described in section 3.2.1 and their concentration was determined using a hemocytometer. The required cell number (table 3.2.5) was seeded and incubated with the transfection mix for 24 h before changing the medium.

After a total incubation time of 48 – 72 h, the cells were harvested and subjected to further analyses.

Table 3.2.5: Cell numbers seeded for reverse transfection.

Cell line	Harvest post transfection start	Plate format	Cells seeded
HCT116	48 h	6-well	200,000
H1299	72 h	6-well	80,000
		96-well	2,600
PANC-1	72 h	6-well	120,000
		96-well	2,500

3.2.6. Immunoblot analysis

For analyzing protein levels in cells, proteins were separated by SDS-Polyacrylamide gel electrophoresis (SDS-PAGE), a method first described by Shapiro and colleagues in 1967 (Shapiro et al., 1967). However, the protocol used was based on the description of immunoblot analysis published by Klusmann et al. in 2016 (Klusmann et al., 2016).

3.2.6.1. Protein extraction from cells

To avoid protein degradation, protein extraction was performed on ice using pre-cooled solutions. Adherent cells were washed twice with cold PBS. In the presence of apoptotic cells, remaining adherent cells were scraped from wells, pelleted for 5 min, 3000 rpm at 4 °C and washed twice with cold PBS. Upon washing, the cells were lysed in cell lysis buffer for protein harvest and the crude lysates were solubilized for 10 min at 4 °C using the *Bioruptor*® sonication device. Relative protein concentrations were determined colorimetrically using the ability of bicinchroninic acid (BCA) to form stable purple complexes with Cu^{1+} ions deriving from the reduction of Cu^{2+} by present proteins (Smith et al., 1985). For BCA measurements, the Pierce BCA protein assay kit (Thermo Scientific) was used according to manufacturer's instructions and colorimetric measurements were performed using the spectrophotometer *DS-11*.

3.2.6.2. SDS-PAGE and immunoblot analysis

To ensure comparable migration of proteins of all sizes towards the anode upon application of an electric field, proteins had to be denaturized in the presence of the anionic detergent sodium dodecyl sulfate (SDS) to establish a negative charge. For this purpose, harvested proteins were boiled for 5 min at 95 °C in the presence of 1x diluted Laemmli buffer.

Separation of proteins was achieved by loading 30 – 50 µg protein (depending on the previous treatment of cells and expression levels of the protein of interest) onto polyacrylamide gels for

electrophoresis. The gels used consisted of two parts, a stacking and a resolving gel (table 3.2.6) that are characterized by different pore sizes and functionalities. The stacking gel exhibits large pores and serves protein stacking prior to separation. Upon application of an electric field, a migrating electric front is established by leading chloride-ions present in casted gels moving towards the anode and trailing glycinate ions originating from the surrounding 1x SDS-running buffer. Loaded proteins are caught by this migrating front, leading to their stacking into thin layers (National Diagnostics, 2010). Further migration of proteins into the resolving gel separates them by size and electrophoretic mobility due to smaller pore sizes. Low range proteins (10-120 kDa) were separated on 12 % acrylamide-bisacrylamide gels run for 3-4 h at 100-120 V while for high range protein electrophoreses (> 120 kDa), 6-10 % gels were used that run for 5 h at 50-60 V.

Table 3.2.6: Composition of gels used for protein electrophoresis.

Component	Stacking gel	Resolving gel
12 % gels		
Acrylamide-bisacrylamide	5 %	12 %
1 M Tris-HCl, pH 6.8	125 mM	-
1.5 M Tris-HCl, pH 8.8	-	378 mM
SDS	0.1 %	0.1 %
APS	0.1 %	0.06 %
TEMED	0.2 %	0.06 %
10 % gels		
Acrylamide-bisacrylamide	5 %	10 %
1 M Tris-HCl, pH 6.8	125 mM	-
1.5 M Tris-HCl, pH 8.8	-	378 mM
SDS	0.1 %	0.1 %
APS	0.1 %	0.06 %
TEMED	0.2 %	0.13 %
6 % gels		
Acrylamide-bisacrylamide	5%	6 %
1 M Tris-HCl, pH 6.8	125 mM	-
1.5 M Tris-HCl, pH 8.8	-	303 mM
SDS	0.1 %	0.1 %
APS	0.1 %	0.1 %
TEMED	0.2 %	0.08 %

Proteins separated using 10 % and 12 % gels were blotted for 3 h at 90 V and 4 °C onto a 0.2 µm nitrocellulose membrane while high range proteins from 6 % gels were blotted onto a PVDF membrane pre-wet in MetOH for 16 h at 25 V and 4°C using the respective transfer buffers. For both protein transfers, a sandwich of Whatman paper and sponges within two plastic holders was prepared to place the gel on the membrane. Blotting efficiency was checked by incubating the membrane with protein-binding Ponceau-S solution for 5 min at RT

that was washed off using 1 % acetic acid. Unspecific epitopes were blocked using 5 % (w/v) milk in TBS containing 1 % Tween-20 (5 % milk/TBS-T) for 1 h at RT before incubating the membrane with primary antibodies overnight at 4°C.

The next day, non-bound primary antibodies were washed off at RT using 5 % milk/TBS-T thrice for 10 min each. Primary antibodies were subsequently labeled with HPR-coupled secondary antibodies for 1 h at RT and non-bound secondary antibodies were washed off. Signal detection was achieved by incubating membranes with *Immobilon Western Chemoluminescent HRP Substrate* for strong protein signals and SuperSignal *West Femto Maximum Sensitivity Substrate* for weak ones. Membranes were imaged using the chemiluminescence imagers *ChemiDoc XRS+* (Bio-Rad) and *Chemocam HR 16 3200* (intas Scientific Imaging Instruments). Analysis of signals was carried out using the *ImageLab* (Bio-Rad) and *Photoshop CS* (Adobe) software.

3.2.7. Quantitative reverse-transcription polymerase chain reaction

3.2.7.1. RNA isolation from cells

Gene expression analysis was performed using reverse transcription of RNA extracted from cells followed by quantitative polymerase chain reaction (qRT-PCR). To harvest RNA, cells were lysed in 1 ml phenol-containing TRIzol™ reagent and incubated for 5-10 min at RT. At this point, RNA samples were either stored at -80°C or processed directly.

RNA isolation was achieved by phenol-chloroform extraction, based on the principles described by Chomczynski and Sacchi (Chomczynski and Sacchi, 1987). For this purpose, 200 µl chloroform were added to 1 ml TRIzol™ cell lysates and mixed. Phase-separation was achieved by centrifugation for at least 30 min at 12,000 g and 4°C and the RNA-containing aqueous phase was transferred to another tube. RNA was precipitated by adding an equal volume of isopropanol and incubation at -80°C overnight. Precipitated RNA was pelleted by centrifugation for at least 1 h at 12,000 g and 4°C and washed twice with 1 ml 75 % EtOH, followed by re-pelleting the RNA for 10 min at 7,600 g and 4°C. Washed RNA was dried for several minutes at 37°C and dissolved in 15-20 µl nuclease-free water. To improve RNA dissolving, samples were incubated at 55°C twice for 3 min each. Quality and quantity of isolated RNA were determined based on absorbance values at 230 nm (organic solvents), 260 nm (nucleic acids) and 280 nm (proteins and phenol) using the *NanoDrop* device.

3.2.7.2. Reverse transcription

For reverse transcription (RT) of RNA into complementary DNA (cDNA), 1 µg RNA was incubated with pre-cDNA-synthesis mix (total volume: 16 µl) for 5 min at 70°C, lid temperature 96 °C. After that, 4 µl of a mix containing the Moloney Murine Leukemia Virus (M-MuLV) reverse transcriptase was added.

Table 3.2.7: Reaction mixes required for cDNA synthesis.

Solution	Composition (per reaction)
Pre-cDNA-synthesis mix	1 µg RNA 2 µl mixed primer 4 µl dNTP mix, 2.5 mM add 16 µl total volume using nuclease-free H_2O
Reverse transcriptase mix	2 µl 10x M-MuLV reverse transcriptase reaction buffer 0.25 µl RNAse inhibitor 0.125µl M-MuLV reverse transcriptase 1.625 µl nuclease-free H_2O

Reverse transcription was carried out for 1 h at 42°C, followed by a final heating for 5 min at 95°C, lid temperature 99 °C.

3.2.7.3. Quantitative polymerase chain reaction

Gene expression analysis was carried out using quantitative polymerase chain reactions (qPCR) in which the amount of DNA amplified during PCR cycles is quantified using a fluorescent dye binding to double-stranded, synthesized DNA (Higuchi et al., 1993). In contrast to the mentioned reference, SYBR Green was used as DNA-binding dye within qPCR reactions.

Synthesized cDNA was diluted 1:10 in nuclease-free water and subsequently subjected to qPCR analysis. The composition of the reaction mix and the amplification protocol used for qPCR are depicted in table 3.2.8 and 3.2.9. Sequences of primers used for gene expression studies are listed in table 3.1.12.

Table 3.2.8: Reaction mixes for qPCR analysis

Solution	Composition (per reaction)
qPCR reaction mix	5 µl cDNA (1:10 diluted) 1x self-made 2x qPCR master mix 0.2 µM forward primer 0.2 µM reverse primer in H_2O

Table 3.2.9: qPCR protocol for gene expression analysis.

Step	Temperature [°C]	Time
1	95	2 min
2	95	15 s
3	60	30 s
4	Fluorescence read	
Back to step 2, 39 times more		
5	Melting curve, 55-95 °C	

All qPCR reactions were performed in triplicates for each biological replicate. Gene expression was subsequently calculated using the $2^{-\Delta\Delta Ct}$ method (Livak and Schmittgen, 2001).

3.2.8. RNA sequencing

3.2.8.1. Sample preparation

Samples for total RNA sequencing (RNA-seq) were prepared as described in section 3.2.7.1. Quality and quantity checks of RNA samples, RNA sequencing library preparation and single-end next-generation sequencing were carried out by the NGS service facility for Integrative Genomics / Institute of Human Genetics Göttingen.

3.2.8.2. RNA sequencing data analysis

For sequencing data analysis, the high-performance computing cluster provided by the Gesellschaft für wisenschaftliche Datenverarbeitung mbH Göttingen (GWDG) and the R environment for statistical computation were used.

External sequencing data (table 3.1.18) was downloaded from the sequence read archive (SRA) using the SRATOOLKIT/2.9.2 and converted into raw sequencing files (.fastq files) using its fastq-dump command. Own raw data and external RNA sequencing experiments were subjected to quality control using FASTQC/0.11.4. If required, raw reads were trimmed using FASTX/0.0.14. The reads were mapped to the hg38 STAR index that was kindly provided by Xin Wang, Clinic for General, Visceral and Pediatric Surgery Göttingen using STAR/2.7.3a to obtain a BAM file sorted by coordinates without strand-specification. The read counts mapped to hg38 reference genes were obtained using HTSEQ/0.6.1 using --stranded=no function.

Differential gene expression analysis was subsequently performed in the R environment using DESeq2/1.26.0. DESeq2 results were visualized as volcano plots and heatmaps using following R packages: EnhancedVolcano/1.4.0, goseq/1.38.0, RColorBrewer/1.1.2, gplots/3.0.3, ggplot2/3.3.0.

Normalized count files generated by DESeq2 were used to carry out gene set enrichment analysis (GSEA) and gene ontology (GO term) analysis using the GSEA tool/4.0.3 along with the C2 curated gene sets and the C5 GO gene sets provided by the Molecular Signature Database v7.0. To ensure that the results obtained from GSEA and GO term analyses are reliable, the genes were pre-filtered based on their normalized counts. In this context, genes exhibiting a normalized count ≥ 30 in at least one sample across all conditions tested were considered to be truly expressed in cells and included in GSEA and GO term analyses.

3.2.9. Chromatin-immunoprecipitation

Chromatin-immunoprecipitation (ChIP) was used to study the binding pattern of a protein of interest to chromatin. The protocol used was based on the ChIP procedure published by Denissov and colleagues (Denissov et al., 2007) with modifications based on the publication by Sen et al. (Najafova et al., 2017; Sen et al., 2019).

3.2.9.1. Crosslinking and chromatin harvest

Cells were seeded at least 24 h prior to ChIP. The cell numbers seeded were chosen depending on the type and duration of treatment prior to ChIP and are listed in table 3.2.10.

Table 3.2.10: Cell numbers seeded for ChIP depending on the respective treatment.

Cell line	Treatment time	Treatment	Cells seeded	Plate format
SJSA-1	4 h	20 µM MG-132	1,000,000	15 cm
	4 h, 6 h	20 µM Nutlin-3a		
	15 h	20 µM Nutlin-3a; DMSO control	1,200,000 1,000,000	
HCT116	4 h	20 µM MG-132		10 cm
H1299	48 h + 4 h	Plasmid expression (seeding + 24 h transfection)+ 20 µM MG-132	600,000 – 900,000	10 cm
PANC-1	-	-	2,500,000	15 cm

To avoid quenching of the crosslinking reaction through components of the cell culture media, the cells were washed twice with 1x PBS at RT prior to crosslinking. To enable detection of proteins that do not directly bind to chromatin but rather interact with a chromatin-binding partner protein, the cells were incubated with protein-protein crosslinking buffer for 40 min at RT. Crosslinked protein complexes were subsequently fixed on chromatin by incubation with formaldehyde-containing protein-DNA crosslinking buffer for 30 min at RT. Importantly, there were no washing steps between both crosslinking methods. The protein-DNA crosslinking was quenched by adding glycine to a final concentration of 125 mM for 5 min at RT.

From now on, chromatin harvest and the subsequent immunoprecipitation were continued on ice using pre-cooled solutions to prevent protein degradation. Upon crosslinking, the cells were washed twice using 1x PBS to remove remaining crosslinking solutions and incubated with Buffer B for 10 min at 4°C to lyse plasma membranes. The released cell nuclei were carefully scraped from cell culture dishes, centrifuged for 5 min at 1600 rpm and 4°C, washed in 2 ml Buffer C and re-pelleted for 10 min at the same speed and temperature.

3.2.9.2. Chromatin shearing

Pelleted nuclei were resuspended in shearing buffer to perforate nuclear membranes and fragment DNA using ultrasound-mediated sonication. Since the SDS concentration within the shearing buffer is a critical parameter affecting the efficiency of the immunoprecipitation (IP), we used different shearing buffers depending on the antibodies used for IP (tale 3.2.11).

Table 3.2.11: Shearing buffer compositions.

Shearing buffer	Composition (per ml)	Used for
0.375 % SDS	1x incubation buffer with SDS 1x proteasome inhibitor cocktail, EDTA-free (Roche) 22.5 µl 10% SDS in H_2O	Fig. 4.1 Fig. 4.2 Fig. 4.3
0.225 % SDS	1x incubation buffer without SDS 1x proteasome inhibitor cocktail, EDTA-free (Roche) 22.5 µl 10% SDS in H_2O	Fig. 4.8 Fig. 4.10
0.1 % SDS	1x incubation buffer without SDS 1x proteasome inhibitor cocktail, EDTA-free (Roche) 10 µl 10% SDS in H_2O	Fig. 4.7 Fig. 4.9 Fig. 4.11 Fig. 4.13

Shearing was performed using a Bioruptor ® Pico with corresponding 1.5 ml Bioruptor ® Microtubes (Diagenode). The volume of shearing buffer used for resuspension of the nuclear pellet and the cycle numbers used for DNA fragmentation highly depended on the cell line, cell number and shearing buffer used. Table 3.2.12 summarizes all shearing conditions used.

Table 3.2.12: Shearing conditions used

Cell line	Shearing buffer		Cycle number (30 sec on, 30 sec off)
	Composition	Volume	
SJSA-1	0.375 % SDS	300 µl / 15 cm plate	15
	0.225 % SDS	300 µl / 15 cm plate	15
	0.1 % SDS	300 µl / 15 cm plate	20
HCT116	0.375 % SDS	600 µl / 10 cm plate	20

H1299	0.375 % SDS	300 µl / 10 cm plate	15
	0.225 % SDS	300 µl / 10 cm plate	15
	0.1 % SDS	600 µl / 10 cm plate	20
PANC-1	0.375 % SDS	900 µl / 15 cm plate	25

Upon shearing, remaining cell debris were pelleted by centrifugation for 5 min at 13,000 rpm and 4°C. Clear chromatin supernatant was transferred into a new tube and further diluted up to a maximum of 500-700 µl chromatin per plate with exception for PANC-1 cells that needed even higher dilutions for shearing.

3.2.9.3. Chromatin-immunoprecipitation

To precipitate DNA associated with the protein of interest, harvested chromatin was incubated with an antibody raised against the desired target and protein A/G agarose beads binding to antibodies. Prior to IP, protein A/G agarose beads were washed twice using bead wash buffer (1x incubation buffer without SDS with 0.2 % BSA) and subsequently resuspended in half of the initial bead volume to obtain 50 % slurry beads. Precipitation reactions for ChIP-qPCR and ChIP-seq experiments without external spike-in controls consist of 120 µl harvested chromatin, 30 µl of 50 % slurry beads and 2 µg of the antibody of interest (table 3.1.11). Each reaction was filled up to a final volume of 300 µl using an IP master mix solution (1x incubation buffer without SDS, 0.1% BSA and 1x diluted EDTA-free proteasome inhibitor cocktail (Roche)) and incubated on a rotator at 4 °C overnight. Input chromatin samples of 12 µl were taken and stored at 4 °C.

For ChIP experiments using *Drosophila melanogaster* chromatin as an external spike-in reference (Active Motif), the composition of ChIP reactions slightly varied. *D. melanogaster* spike-in chromatin was added to the experimental chromatin pool prior to IP in a fixed ratio of 20 ng *D. melanogaster* chromatin per 25 µg experimental chromatin (Active Motif). To obtain DNA concentrations of experimental chromatin, a small aliquot was taken and incubated with 0.2 µg/ml RNAse A for 30 min at 37 °C and 800 rpm shaking. The DNA was subsequently decrosslinked in 1x diluted decrosslinking buffer supplemented with 0.2 mg/ml proteinase K for 2 h at 65 °C and 800 rpm shaking. DNA isolation was performed using the MinElute PCR Purification Kit (Qiagen) according to manufacturer's instructions. The DNA concentration was determined using the *NanoDrop* device and the spike-in chromatin was added to the experimental chromatin accordingly. IP reactions were composed of 25 µg of experimental chromatin, 20 ng of *D. melanogaster* chromatin, 30 µl of 50 % slurry beads, 5 µg of the antibody of interest and 2 µg of the spike-in antibody targeting the *Drosophila*-specific histone variant H2Av (Active Motif). The total volume of IP reactions varied depending on the concentration of experimental chromatin but the proportion of BSA, proteasome inhibitors and 1x diluted

incubation buffer without SDS were kept the same as previously described. Due to the high volume of chromatin per IP, only 1/100 of the chromatin volume used per IP was kept as input at 4 °C.

Upon overnight incubation, the IPs were washed the next day using washbuffer 1 twice, once using washbuffer 2, once using washbuffer 3 and twice using washbuffer 4 again. For this purpose, 400 µl washbuffer were added to each reaction, the tubes were inverted 16 times and the beads were subsequently pelleted by centrifugation for 2 min at 4000 rpm and 4°C. After washing, the beads were aspirated entirely and subjected to decrosslinking.

3.2.9.4. Decrosslinking and DNA isolation

Decrosslinking of ChIP samples and subsequent DNA isolation were performed at RT to avoid precipitation of SDS present in decrosslinking solutions. Importantly, input samples were included from this step on to ensure equal treatment of all samples.

Within this work, we have used two different protocols for decrosslinking. In ChIP experiments of Fig. 4.1-3, the washed beads and the respective inputs were incubated with 200 µl elution buffer on a rotator for 20 min at RT to disrupt bead-antibody interactions. The beads were briefly pelleted for 1 min at maximum speed and the supernatant was transferred into new tubes. Decrosslinking of DNA and proteins was achieved by incubation of samples with 200 mM NaCl for 4-5 h at 65 °C and 1100 rpm shaking. In all other experiments, the RNA within samples was degraded by incubation of beads and inputs with 0.2 µg/ml RNAse A for 30 min at 37 °C and 800 rpm shaking. Following this, the samples were incubated in 1x decrosslinking buffer complemented with 0.2 mg/ml proteinase K overnight at 65 °C and 800 rpm shaking to remove the DNA-protein crosslinking. The following day, the beads were pelleted for 2 min at 2,000 g and the supernatant was transferred into new tubes. Remaining DNA was eluted from beads by resuspending them in 100 µl 10 mM Tris-HCl p 8.0. Upon incubation for 10 min at 65 °C and 800 rpm shaking, the beads were re-pelleted for 5 min at 2,000 g and the supernatant was added to the remaining samples.

Regardless of the decrosslinking method used, the DNA isolation from samples was performed using the MinElute PCR Purification Kit (Qiagen) according to manufacturer's instructions.

3.2.9.5. Analysis of ChIP experiments using qPCR

The occupancy of a certain factor on chromatin was determined using qPCR. With exception of input samples deriving from ChIP experiments with external spike-in references, the input DNA was diluted 1:10 prior to qPCR. Since qPCR signals of ChIP DNA are generally quite low, the more potent, commercially available 2x Maxima SYBR Green master mix (Thermo Scientific) was used. The composition of the reaction mix and the thermocycler protocol used

for qPCR are depicted in table 3.2.13 and 3.2.14. Sequences of primers used for chromatin binding studies are listed in table 3.1.12.

Table 3.2.13: Reaction mixes for ChIP-qPCR analysis

Solution	Composition (per reaction)
ChIP-qPCR reaction mix	5 µl ChIP DNA / 1:10 diluted input DNA 1x Maxima SYBR Green master mix 0.4 µM forward primer 0.4 µM reverse primer in H_2O

Table 3.2.14: qPCR protocol for ChIP-qPCR analysis.

Step	Temperature [°C]	Time
1	95	10 min
2	95	15 s
3	60	60 s
4	Fluorescence read	
Back to step 2, 39 times more		
5	Melting curve, 50-95 °C	

3.2.10. ChIP sequencing

DNA isolated from ChIP experiments was also subjected to next-generation sequencing (ChIP-seq). For this purpose, single-end DNA-sequencing libraries were prepared from ChIP-DNA and submitted to the NGS service facility for Integrative Genomics / Institute of Human Genetics Göttingen to perform next-generation sequencing on a HiSeq4000 system (Illumina).

3.2.10.1. ChIP-seq library preparation

Prior to ChIP-seq library preparation, the concentration of ChIP-DNA was determined using the Qubit™ dsDNA High Sensitivity Assay Kit (Thermo Scientific) according to manufacturer's instructions.

Following this, ChIP-DNA libraries were prepared using the KAPA Hyper Prep Kit with the corresponding KAPA SI Adapter Kit Set A+B and KAPA AMP Pure beads (Roche). Due to non-detectable DNA concentrations for the first ChIP-seq approach (Fig. 4.2), 50 µl of each sample were used for library preparation, irrespective of its concentration. In contrast, library preparation of the quantitative ChIP-seq (Fig. 4.13) was performed using 1 ng input DNA of each sample. Each step of the library preparation was performed according to manufacturer's instructions. In short, isolated DNA fragments were subjected to a one-step end-repair and dA-tailing reaction to obtain blunt-ended DNA fragments exhibiting a 5' phosphorylation and a 3' dA-tail. These modifications enable the subsequent adapter ligation that is followed by a post-

ligation cleanup step to remove non-ligated excess adapters and adapter dimers. Following this, library fragments were amplified using PCR and excess primers were removed from samples using another post-amplification cleanup step. Finally, the library samples were filtered for fragments of the desired size (250-350 bp) using double-sided size selection.

Upon preparation, the average fragment size of each library sample was determined using the Bioanalyzer 2100 with the corresponding High Sensitivity DNA Analysis Kit (Agilent Technologies) and its concentration was measured using the Qubit™ device as previously described. Based on the average fragment size and the library DNA concentration, the ChIP-seq libraries were diluted to a final concentration of 2 nmol/L. These diluted samples were then mixed in equal ratios to obtain sequencing pools that were submitted for sequencing.

3.2.10.2. Analysis of ChIP-seq data without spike-in references

For ChIP-seq data analysis, the same platforms were used as for RNA-seq data. Again, download of external data (table 3.1.18) as well as its conversion into FASTQ files was achieved using the SRATOOLKIT/2.9.2 and the additional --split-files setting to obtain two separate files for paired-end read files. Quality control and trimming of raw data were performed as already described in section 3.2.8.2. Trimmed raw data files were mapped to the human UCSC hg38 reference genome (iGenomes Illumina) using BOWTIE2/2.3.4.1 with --very-sensitive end-to-end setting. In case of paired-end sequencing data, both complementary FASTQ files were used for mapping, resulting in one common SAM file. SAM files were further processed using SAMTOOLS/1.9. At first, SAM files were converted into BAM files using samtools view and, if present, sequencing replicates were then merged to one file using samtools merge.

Single-end sequencing data was subsequently sorted by coordinates using samtools sort and PCR duplicates were removed by samtools markdup taking an estimated fragment length of 200 bp for external data and the previously determined fragment length for own data. Paired-end data had to be processed differently to be able to remove PCR duplicates. In this case, converted BAM files were first sorted by the respective read name using samtools sort with additional -n setting. The corresponding mate score for each read pair was then calculated by samtools fixmate. The resulting file was subsequently re-sorted by coordinates and PCR duplicates were removed as described for single-end sequencing data. Upon removal of PCR duplicates, index files corresponding to the resulted BAM files were generated using samtools index.

The generated BAM files and their corresponding index files served as input for further computations. To identify binding sites for a factor of interest, peaks were called using MACS2/2.1.2. Since the signal of some factors was very low in certain systems, peak calling

was performed without using an input reference file in special cases. Furthermore, non-specific binding sites inadvertently called as peaks had to be filtered out based on peak scores in some cases. Hence the table 3.2.15 provides an overview of all settings used and filters applied to generate peak files.

Table 3.2.15: Settings used for peak calling

Factor	Cell	Settings	Threshold filtering based on peak score
MDM2	SJSA-1	-nomodel, --broad, --broad-cutoff 0.05, --max-gap 200	Peak score ≥ 39
	HCT116	-nomodel, --broad, --broad-cutoff 0.1, --max-gap 300, --fe-cutoff 0.3	No additional filtering
	H1299	-nomodel, --broad, --broad-cutoff 0.1, --max-gap 300, --fe-cutoff 0.3 peak calling without reference file	No additional filtering
	PANC-1	-nomodel. --broad, --broad-cutoff 0.1, --max-gap 300, --fe-cutoff 0.3, peak calling without reference file	Overlap with SJSA-1 peaks (at least 1 bp)
H3K27ac	SJSA-1	-nomodel, --broad, --broad-cutoff 0.05, --max-gap 50	Peak score ≥ 30
	HCT116	-nomodel, --broad, --broad-cutoff 0.05, --max-gap 200	Peak score ≥ 20
	H1299	-nomodel, --broad, --broad-vutoff 0.05, --max-gap 100	Peak score ≥ 30
	PANC-1	-nomodel, --broad, --broad-cutoff 0.05, --max-gap 200	Peak score ≥ 20
CGI	blood	-nomodel. --broad, --broad-cutoff 0.05, --max-gap 200 peak calling without reference file	No additional filtering
	cerebellum	-nomodel. --broad, --broad-cutoff 0.05, --max-gap 200 peak calling without reference file	No additional filtering
	sperm	-nomodel. --broad, --broad-cutoff 0.05, --max-gap 200 peak calling without reference file	No additional filtering

The resulting peak coordinate files (BED files) were intersected with other coordinate files using the intersectBed and subtractBed functions of BEDTOOLS/2.24. Called H3K27ac peaks were used as input file for super enhancer calling using the Ranking Of Super Enhancer (ROSE) algorithm. To identify these regions, a minimum distance of at least 2500 bp to annotated hg38 TSS was set as a requirement.

The package DEEPTOOLS/3.0.1 was used to visualize aligned sequencing data. ChIP-seq track (BIGWIG) files were computed using bamCoverage with an average read extension of 200 bp for external data and the respective fragment length minus 120 bp for own data. This

subtraction excludes bases added through the ligation of sequencing adapters, thus reflecting the actual length of the isolated DNA fragment. Additional settings used for BIGWIG file computation were --ignoreDuplicate, --smoothLength 60, --binSize 20 and --normalizeUsing RPKM. Computed ChIP-seq tracks were visualized using the Integrative Genomics Viewer (IGV) v2.3.

Matrices used as input files to generate heatmaps and aggregate plots of ChIP-seq data were generated using computeMatrix. The settings used to compute matrices varied depending on the intended application, but a bin size of 50 was commonly used in all cases. Visualization of computed matrices as heatmaps was achieved using plotHeatmap, while aggregate plots were generated using plotProfile.

The comprehensive gene set enrichment analysis web server Enrichr was used to identify factors associated with called peak regions. Furthermore, transcription factor consensus sites enriched in the regions of interest were determined using the Hypergeometric Optimization of Motif EnRichment (HOMER) analysis software version v4.11.1.

3.2.10.3. Analysis of ChIP-seq data with additional spike-in references

To monitor global changes of ChIP-seq signals, normalization factors were calculated to adjust samples to each other based on the number of reads mapped to the *Drosophila melanogaster* genome. For this purpose, trimmed raw data of experiments using *D. melanogaster* chromatin as external spike-in reference were mapped to the dm6 reference genome (iGenomes, Illumina) to obtain SAM files of dm6 aligned reads. The subsequent conversion into BAM files, merging of technical replicates, sorting and PCR duplicate removal were performed as previously described for hg38-aligned data. The number of de-duplicated reads mapped to the dm6 reference genome were determined using the samtools flagstat function of the SAMTOOLS/1.9 package.

The normalization factors required to adjust samples to each other in later analyses were calculated based on the determined dm6-aligned reads according to the kit manufacturer's instructions (Active Motif). The calculation of those factors varied depending on whether the tool that should be used for further analysis multiplies or divides by normalization factors. For tools multiplying by normalization factors such as bamCoverage, the factors were calculated as (# dm6 reads sample / smallest # dm6 reads of all samples compared) and vice versa for tools dividing through normalization factors such as DESeq2.

To visualize global changes in ChIP-seq results, the resulting normalization factors were included into BIGWIG computations using the --scaleFactor function of bamCoverage. Track files derived from single technical replicates were merged for visualization in IGV using bigwigCompare with the --operation add setting.

Furthermore, differential binding analysis was performed using a DESeq2 script for R provided by Dr. Michael Lidschreiber, Department of Molecular Biology, Max-Planck-Institute of Biophysical Chemistry Göttingen. To run DESeq2 analysis, the mapped read counts within a region of interest were determined using HTSEQ/0.6.1. Following this, a DESeq2 data set was created containing the conditions that should be compared and their respective read counts. To analyze global changes in binding patterns, the normalization factors that are automatically calculated by DESeq2 were replaced by the ones that were previously calculated. With these new normalization factors, DESeq2 was run to identify differentially bound regions and the results were displayed as MA plots.

3.2.11. Complex-immunoprecipitation

Complex-immunoprecipitation (Co-IP) was performed to check for potential protein-protein interactions. Co-IPs were all performed by Antje Dickmanns, Institute of Molecular Oncology, University Medical Center Göttingen and the protocol used was based on the Co-IP procedure described by Wienken and colleagues (Wienken et al., 2016).

3.2.11.1. Protein harvest

Co-IPs of endogenous proteins were performed in SJSA-1 cells using one confluent 15 cm plate per antibody. In contrast, Co-IPs of proteins that were exogenously expressed in H1299 cells were done using one confluent 6-well per condition per antibody. In general, cells were always pre-treated with 20 µM MG-132 for 4 h prior to elevate protein levels prior to Co-IP.

Upon treatment, the cells were washed twice using 1x cold PBS and subsequently lysed using 500 µl Co-IP buffer supplemented with 1x diluted proteinase inhibitor cocktail (Roche) per 6-well. The cell lysates were scraped from cell culture dishes and transferred to a 50 ml reaction tube where all lysates of one condition were pooled. Within this tube, the cell lysates were homogenized by pushing them five times through a 26 G syringe. These homogenized lysates were then divided into 1.5 ml aliquots for sonication-mediated breakdown of protein-DNA interactions. The sonication was carried out using a *Bioruptor*® sonication devicce for 10 min at medium power and cell debris were subsequently pelleted for 10-15 min at 13,000 rpm and 4 °C. The clear cell lysates were pooled in one tube per condition while the cell debris pellet was lysed in 100 µl cell lysis buffer for protein harvest with 50 µl 6x Laemmli buffer to check for protein solubility later on.

3.2.11.2. Pre-clearing and immunoprecipitation

Prior to IP, the harvested cell lysates were pre-cleared to remove components that are non-specifically binding to sepharose beads. For this purpose, the required volume of beads was equilibrated. The type of beads used depended on the antibody used for IP. While protein-G-sepharose beads were used for monoclonal antibodies, protein-A-sepharose was used for polyclonal ones. To equilibrate beads, 100 µl 20/80 slurry beads were taken per IP and pelleted for 2 min at 3000 rpm and 4 °C. The pelleted beads were washed in 800 µl Co-IP buffer supplemented with protease inhibitors and re-pelleted again. This washing step was repeated three times in total before diluting the beads to their initial volume using Co-IP buffer supplemented with protease inhibitors. Upon washing, 300 µl beads were added to the pooled cell lysates and incubated on a rotator for at least 1 h at 4 °C. Then, the samples were centrifuged for 4 min at 3000 rpm and 4°C to pellet beads and the pre-cleared lysates were collected. 50 µl of each lysate were taken as an input control prior to IP, mixed with 50 µl 6x Laemmli buffer and boiled for 5 min at 95 °C. The remaining volume was equally distributed to 1.5 ml reaction tubes to perform IP reactions. For this purpose, 2-3 µg of the antibody of interest were added to each sample and incubated on a rotator at 4 °C overnight.

3.2.11.3. Bead coupling and washing

The following day, 50 µl of the respective beads were aliquoted per sample and equilibrated as previously described. 50 µl of washed beads were then added to each IP sample and incubated for 2 h on a rotator at 4 °C. Antibody-coupled beads were pelleted for 2 min at 3000 rpm and 4°C and washed five times using 800 µl Co-IP buffer supplemented with protease inhibitors. After the final washing step, the beads were pelleted for 2 min at 6000 rpm and 4 °C and subsequently resuspended in 50 µl 6x Laemmli buffer. The resuspended beads were boiled for 5 min at 95 °C to equally charge linearized proteins and protein interactions were determined using immunoblot analysis of the prepared samples.

3.2.12. Fluorescence-based apoptosis assay

To check for the induction of apoptosis, the activation of caspase 3 and 7 was determined in real-time using the ViaStain™ Live Caspase 3/7 Detection Kit for 2D/3D Cultures (Nexcelom) according to manufacturer's instructions. This assay relies on the membrane-permeable reagent NucView™ that consists of a nucleic acid-specific dye that is attached to a fluorescent probe. Additionally, it is linked to the small peptide sequence DEVD mimicking the cleavage site of activated caspases 3 and 7. Upon apoptosis induction, these caspases get cleaved and activated, resulting in the cleavage of the DEVD peptide sequence and the subsequent release

of the nucleic acid-binding dye. Upon DNA binding, this dye emits a green fluorescent signal that can be detected using the image cytometer Celigo (Nexcelom).

3.2.13. Statistical analysis

Statistical analysis was carried out using the GraphPad Prism v5.04 software (GraphPad Software Inc). Statistical analyses were performed using unpaired, two-tailed Student's t-tests with 95 % confidence intervals. A p-value of 0.05 served as threshold to determine significance. The grade of significance was depicted as stars, representing * $p \leq 0.05$ and ** $p \leq 0.01$.

4. Results

4.1. Declaration of contributions

The results presented in this section were produced in collaboration with other scientists. Contributions of collaborators are stated in the respective figure legends. The remaining experimental data as well as data analyses were performed by Sabrina Gerber. Bioinformatic analyses were assisted by Ana P. Kutschat, Xin Wang and Dr. Zeynab Najafova, Clinic for General, Visceral and Pediatric Surgery, University Medical Center Göttingen, as well as Dr. Michael Lidschreiber, Department of Molecular Biology, Max-Planck-Institute for Biophysical Chemistry Göttingen.

4.2. Establishment of an MDM2 ChIP protocol

To investigate and characterize the global binding pattern of MDM2 on chromatin, a sufficient amount of DNA over background (IgG) has to be precipitated. However, previous attempts of our group to precipitate MDM2-bound chromatin resulted in poor signals over background. For this purpose, the previously used ChIP protocol (Wienken et al., 2016) was adapted to detect chromatin-bound MDM2 with higher efficiency.

Since MDM2 lacks a DNA binding domain, we anticipated that it associates with chromatin via interaction with a DNA or chromatin-binding factor. For this purpose, it was tested whether additional incubation with the protein-protein crosslinker ethylene glycol bis(succinimidyl succinate) (EGS), as reported by Sen and colleagues (Sen et al., 2019), would increase MDM2 ChIP efficiency.

Indeed, adding a protein-protein crosslinking step prior to protein-DNA crosslinking resulted in a 5-fold increased MDM2 ChIP efficiency at the *CDKN1A* (referred to as *P21*) promoter. An even 7-fold increase in efficiency was observed at the *MDM2* TSS using the MDM2 antibody provided by Abcam (Fig. 4.1 A). This effect was confirmed using another MDM2 antibody (IF2) that was already shown to work in MDM2 IPs (Wienken et al., 2016), albeit with a lower efficiency in ChIP than the Abcam antibody.

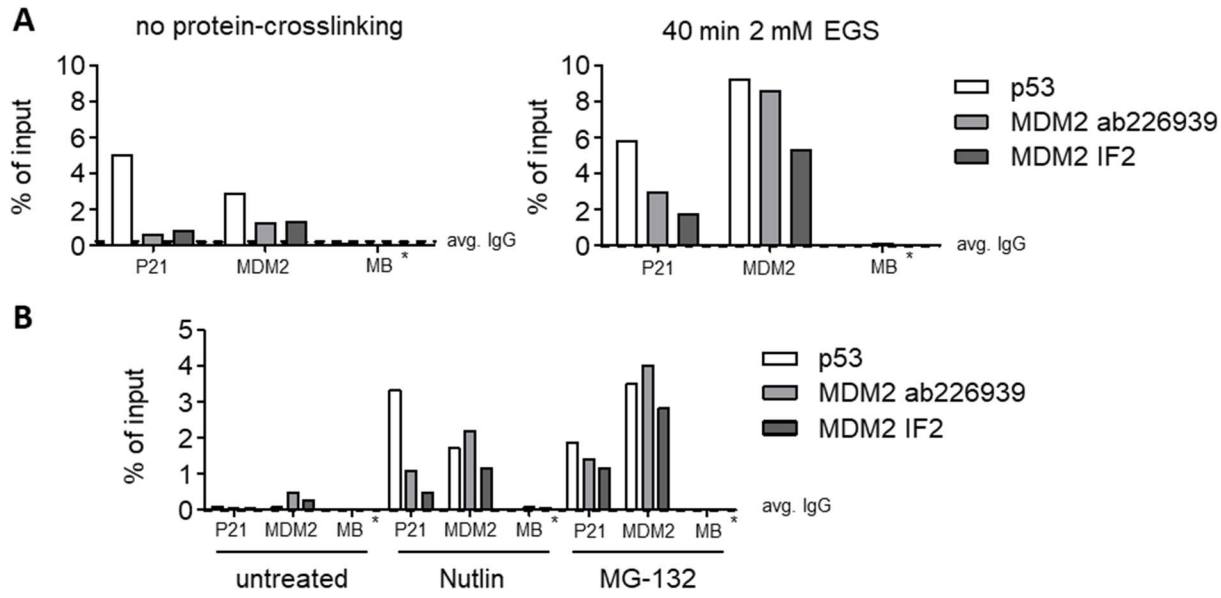

Fig. 4.1: Optimization of the MDM2 ChIP protocol. (A) Comparison of the MDM2 ChIP efficiency in SJSA-1 cells using the established ChIP protocol (no protein-crosslinking) and an optimized version with additional protein-protein crosslinking (40 min 2 mM EGS). (B) MDM2 antibody specificity was tested by detecting increased MDM2 levels on chromatin in SJSA-1 cells treated with 20 µM Nutlin-3a or 20 µM MG-132 for 4 h. In (A) and (B), two different MDM2-targeting antibodies were tested in parallel. Background precipitations (avg. IgG) are indicated as a dotted line. MDM2 ChIP efficiency was tested via qPCR at the TSS of two p53 target genes and a p53 ChIP served as positive control. Primers targeting the gene body of the myoglobin gene (MB) served as negative control. ChIP data is presented as bar diagram showing the mean ± SEM (n=1).

To confirm the specificity of both MDM2 antibodies used, MDM2 levels were elevated in SJSA-1 cells using the small-molecule inhibitor Nutlin-3a (referred to as Nutlin in the text from now on) and the resulting MDM2 occupancy was measured by ChIP-qPCR. Nutlin binds to the hydrophobic p53-binding pocket of MDM2, thus leading to an accumulation and activation of p53 and increased p53-target gene expression, such as *MDM2* (Vassilev et al., 2004). Therefore, treatment of cells with Nutlin is a convenient way to quickly elevate p53 and MDM2 protein levels in p53 wild-type cells. As expected, treatment of SJSA-1 cells with 20 µM Nutlin for 4 h markedly increased MDM2 occupancy at p53 target gene TSS with both antibodies tested (Fig. 4.1 B). The same is true for the correlating p53 occupancy, confirming Nutlin efficiency. Additionally, treatment of SJSA-1 cells with 20 µM of the proteasome-inhibitor MG-132 for 4 h resulted in elevated MDM2 chromatin binding as well. Taken together, additional protein-protein crosslinking prior to protein-DNA crosslinking is a suitable way to increase MDM2 ChIP efficiency. The increments of MDM2 protein levels using chemical compounds further elevates the MDM2 signal over background. Furthermore, it is recommended to use the MDM2 antibody provided by Abcam for ChIP due to its higher efficiency, while the established MDM2 IF2 antibody is still a reliable control to test for MDM2 antibody specificity.

4.3. MDM2 globally colocalizes with p53 at MDM2 binding sites

Upon establishment of a working ChIP protocol, global MDM2 chromatin binding sites were identified using ChIP-seq. To test for the consistency of identified MDM2 peaks, this experiment was performed in four different cell lines with different p53 status and varying MDM2 levels (Fig. 4. 2). To increase the chance of yielding a robust MDM2 signal in ChIP-seq analysis, p53 wild-type SJSA-1 and HCT116 cells were treated with 20 µM MG-132 for 4 h to elevate endogenous MDM2 levels prior to ChIP. In contrast, in H1299 cells transfected with an empty control vector as well as in PANC-1 cells, physiological MDM2 levels were detected. This resulted in very high endogenous MDM2 levels in SJSA-1 cells decreasing in HCT116, H1299 and PANC-1 cells (Fig. 4.2 A).

In line with the determined MDM2 levels, MDM2 ChIP-seq conducted in SJSA-1 cells yielded the highest MDM2 signals of all four cell lines tested, followed by HCT116, H1299 and PANC-1 cells. This is illustrated by heatmaps representing the calculated MDM2 signal at MDM2 peaks identified in SJSA-1 cells (Fig. 4.2 B). The differences in MDM2 ChIP-seq efficiency were mirrored by the number of called MDM2 peaks, ranging from 30,044 identified peaks in SJSA-1 cells, to 6,609 peaks in HCT116, 4,552 peaks in H1299 and 2,378 peaks in PANC-1 cells (data not shown). Despite large differences in MDM2 signal intensities, a large proportion of MDM2 binding sites was conserved across all cell systems tested as indicated by comparing the MDM2 heatmaps of the different cell lines (Fig. 4.2 B). In addition to MDM2, the correlating p53 occupancy was determined in SJSA-1 cells using ChIP-seq. Being the major interaction partner of MDM2, it is possible that chromatin-bound p53 could mediate MDM2 chromatin recruitment. To test for a potential correlation of MDM2 and p53 occupancy, p53 enrichment at MDM2 peaks identified in SJSA-1 cells was calculated and illustrated in a heatmap. Indeed, comparing the MDM2 signal with the corresponding p53 occupancy revealed nearly identical binding patterns of both proteins at MDM2 peaks, testifying a high MDM2 and p53 colocalization within these regions (Fig. 4.2 B).

To further confirm this high correlation, the MDM2 and p53 signals determined in SJSA-1 cells were correlated at MDM2 peak sites (Fig. 4.2 C). To exclude any bias due to a varying genetic background, both signals were normalized using the $\log_2$ fold-change of each signal over input before correlating them in a smooth-scatter plot. As already indicated by visual evaluation of MDM2 and p53 binding heatmaps, the smooth-scatter plot proved a high correlation of MDM2 and p53 on chromatin, which was further confirmed by a high correlation coefficient of 0.73.

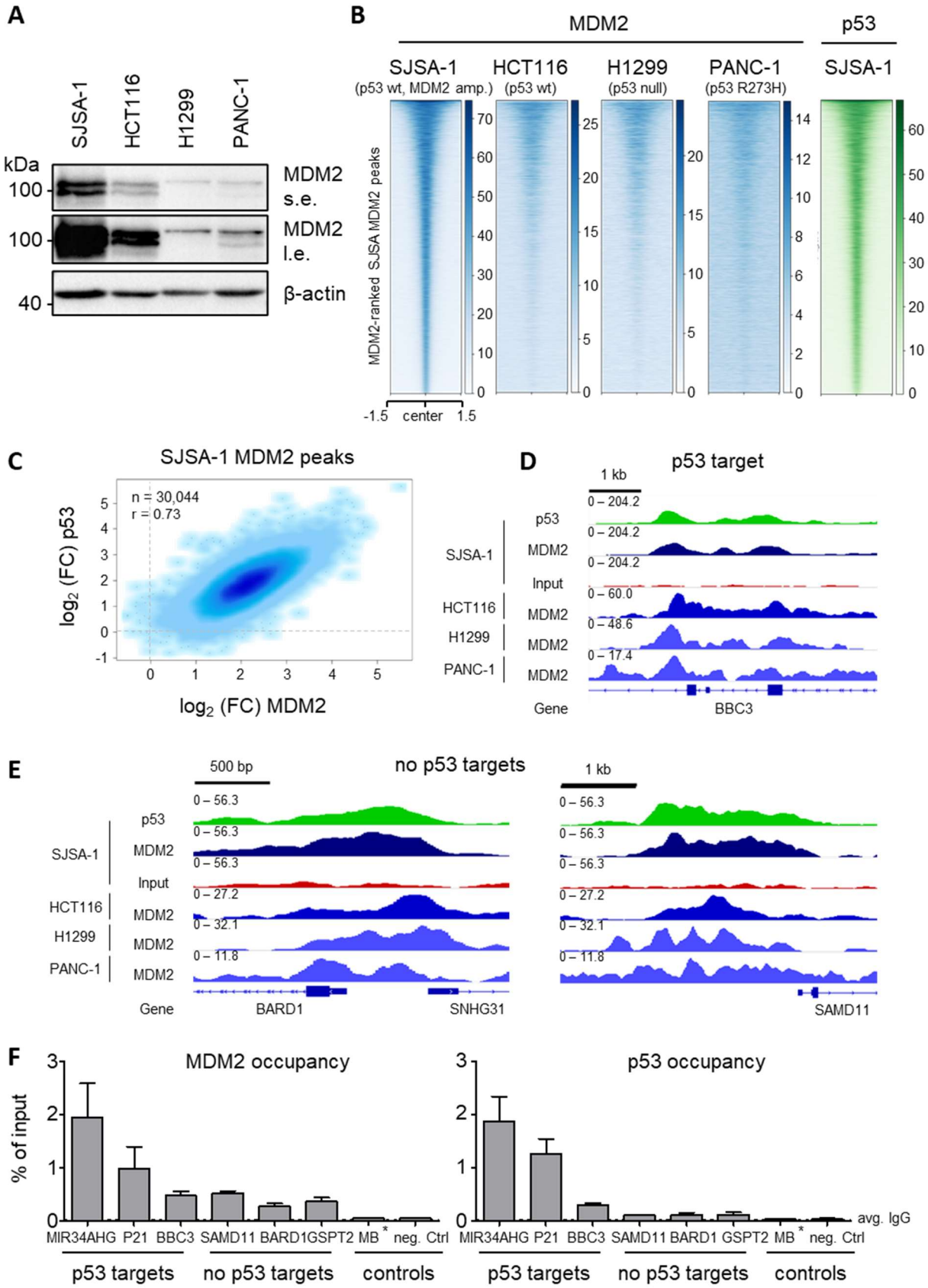

(Figure legend on next page)

Fig. 4.2: MDM2 and p53 highly colocalize across the genome. (A) Immunoblot analysis of whole-cell lysates showing endogenous MDM2 levels of all four cell lines used for ChIP-seq. SJSA-1 and HCT116 cells were treated for 4 h with 20 µM MG-132 while H1299 and PANC-1 cells were not treated with proteasome inhibitors and thus MDM2 levels did not change prior to ChIP. Staining of β-actin served as loading control. (B) Heatmaps displaying MDM2 binding in SJSA-1, HCT116, H1299 and PANC-1 cells at MDM2 peaks identified in SJSA-1 cells (blue). The corresponding p53 occupancy monitored at MDM2 peaks in SJSA-1 cells is shown to the right (green). (C) Smooth scatter plot illustrating the correlation of MDM2 and p53 signals in SJSA-1 cells at MDM2 peaks. Signals were calculated as the log_2 fold-change of the respective signal over input. (D+E) Visualization of p53 (green) and MDM2 (blue) ChIP-seq tracks at the p53 target gene *BBC3* (D) and the non-p53 target genes *SAMD11* and *BARD1* (E). The levels of endogenous MDM2 protein were indicated by different shades of blue, representing high MDM2 levels in dark blue and lower ones in light blue. (F) ChIP-qPCRs confirming MDM2 and p53 occupancy at predicted MDM2 binding sites in SJSA-1 cells. Primer binding sites were randomly chosen based on visualized MDM2 tracks and classified into p53 target and non-target genes. Asterisks indicate primer binding sites not associated with the gene's TSS. Binding sites within the myoglobin gene (MB) and an intergenic region with low MDM2 signal (neg. Ctrl) served as negative controls. Background precipitation (avg. IgG) is indicated as a dotted line. Bar diagrams visualize the mean ± SEM (n=3). One biological replicate was done by Kester Henningsen. ChIP experiments of the remaining replicates were performed by Antje Dickmanns while qPCR analyses were done by Sabrina Gerber.

Visual evaluation of MDM2 and p53 ChIP-seq tracks at the p53 target *BBC3* (Fig. 4.2 D) and genes that are no p53 targets (Fig. 4.2 E) further confirmed the high correlation of MDM2 and p53 binding. As already shown, MDM2 and p53 colocalized at both, p53 target and non-target genes, and highly correlated even in their binding pattern. Comparison of MDM2 ChIP-seq tracks from SJSA-1 cells with the ones raised in other cell systems proved that this is not a SJSA-specific phenomenon but a general effect conferrable to all systems tested (Fig. 4.2 D+E).

In addition to bioinformatic analyses (Fig. 4.2 B+C), the colocalization of MDM2 and p53 at MDM2 peaks was further verified using site-specific ChIP-qPCRs. For this purpose, primers targeting randomly chosen MDM2 peaks were designed and classified into p53 target and non-target genes. Quantitative PCRs using DNA obtained from ChIP conducted in SJSA-1 cells treated with 20 µM Nutlin for 4 h revealed that MDM2 and p53 bound equally well to all sites tested, confirming the high colocalization of both proteins again (Fig. 4.2 F). Collectively, the results presented so far attested a very high colocalization of MDM2 and p53 as well as a correlation in their binding pattern at MDM2 peaks.

4.4. MDM2 can bind to chromatin independently of p53

The high colocalization of MDM2 and p53 raised the question whether p53 is involved in MDM2 chromatin binding. Indeed, MDM2 was already shown to bind to the promoter region of the p53 target gene *P21* via p53 (Minsky and Oren, 2004). However, the fact that a large proportion of MDM2 peaks is conserved in systems lacking endogenous wild-type p53 suggests that there could be another, p53-independent way of MDM2 chromatin recruitment as well (Fig. 4.3 A). Indeed, since MG-132 treatment elevates MDM2 and p53 protein levels without disturbing their interaction, it is possible that MDM2 gets recruited to chromatin in a p53-independent fashion and that p53 binds to the potentially accessible p53-binding pocket of chromatin-bound MDM2. This would result in a high correlation of MDM2 and p53 binding as well. To overcome this problem, MDM2 chromatin binding studies were performed using Nutlin. As already mentioned in chapter 4.1, Nutlin blocks the MDM2-p53 interaction resulting in elevated MDM2 and p53 protein levels (Fig. 4.3 B). This enables the monitoring of MDM2 chromatin recruitment independently of p53 binding.

As expected, treatment with 20 µM Nutlin for 4 h elevated MDM2 and p53 protein levels in SJSA-1 cells, thus proving Nutlin efficiency (Fig. 4.3 C). Furthermore, Nutlin treatment enhanced the overall levels of chromatin-bound MDM2 at all MDM2 peaks tested, of which six out of ten non-p53 target genes tested showed a significant increase of MDM2 binding compared to DMSO controls (Fig. 4.3 D). In contrast, p53 binding solely increased at the TSS of the p53 target genes *P21* and *BBC3* to a significant level, while the p53 occupancy at tested non-p53 target sites largely remained unchanged (Fig. 4.3 D).

Since these findings strongly point to a p53-independent mechanism of MDM2 chromatin recruitment, this hypothesis was further tested in a system lacking endogenous p53. For this purpose, human MDM2 protein was exogenously expressed in H1299 cells for 24 h, either alone or in combination with human wild-type p53 and the expression efficiency was confirmed by immunoblot analysis (Fig. 4.3 F). MDM2 chromatin recruitment was subsequently analyzed using ChIP-qPCR. In line with previous results, the co-expression of p53 together with MDM2 significantly increased MDM2 binding specifically at the p53 target *MIR34AHG*, while MDM2 recruitment to non-p53 target genes was comparable in the presence and absence of p53 (Fig. 4.3 E). These results were further supported by ChIP-seq tracks obtained from H1299 cells overexpressing either MDM2 alone (Fig. 4.3 G+H, upper track) or in combination with p53 (Fig. 4.3 G+H, lower track).

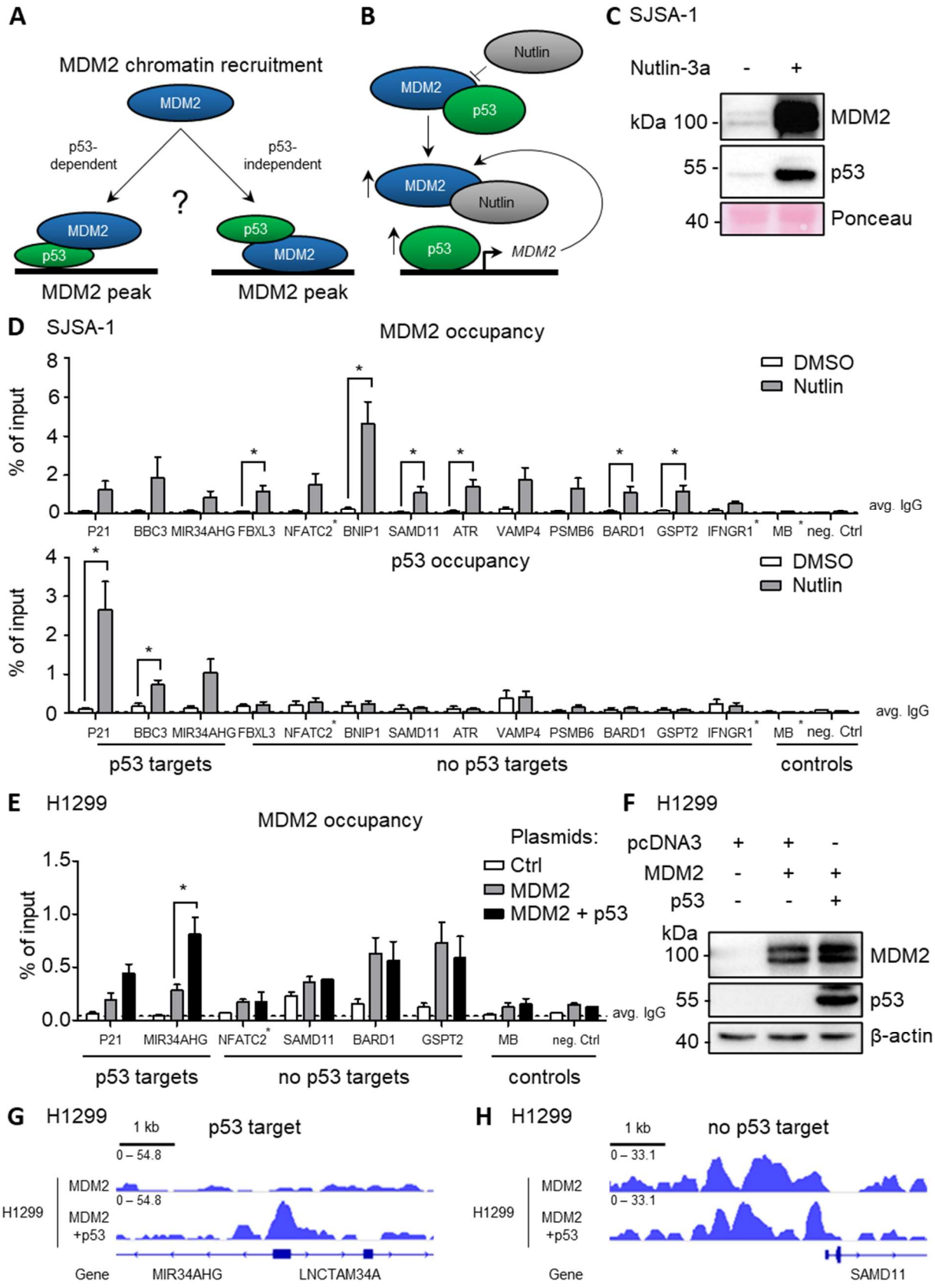

(Figure legend on next page)

Fig. 4.3: MDM2 can bind to chromatin independently of p53. (A) Scheme displaying potential mechanisms of MDM2 chromatin recruitment. Firstly, p53 mediates MDM2 chromatin recruitment to all MDM2 binding sites identified (left). Secondly, MDM2 is recruited first and p53 binds to the potentially still accessible p53-binding domain of chromatin-bound MDM2 (right). (B) Effect of the small-molecule inhibitor Nutlin-3a. (C) Immunoblot analysis of SJSA-1 cells treated with 20 µM Nutlin-3a for 4 h. Ponceau-S staining served as loading control. (D) MDM2 and p53 occupancy at MDM2 peaks, measured in SJSA-1 cells upon treatment with 20 µM Nutlin-3a for 4 h using ChIP-qPCR. Asterisks indicate primer binding sites not associated with the gene's TSS. Background precipitation (avg. IgG) is indicated as a dotted line. Data is shown as bar diagrams of the mean ± SEM (n=3). One biological replicate was conducted by Kester Henningsen. ChIP experiments of the remaining replicates were performed by Antje Dickmanns while qPCR analyses were done by Sabrina Gerber. (E) MDM2 occupancy determined by ChIP-qPCR in H1299 cells upon exogenous expression of wild-type MDM2 with and without co-expression of wild-type p53. Transfection of an empty pcDNA3 vector served as transfection control. Asterisks indicate primer binding sites not associated with the gene's TSS. Background precipitation (avg. IgG) is indicated as a dotted line. Bar diagrams visualize the mean ± SEM (n=3) (F) Immunoblot analysis of whole-cell lysates corresponding to (E). (G+H) Visualization of MDM2 ChIP-seq tracks determined upon overexpression of MDM2 alone (upper track) and in combination with wild-type p53 (lower track) for 24 h in H1299 cells at the p53 target gene *MIR34AHG* (G) and the non-p53 target gene (H). Statistical analyses of samples were performed using two-tailed, unpaired Student's t-tests with a confidence interval of 95 %; * $p \leq 0.05$.

Taken together, the depicted results prove that there is indeed a p53-independent mechanism mediating MDM2 chromatin recruitment to the vast majority of the identified MDM2 binding sites. For this purpose, the exact underlying mechanism and correlating interaction partners of MDM2 were further investigated.

4.5. MDM2 is recruited to CpG islands

To get an idea of how MDM2 chromatin recruitment is mediated, it was tested whether MDM2 preferably associates with specific transcriptional regulatory elements such as the gene's TSS, enhancer or super enhancer sites. This categorization may help to restrict the number of potential interaction partners mediating MDM2 recruitment, depending on the respective regulatory region to which MDM2 binds.

As a prerequisite for this study, transcriptionally relevant regulatory elements were defined bioinformatically. Annotated hg38 TSS coordinates were kindly provided by Xin Wang, member of the General, Visceral and Pediatric Surgery department Göttingen. Enhancer and super enhancer elements were defined using cell line-specific H3K27ac ChIP-seq data. Enhancer elements were generally defined as H3K27ac peaks that did not overlap with annotated gene TSSs. Super enhancer sites were called using the ROSE algorithm and subsequently subtracted from enhancer sites to identify enhancers that were not included in super enhancers. To test whether MDM2 preferably associates with any of these regulatory

elements, the MDM2 peaks were intersected with the coordinates of the respective regulatory elements. A positive correlation was defined as an overlap of at least 1 bp. The bioinformatic analyses indicate that MDM2 binds more to TSSs than to enhancers and super enhancers (Fig. 4.4 A). However, there was a comparable proportion of MDM2 peaks bound to none of these regulatory elements, suggesting a more general recruitment mechanism that is spread across the whole genome.

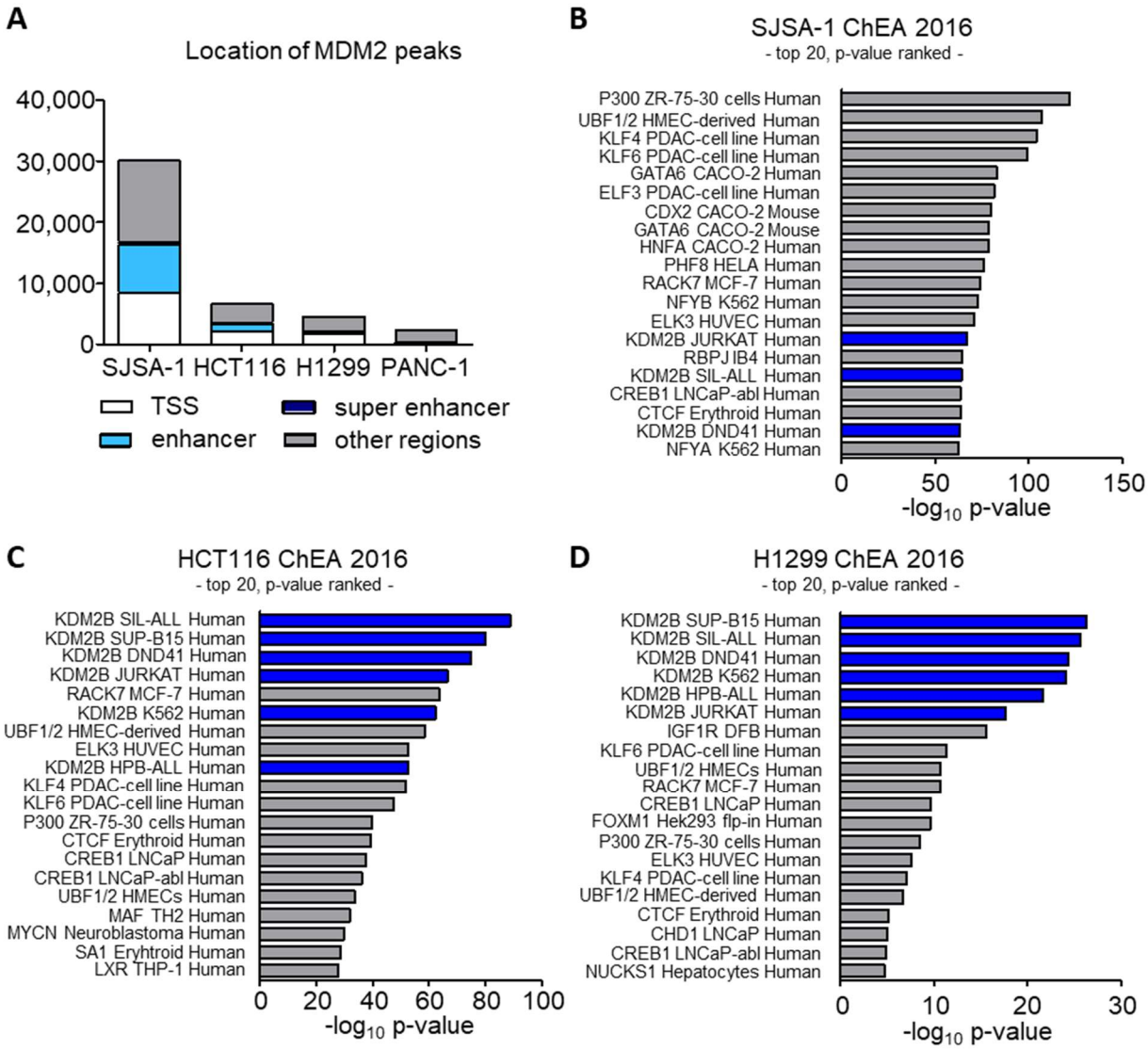

Fig. 4.4: KDM2B associates with MDM2 binding sites. (A) Overlap of cell line specific MDM2 peaks with TSSs, enhancer and super enhancer sites (criteria for association: at least 1 bp overlap) revealed no preferential binding of MDM2 to any regulatory elements across all systems tested. (B-D) Analysis of the top 20 transcription and chromatin-binding factors associated with MDM2 peaks called in SJSA-1 (B), HCT116 (C) and H1299 cells (D). Factors were identified by comparing MDM2 peaks with transcription factor gene sets of the ChEA 2016 database using the Enrichr platform.

In order to identify binding patterns underlying this wide-spread MDM2 recruitment, cell-line specific MDM2 peaks were submitted to the comprehensive gene set enrichment analysis web server Enrichr. This website compares the submitted coordinates with publicly available sequencing data of numerous gene-set libraries, giving a list of factors that highly associate with the provided loci. Correlating chromatin binding factors identified through comparison with transcription factor gene sets listed in the ChEA 2016 library (Lachmann et al., 2010) were ranked according to descending p-values. The top 20 of these ranked transcription factors were displayed in a bar diagram showing the negative $\log_{10}$ p-value for SJSA-1, HCT116 and H1299 cells (Fig. 4.4 B-D). Comparing the results of the different cell lines, it is striking that more than 50 % of the top 20 transcription factors associated with MDM2 peaks in SJSA-1 cells were also found in the top hits of HCT116 and H1299 cells. This confirms the finding that a large proportion of MDM2 peaks is conserved across the different cellular systems. Of these common associated factors, the histone demethylase KDM2B stood out being the predominant factor correlating with MDM2 peaks in HCT116 and H1299 cells (Fig. 4.4 C+D). This suggests that KDM2B could be an important factor involved in MDM2 chromatin recruitment even in systems with low endogenous MDM2 protein levels.

KDM2B has been published to function as both, an H3K36me2 demethylase depending on its N-terminal JmjC domain as well as a CGI-binding protein based on its CxxC-domain (Farcas et al., 2012; Tzatsos et al., 2008). Hence it was tested whether MDM2 associates with CGIs as well. For this purpose, persistent CGIs within the human genome were defined based on CxxC affinity purification (CAP)-sequencing data provided by Illingworth and colleagues (Illingworth et al., 2010). After mapping the CGI data of human sperm, blood and cerebellum cells to the hg38 reference genome, tissue-specific peaks were called and subsequently intersected to identify persistent human CGIs. The MDM2 signal detected in SJSA-1, HCT116, H1299 and PANC-1 cells as well as KDM2B and RNF2 occupancy derived from PC3 cells (Su et al., 2019) was assessed at persistent CGIs. Heatmaps illustrating the results of this correlation revealed an enrichment of MDM2 at CGIs in all cell lines tested, along with a colocalization of KDM2B and RNF2 (Fig. 4.5 A). This is a first hint pointing to an association of MDM2 with CGIs.

Looking at the distribution of MDM2, KDM2B and RNF2 at persistent CGIs, there was a subset of CGIs missing their colocalization. To identify factors potentially supporting the recruitment of MDM2, KDM2B and RNF2, the first and last 20 % of MDM2 signal-ranked CGIs were analyzed regarding transcription factor consensus sites present within these regions. To specifically search for motifs that are present in the “MDM2 high” CGI subset but missing within the “MDM2 low” one, the “MDM2 low” CGIs were used as background file for motif analysis in the “MDM2 high” group (Fig. 4.5 B).

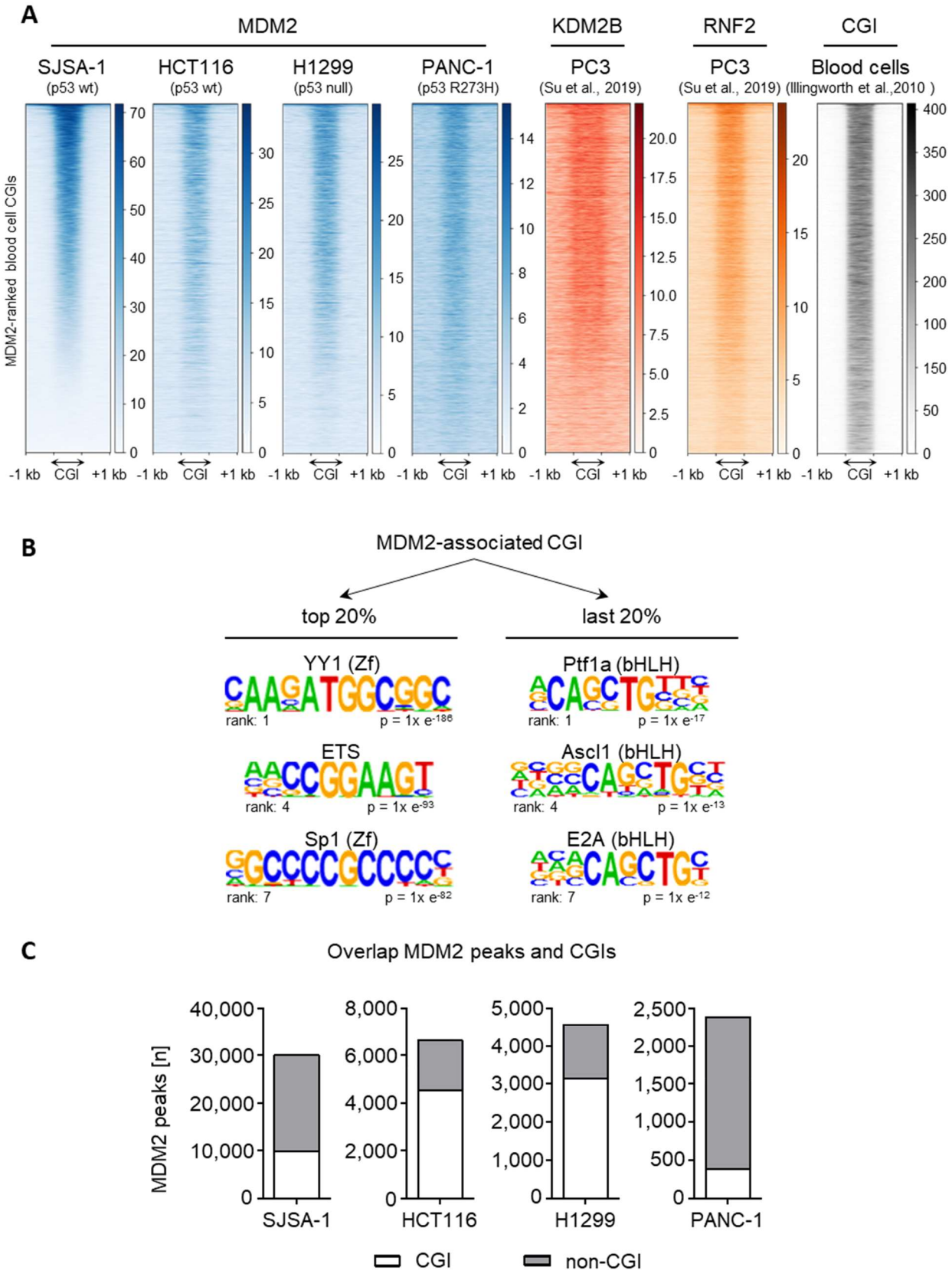

(Figure legend on next page)

Fig. 4.5: MDM2 associates with Polycomb repressor complexes at CpG islands. (A) Heatmaps displaying an enrichment of MDM2 (blue), KDM2B (red) and RNF2 (orange) at persistent human CGIs. KDM2B and RNF2 data in PC3 cells were derived from Su et al., 2019. Persistent CGIs were ordered according to the descending MDM2 signal measured in SJSA-1 cells. (B) Transcription factor motifs identified in the first and last 20 % of blood cell CGIs ranked according to a descending SJSA-1 MDM2 signal using the HOMER algorithm. Motif analysis revealed higher GC content as well as a higher CpG dinucleotide frequency in motifs found in the top 20 % compared to the last 20 %. (C) Overlap of MDM2 peaks identified in SJSA-1, HCT116, H1299 and PANC-1 cells with persistent CGIs identified based on the data from Illingworth et al., 2010. Criteria for association was at least 1 bp overlap.

Surprisingly, consensus sites of the transcription factor YY1 was the top motif enriched within CGIs exhibiting a high MDM2 occupancy (Fig. 4.5 B). YY1 has been shown to interact with both, p53 and MDM2 (Sui et al., 2004), hence this interaction could represent a mechanism of MDM2 chromatin recruitment. However, the fact that motifs of other transcription factors families, such as ETS, SP1 and AP-1, were also highly enriched within MDM2-bound CGIs suggests that the MDM2-YY1 interaction is not the predominant mechanism mediating MDM2 chromatin recruitment. Instead, there was a striking difference in the sequence composition of transcription factor motifs when comparing the “MDM2 high” and “MDM2 low” groups. While the motifs extracted from “MDM2 high” CGIs showed a high GC content and several CpG dinucleotides in close neighborhood to each other, these features were largely missing in the “MDM2 low” group (Fig. 4.5 B). This indicates that the CGIs in the “MDM2 high” group exhibit more of the typical CGI characteristics than CGIs of the “MDM2 low” group, again supporting the idea that MDM2 is preferably recruited to CGI sites.

To further test this hypothesis, the cell-line specific MDM2 peaks were intersected with persistent human CGIs to identify the proportion of MDM2 peaks that directly colocalize with CGIs. Criteria for such a colocalization was an overlap of at least 1 bp. Indeed, overlapping studies proved a colocalization of MDM2 and CGIs ranging from 33 % overlap in SJSA-1 cells to even 68 % in HCT116 and H1299 cells (Fig. 4.5 C). Of note, this effect was less pronounced in PANC-1 cells showing only 16 % colocalization of MDM2 and CGIs. This is most probably caused by problems of MDM2 peak calling in PANC-1 cells. Due to very low MDM2 signals, non-specific MDM2 peaks were called by MACS2 in this cell line. To filter for MDM2-specific peaks, these peaks were intersected with the SJSA-specific ones. However, since the exact location and the shape of MDM2 peaks slightly varies from cell line to cell line even if they all associate with CGIs, it is very likely that a large proportion of PANC-1 MDM2 peaks will be missed when intersecting them with SJSA-1 peaks. Hence the results of independently called MDM2 peaks in SJSA-1, HCT116 and H1299 cells are more reliable in this context than the PANC-1 data. Nonetheless, the fact that all cell lines showed a colocalization of MDM2 peaks and CGIs further supports the hypothesis that MDM2 preferably binds to CGIs.

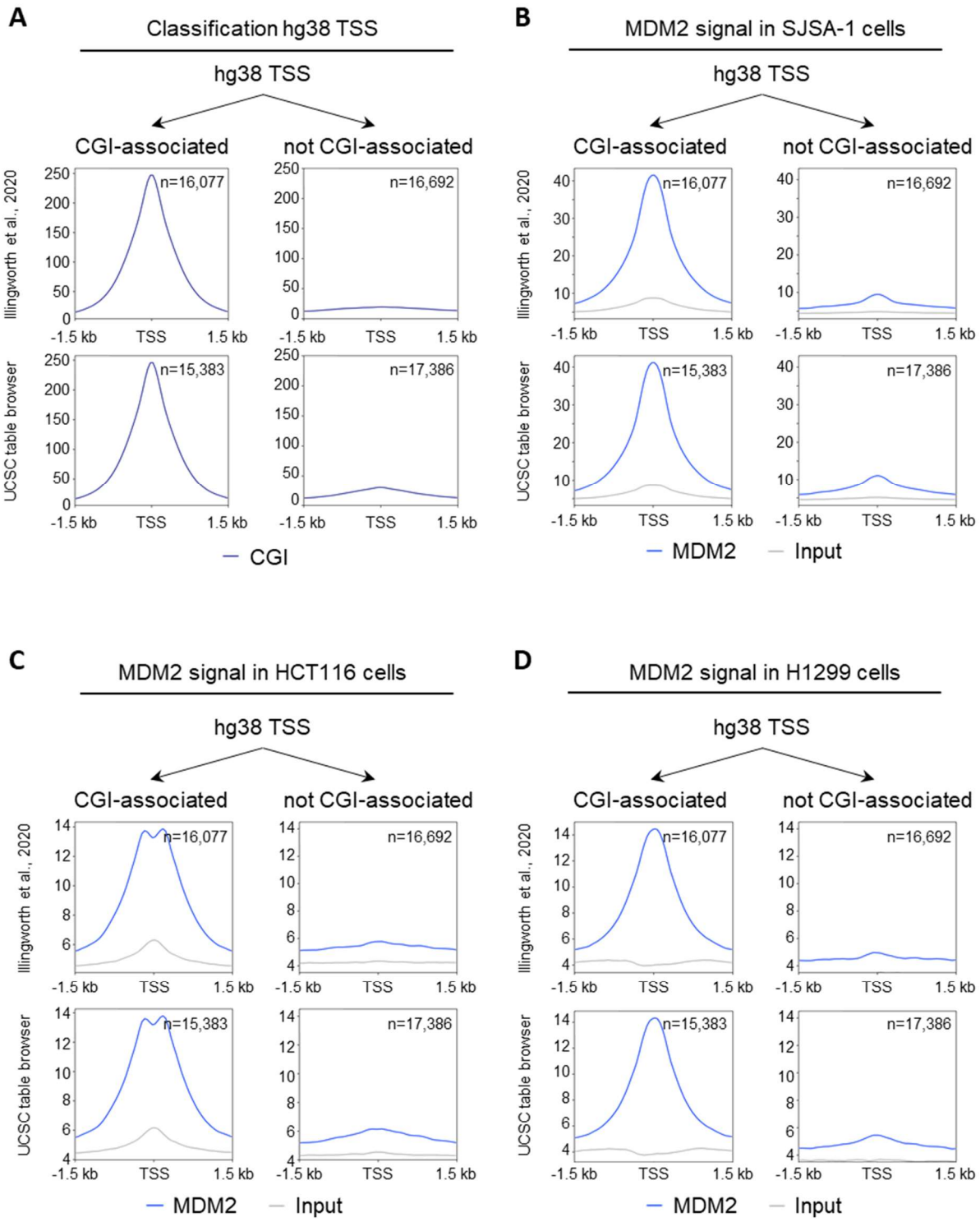

Fig. 4.6: MDM2 binding correlates with CGI-associated TSSs. (A) Classification of annotated hg38 TSSs into CGI and non-CGI-associated TSSs. TSSs were characterized based on their overlap with persistent human CGIs (Illingworth et al., 2010, upper panel) and with CGIs derived from the UCSC table browser (lower panel). (B-D) Aggregate plots illustrating the MDM2 enrichment (blue) at CGI-associated TSSs of hg38 reference genes (left) in comparison to TSSs that are not associated with CGIs (right) in SJSA-1, HCT116 and H1299 cells. Input signals (grey) within these regions served as negative controls.

Another characteristic of CGIs is their association with gene TSSs (Saxonov et al., 2006). Assuming that MDM2 colocalizes with CGIs, it was tested whether MDM2 preferentially associates with the TSSs of genes overlapping with CGIs as well. For this purpose, the TSSs of hg38 genes were classified into CGI-associated and non-CGI-associated TSSs by overlapping them with CGI sites. The coordinates of persistent CGIs and annotated CGIs downloaded from the UCSC table browser were used for this analysis. To test for a successful classification, the CGI signal derived from human blood cells was calculated at the defined hg38 TSS subsets and visualized in an aggregate plot. Since the enrichment of CGI signals was specific to CGI-associated TSSs (Fig. 4.6 A), the successful classification of hg38 TSSs was confirmed. Upon classification, the MDM2 signal detected in SJSA-1 (Fig. 4.6 B), HCT116 (Fig. 4.6 C) and H1299 cells (Fig. 4.6 D) was calculated around the TSSs of each subclass and displayed as aggregate plots. In line with previous results, MDM2 accumulated around TSSs associated with CGIs in all three cell lines tested (Fig. 4.6 B-D, left panels). This effect was consistent for both CGI classes, the persistent ones and the ones downloaded from UCSC. In contrast, there was no MDM2 binding detectable at TSSs that are not associated with CGIs (Fig. 4.6 B-D, right panels), again confirming the hypothesis of a CGI-dependent MDM2 recruitment. Collectively, the latest results strongly suggest that MDM2 enriches at CGIs across the genome in multiple different cell systems and that it selectively binds to TSSs associated with these structures.

4.6. Recruitment of MDM2 to CpG islands depends on KDM2B

Due to the high colocalization of MDM2 and KDM2B at CGIs, a potential interaction of both proteins would be a promising candidate mechanism explaining MDM2 chromatin recruitment. To test this, MDM2 was exogenously expressed alone or in combination with wild-type KDM2B for 24 h in H1299 cells and a potential interaction was tested using complex-immunoprecipitation. As a prerequisite for chromatin binding studies, the same experiment was performed in parallel co-expressing a CxxC-domain deletion mutant of KDM2B (ΔCxxC) instead of the wild-type version. Due to the lack of expression plasmids coding human KDM2B, the plasmids used contained the murine KDM2B homologs (He et al., 2013). However, since the KDM2B gene is conserved in human and murine species (National Center for Biotechnology Information, 2020), this was not considered to inhibit a potential interaction between human MDM2 and murine KDM2B. Complex-immunoprecipitation studies of exogenously expressed proteins revealed a strong interaction of MDM2 with both, wild-type KDM2B and its ΔCxxC mutant version as shown by positive stainings for KDM2B Flag-tags upon precipitation using an MDM2-targeting antibody (Fig. 4.7 A, α-MDM2 panel, lanes 4+6).

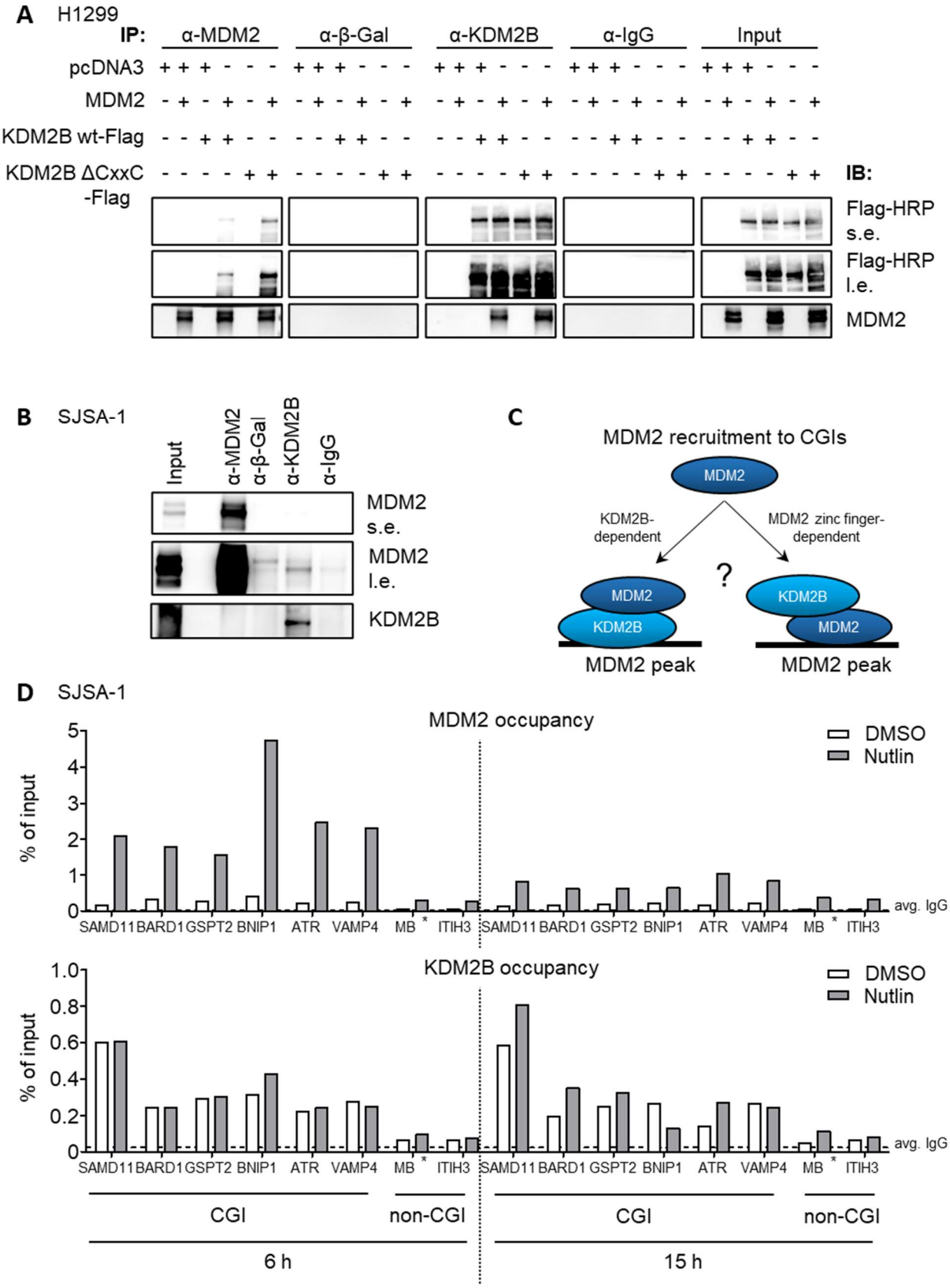

(Figure legend on next page)

Fig. 4.7: MDM2 interacts with KDM2B. (A) Co-IP of exogenously expressed human wild-type MDM2 in combination with murine Flag-tagged wild-type KDM2B and a CxxC-domain deletion KDM2B mutant (He et al., 2013) in H1299 cells. Precipitation with β-Gal and isotype IgG antibodies served as negative controls. Input samples represent the levels of exogenously expressed proteins prior to IP. All blots were developed simultaneously to ensure comparable exposure of samples. Co-IPs and their analysis were done by Antje Dickmanns. (B) Co-IP of endogenous MDM2 and KDM2B protein in SJSA-1 cells treated for 4 h with 20 μM MG-132. Experiments were performed by Antje Dickmanns. (C) Scheme displaying two potential mechanisms of MDM2 recruitment to CGIs. On the one hand, MDM2 could be recruited to CGIs by KDM2B. On the other hand, MDM2 could bind to CGIs via its central zinc finger and recruit KDM2B to these sites. (D) KDM2B occupancy at MDM2-associated CGIs determined in SJSA-1 cells treated with 20 μM Nutlin-3a for 6 h (left) and 15 h (right) using ChIP-qPCR. Non-CGI sites served as negative controls and asterisks indicate primer binding sites that are not associated with the gene's TSS. Background precipitation (avg. IgG) is indicated as a dotted a line. Bar diagrams illustrate the mean ± SEM (n=1).

This interaction was confirmed by the reverse precipitation using a KDM2B-targeting antibody to enrich proteins and staining for MDM2 (Fig. 4.7 A, α-KDM2B panel, lanes 4 and 6). Since the negative control precipitations did not show any signal neither for MDM2 nor for KDM2B (Fig. 4.7 A, α-β-Gal and α-IgG panels), it was proven that the detected interactions between MDM2 and KDM2B were highly specific.

As a next step, it was further tested whether the interaction between MDM2 and KDM2B is also detectable using endogenous protein. For this purpose, SJSA-1 cells were treated with 20 μM MG-132 for 4 h followed by Co-IP. In accordance with previous results, the KDM2B antibody successfully precipitated endogenous MDM2 protein in SJSA-1 cells (Fig. 4.7 B, MDM2 l.e. panel, lane 4). But in contrast to exogenous complex-immunoprecipitations, the reciprocal precipitation did not work (Fig. 4.7 B, KDM2B panel, lane 2). This could be caused by a potential epitope shielding through MDM2-interacting proteins. Thus, this precipitation should be repeated using different MDM2 antibodies targeting other domains than the one used.

Although the interaction between MDM2 and KDM2B was clearly shown, its consequences for the chromatin recruitment of both proteins are still elusive. Similar to the CxxC zinc finger domain of KDM2B, MDM2 exhibits a central zinc finger containing two repeats of the CxxC-motif (Yu, 2006). Although the MDM2 zinc finger possesses less repeats of the DNA-binding CxxC-motif compared to other ZF-CxxC-domain-containing proteins (Long et al., 2013), its presence still discloses two potential mechanisms taking place at CGIs (Fig. 4.7 C): On the one hand, chromatin-bound KDM2B could recruit MDM2 to CGIs. On the other hand, MDM2 could potentially bind to CGIs via its central zinc finger domain, leading to the subsequent recruitment of KDM2B and variant PRC1 complexes.

To test which of the depicted hypotheses is true, SJSA-1 cells were treated with 20 µM Nutlin for 15 h and subjected to ChIP to test whether MDM2 chromatin recruitment affects KDM2B occupancy. Since 15 h of Nutlin treatment induces a cell cycle arrest in SJSA-1 cells, an additional timepoint of 6 h Nutlin treatment was added to rule out cell cycle-dependent effects. As expected, Nutlin increased the recruitment of MDM2 to CGIs upon 6 h of treatment (Fig. 4.7 D, upper panel left). These elevated MDM2 levels were still present after 15 h of Nutlin, albeit to a much lower extent. This is shown by reductions of the MDM2 occupancy ranging from 58 % at the ATR TSS to even 86 % at the BNIP1 TSS compared to the 6 h Nutlin condition (Fig. 4.7 D, upper panel right). This indicates that MDM2 chromatin recruitment is an event of the early Nutlin-response in cells that declines with prolonged treatment time. However, increased MDM2 recruitment to CGIs did not affect the levels of chromatin-bound KDM2B, neither upon 6 h nor 15 h of Nutlin treatment in a first pilot experiment (Fig. 4.7 D, lower panel). This suggests that MDM2 is not the driving force mediating CGI chromatin recruitment of KDM2B, but to be able to draw a conclusion on any significant changes in MDM2 and KDM2B chromatin recruitment, these experiments need to be repeated at least thrice.

To further investigate whether MDM2 can bind directly to chromatin, exogenous expression experiments were performed in H1299 cells to further characterize MDM2 chromatin binding. For this purpose, wild-type MDM2 was expressed in parallel to MDM2 deletion mutants missing different functional domains and an MDM2 RING finger mutant for 48 h. The cells were then treated with 20 µM MG-132 for 4 h and subjected to ChIP-qPCR. Exogenous expression of wild-type MDM2 elevated the overall levels of MDM2 bound to defined MDM2 peaks, of which the *MIR34AHG* locus was the only one showing a significant increase (Fig. 4.8 A). Comparing the binding pattern of the different deletion mutants, there was no mutant that significantly abolished MDM2 recruitment (Fig. 4.8 A). Since all MDM2 mutants were equally expressed in H1299 cells (Fig. 4.8 B), it is excluded that this is a side-effect of an increased stabilization of one specific deletion mutant compensating reduced chromatin recruitment. Hence, this data shows that none of the functional domains tested, including the central zinc finger (Δ222-325 mutant), is exclusively required for MDM2 chromatin recruitment. Furthermore, this suggests that MDM2 does not bind to CGIs independently. However, it needs to be mentioned that the MDM2 occupancy highly varied between the biological replicates as indicated by high error bars. Therefore, it would be advisable to further increase the n-number of this experiment to clearly state whether the central zinc finger is not required for MDM2 chromatin recruitment.

To further test whether KDM2B is responsible for MDM2 recruitment to CGIs instead, another set of exogenous expression experiments was performed in H1299 cells. For this purpose, wild-type MDM2 was expressed in combination with either murine wild-type KDM2B or its ΔCxxC deletion mutant for 24 h and MDM2 chromatin recruitment was determined using ChIP.

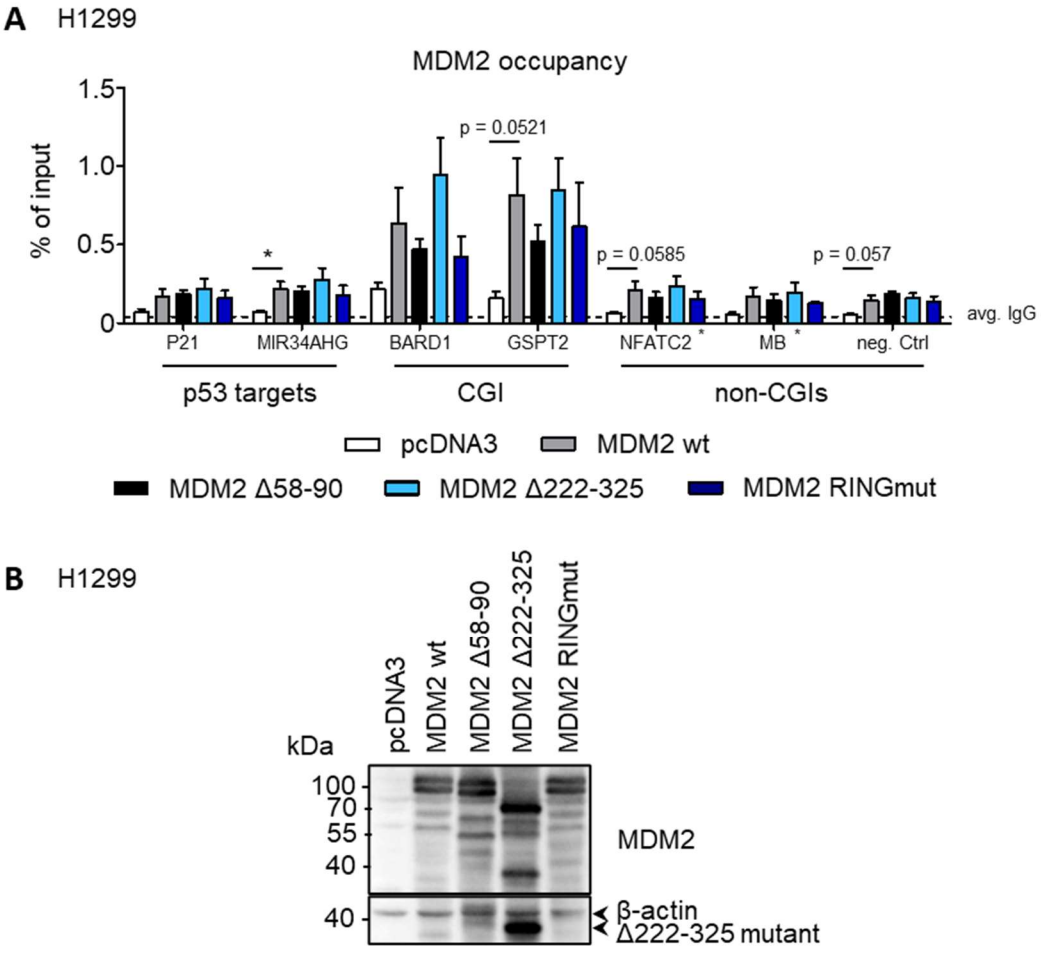

Fig. 4.8: MDM2 chromatin recruitment occurs independently of its central zinc finger domain. (A) MDM2 occupancy determined at MDM2 binding sites upon exogenous expression of wild-type MDM2, MDM2 deletion mutants missing different functional domains and an MDM2 mutant with a point mutation within the RING finger in H1299 cells for 48 h. Prior to ChIP, cells were treated with 20 µM MG-132 for 4 h. Non-CGI sites served as negative controls and asterisks indicate primer binding sites that are not associated with the gene's TSS. Background precipitation (avg. IgG) is indicated as a dotted line. Bar diagrams illustrate the mean ± SEM (n=3). (B) immunoblot analysis corresponding to (A).

Again, the cells were treated with 20 µM MG-132 for 4 h prior to ChIP to increase ChIP efficiency. In accordance with previous reports showing KDM2B being a CGI-binding protein, wild-type KDM2B was capable to bind to CGIs upon expression (Fig. 4.9, lower panel). Additionally, its expression markedly increased MDM2 and at these sites in comparison to MDM2 expression alone (Fig. 4.9 A, upper panel). Importantly, these effects were restricted to CGI sites and were completely reversible when co-expressing MDM2 with the ΔCxxC mutant of KDM2B that was not able to bind to CGIs.

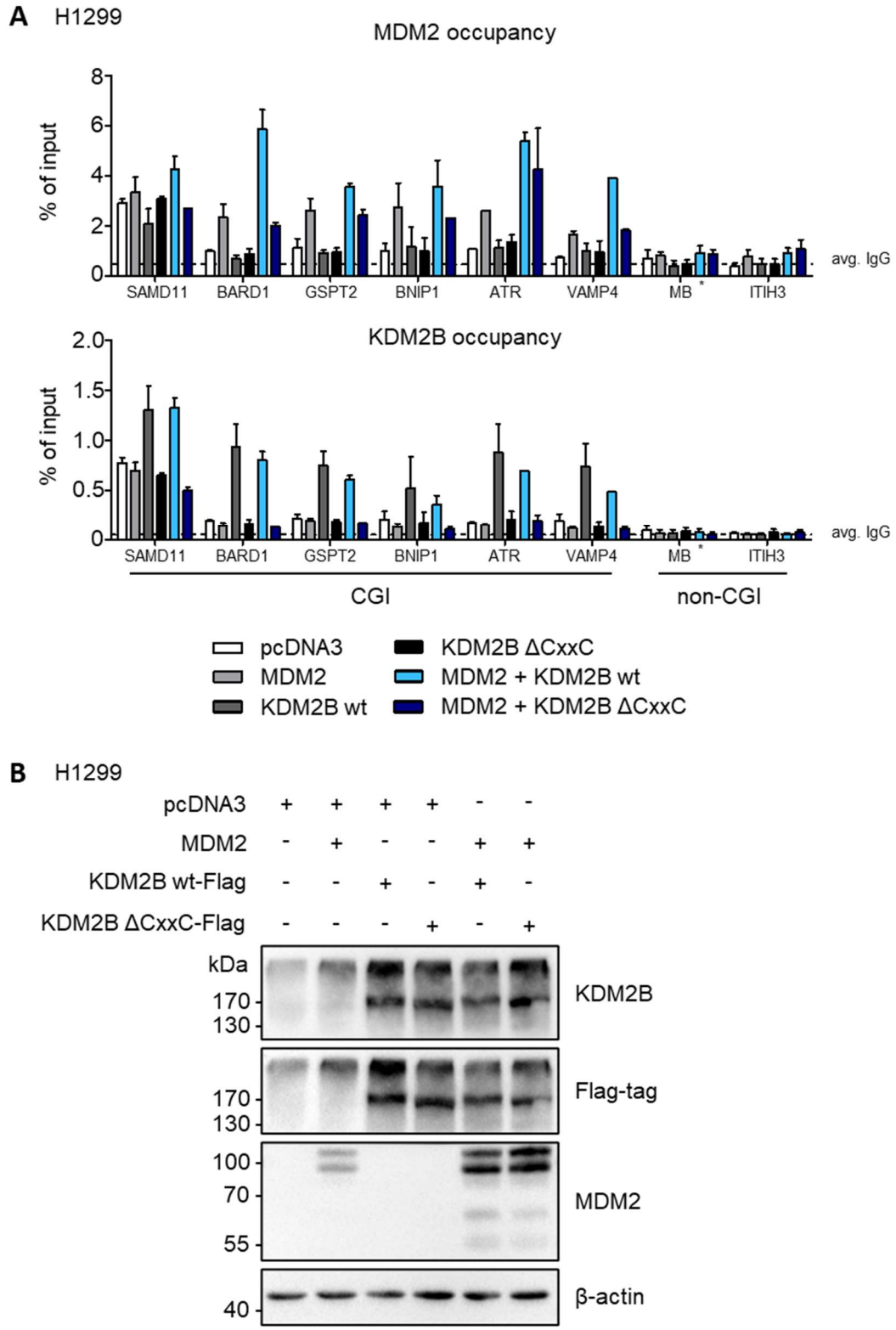

Fig. 4.9: Recruitment of MDM2 to CGI depends on KDM2B. (A) Chromatin binding of exogenously expressed MDM2 in combination with wild-type KDM2B and a CxxC-domain deletion mutant, determined in H1299 cells using ChIP-qPCR. Non-CGI sites served as negative controls and asterisks indicate primer binding sites that are not associated with the gene's TSS. Background precipitation (avg. IgG) is indicated as a dotted line. Data is visualized using bar diagrams of the mean ± SEM (n=2). (B) Immunoblot analysis corresponding to (A), confirming expression efficiency.

But again, these are only preliminary results since this experiment was performed only twice so far and needs to be repeated at least once more. Nonetheless, the fact that both biological replicates show a high similarity in MDM2 and KDM2B occupancy as demonstrated by small error bars supports the idea that this is a reliable consequence of the KDM2B and MDM2 interaction. In addition to increased chromatin recruitment, the co-expression of MDM2 and KDM2B elevated MDM2 protein levels in comparison to MDM2 expression alone (Fig. 4.9 B, lanes 5 and 6), pointing to a potential stabilization of MDM2 protein by KDM2B. This could be caused through the prevention of the MDM2 auto-ubiquitination, supporting the hypothesis that both proteins closely interact. Importantly, the increased MDM2 chromatin recruitment is no consequence of elevated MDM2 protein levels upon MDM2 and KDM2B co-expression since it was specifically monitored upon co-expression of MDM2 and wild-type KDM2B and not with the ΔCxxC mutant (Fig. 4.9 A, upper panel). Taken together, the depicted results suggest that MDM2 recruitment to CGIs occurs shortly upon MDM2 induction, e.g. by Nutlin treatment, and that MDM2 chromatin recruitment strongly depends on the interaction of MDM2 and KDM2B.

4.7. MDM2 reduces Pol II occupancy at CGI-associated genes

Upon identification of a potential mechanism, the consequences of MDM2 recruitment to CGIs should be further investigated. MDM2 has already been shown to repress Polycomb repressor target genes by supporting the formation of H3K27me3 and H2AK119ub1 (Wienken et al., 2016). Furthermore, KDM2B was recently shown to affect the occupancy of Pol II at CGI-associated genes thus leading to their repression (Turberfield et al., 2019). Hence it was tested whether MDM2 fulfills any of these repressive functions in the context of CGI-associated gene expression as well.

To test whether MDM2 represses CGI-associated genes by recruiting Polycomb repressor complexes, the formation of H3K27me3 and H2AK119ub1 at MDM2 peaks was detected in SJSA-1 cells treated with 20 μM Nutlin for 15 h (Fig. 4.10 A). Similar to previous experiments, Nutlin treatment elevated MDM2 occupancy at all sites tested (Fig. 4.10 A, upper panel). However, there was hardly any effect neither on H3K27me3 nor H2AK119ub1 (Fig. 4.10 A, middle and lower panel). While there was a slight reduction of H2AK119ub1 occupancy at the promoter of the p53-target gene *MIR34AHG*, there were no changes in H3K27me3 or H2AK119ub1 occupancy monitored at the *BARD1* and *GSPT2* promoters. The promoter region of *SAMD11* was the only non-p53 target gene showing a slight upregulation of both repressive histone modifications upon Nutlin treatment while the repression of the negative control *MB* was constantly high for both modifications in all conditions.

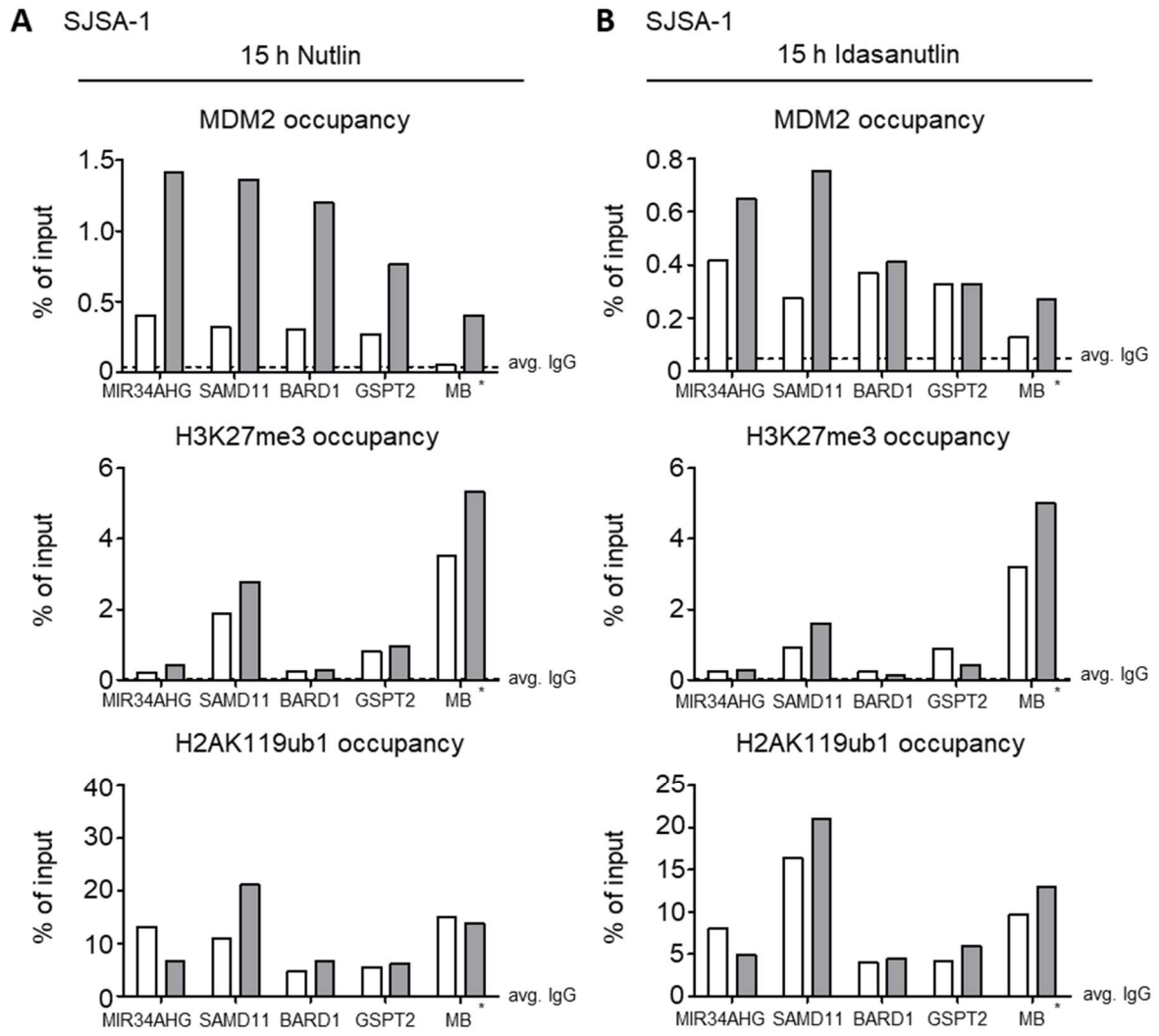

Fig. 4.10: MDM2 does not strongly affect H3K27me3 or H2AK119ub1 formation at CGI. (A+B) ChIP-qPCR experiments determining MDM2, H3K27me3 and H2AK119ub1 occupancy in SJSA-1 cells upon treatment with 20 µM Nutlin-3a (A) or 1 µM Idasanutlin (B) for 15 h. A primer binding site within the *MB* gene served as negative control. Asterisks indicate primer binding sites not associated with the gene's TSS. Background precipitation (avg. IgG) is indicated as a dotted line. Bar diagrams visualize the mean ± SEM (n=1).

These preliminary results were confirmed in another pilot experiment using SJSA-1 cells treated with 1 µM Idasanutlin, a more potent Nutlin derivate that is currently being tested in several clinical trials (Ding et al., 2013; U.S. National Library of Medicine, 2020). Similar to Nutlin, treatment of cells with Idasanutlin increased MDM2 binding to the predicted sites but only slightly changed H3K27me3 and H2AK119ub1 occupancy at these sites (Fig. 4.10 B). Based on these preliminary results, the hypothesis that MDM2 could affect the formation of H3K27me3 or H2AK119ub1 at MDM2 peak sites was rejected.

To check instead whether MDM2 recruitment could affect RNA Pol II occupancy at CGI-associated genes in a similar way as KDM2B does (Turberfield et al., 2019), the total Pol II occupancy was monitored in SJSA-1 cells upon treatment with 20 µM Nutlin. These experiments were performed in parallel to the ChIP-qPCR experiments shown in Fig. 4.7 D, hence the graph showing the MDM2 occupancy is identical and was only added to provide a better overview of all conditions (Fig. 4.11 A). Furthermore, two different Pol II antibodies were used to monitor Pol II occupancy, one targeting the Pol II CTD and one raised against the N-terminus of the Pol II subunit Rbp1. By doing so, any bias that could derive from epitope shielding through post-translational modifications of the Pol II CTD were excluded. The results obtained with both Pol II antibodies were highly comparable (Fig. 4.11 B+C). In general, Pol II binding was higher at CGI-associated genes compared to non-CGI sites as shown by low Pol II occupancies at the *MB* and *ITIH3* control sites in both conditions after 6 h of Nutlin treatment (Fig. 4.11 B+C, left panel). This effect was still present upon 15 h Nutlin treatment, albeit less pronounced. Surprisingly, vehicle treatment of cells for 15 h heavily reduced Pol II binding to chromatin compared to a 6 h vehicle treatment, as shown by Pol II occupancies reduced by 65 % at the *SAMD11* site and up to 86 and 87 % at the *ATR* and *BARD1* promoters respectively (Fig. 4.11 B, right panel). Nonetheless, Nutlin treatment further diminished Pol II binding to CGI sites compared to DMSO upon both, 6 h and 15 h of treatment (Fig. 4.11 B+C), indicating that MDM2 could reproduce effects that were already reported for KDM2B.

However, there is no mechanism published how the presence of KDM2B reduces Pol II occupancy at CGI-associated genes. In contrast, MDM2 has already been shown to physically interacts with the TFIID subunits TBP and $TAF_{II}250$, leading to a repression of genes (Léveillard and Wasylyk, 1997). Hence it was tested whether the recruitment of MDM2 affects the binding of transcriptional PIC components to CGI-associated gene promoters as well. To test for the persistency of PIC binding to promoters, the occupancy of TBP, representing TFIID, and of the TFIIEα subunit were determined at CGI-associated genes (Yudkovsky et al., 2000). Like Pol II, TBP and TFIIEα occupancy decreased upon treatment of cells with 20 µM Nutlin, albeit to a lesser extent than Pol II (Fig. 4.11 D+E). This effect was present in both conditions, upon 6 h and 15 h of Nutlin treatment, pointing to a potential destabilization of the Pol II pre-initiation complex. However, these are only preliminary results again and the experiments shown need to be repeated at least twice to obtain reliable results. Furthermore, it is not clear whether the decrease in PIC component binding to CGI sites is the cause or the consequence of reduced Pol II occupancy. Assuming that Pol II occupancy is reduced by any other mechanism than the destabilization of the PIC through MDM2, it would be conceivable that a subsequent lack of Pol II on the chromatin will result in a destabilization of the present PIC scaffold.

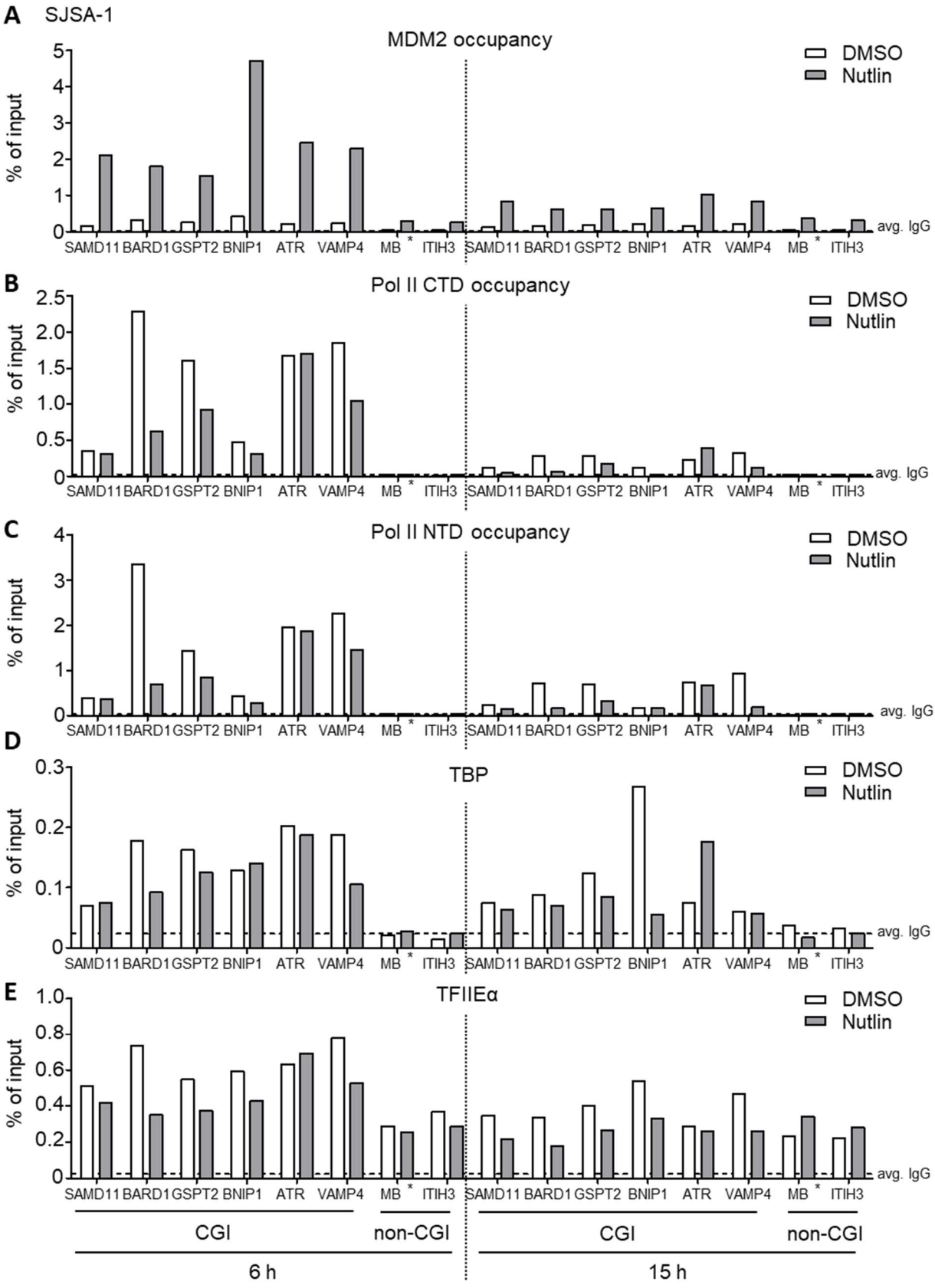

(Figure legend on next page)

Fig. 4.11: MDM2 chromatin recruitment correlates with reduced binding of Pol II and PIC components. (A-E) MDM2 (A), total Pol II (B+C), TBP (D) and TFIIEα (E) occupancy determined at MDM2 bound CGIs in SJSA-1 cells treated with 20 µM Nutlin-3a for 6 h (left side) and 15 h (right side) using ChIP-qPCR. Non-CGI sites served as negative controls and asterisks indicate primer binding sites that are not associated with the gene's TSS. Background precipitation (avg. IgG) is indicated as a dotted line. Bar diagrams illustrate the mean ± SEM (n=1).

To exclude that the reduction in Pol II chromatin occupancy is caused by a decrease of total Pol II protein levels, immunoblot analysis of whole-cell lysates derived from SJSA-1 cells treated with 20 µM Nutlin and varying concentrations of Idasanutlin for 4 h and 15 h were performed (Fig. 4.12). Although Nutlin-treatment led to a reduction of Pol II occupancy at CGI-associated genes (Fig. 4.11 B+C), total Pol II protein levels remained in all tested conditions. Furthermore, the efficiency of Nutlin-treatment was confirmed by the accumulation of p53 protein as well as increased MDM2 and p21 protein levels, both of which are encoded by p53 target genes. This result suggests that Pol II chromatin binding is specifically reduced upon Nutlin treatment. However, the exact mechanism how Nutlin-treatment affects Pol II chromatin occupancy and whether this is a direct consequence of MDM2 recruitment is still elusive and needs to be addressed in further studies.

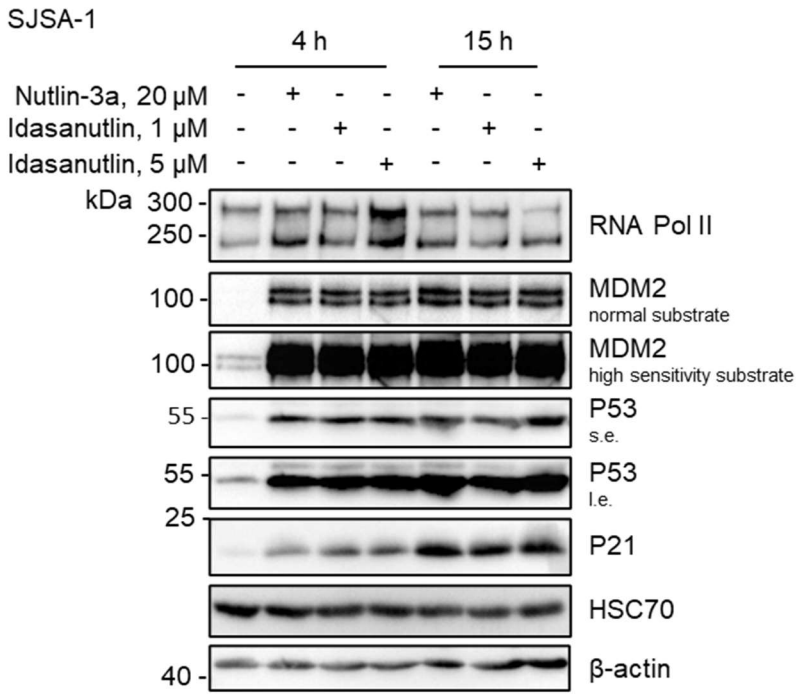

Fig. 4.12: Pol II protein levels remain stable upon Nutlin treatment. Immunoblot analysis showing total Pol II protein levels in SJSA-1 cells treated with the indicated concentrations of Nutlin-3a and its derivate Idasanutlin for 4 h and 15 h. MDM2, p53 and p21 protein levels were used to control the efficiency of Nutlin treatment while stainings for HSC70 and β-actin served as loading controls.

4.8. MDM2 represses genes with CGI-associated promoters

Although its mechanism is not clarified yet, the preliminary result that Pol II occupancy was reduced upon Nutlin treatment raised the question whether increased MDM2 chromatin recruitment results in the repression of CGI-associated genes similar to KDM2B. One reliable readout for gene activity is the formation of H3K37ac at histones of actively transcribed genes (Creyghton et al., 2010; Hilton et al., 2015). In order to test for a potential repression of genes, H3K27ac occupancy was determined at MDM2 peaks using ChIP-qPCR conducted in SJSA-1 cells treated with 20 µM Nutlin for 6 h and 15 h. In line with the observed Pol II binding, H3K27ac occupancy decreased at CGI-associated MDM2 peaks while the levels at non-CGI control sites remained largely unaffected (Fig. 4.13 A). This effect was conserved at both time points, proving that this is no cell cycle-dependent effect. However, this a preliminary result as well and needs to be repeated to make any statements on significant changes.

Nonetheless, since the decrease of H3K27ac was in accordance with other preliminary results and suggests an involvement of MDM2 in CGI-associated gene repression, it was further tested whether this reduced gene activity could also be observed on a global scale. For this purpose, H3K27ac ChIP-seq was conducted in SJSA-1 cells treated with 20 µM Nutlin for 15 h. To be able to monitor quantitative changes in ChIP-seq, chromatin derived from *Drosophila melanogaster* was added to the human chromatin pool prior to IP to serve as external spike-in control. In accordance with the preliminary results obtained from ChIP-qPCR experiments, visual evaluation of the quantitative ChIP-seq revealed a strong decrease of H3K27ac upon Nutlin-treatment that correlated with previously defined MDM2 peaks and CGIs (Fig. 4.13 B).

To test whether H3K27ac is significantly changed at CGIs on a global scale, differential binding analysis of spike-in normalized H3K27ac was performed within a region ± 2000 bp around the gene's TSS. In line with previous results, global H3K27ac occupancy decreased at the tested TSSs as indicated by a shift of the scatter plot median below the $\log_2$ fold-change threshold line (Fig. 4.13 C, red line). Additionally, a large proportion of these TSSs exhibited significant changes of H3K27ac occupancy ($|\log_2 (FC) > 1|$, padj. < 0.05; Fig. 4.13 C, red dots). Again, this finding supports the hypothesis that Nutlin-treatment and subsequent MDM2 chromatin recruitment represses CGI-associated genes.

Since the activating histone mark significantly decreased at most genes upon Nutlin treatment, it was further tested whether these changes are also observable in global gene expression. For this purpose, publicly available gene expression data obtained from SJSA-1 cells treated with 20 µM Nutlin for 6 h (Sriraman et al., 2018) was re-analyzed.

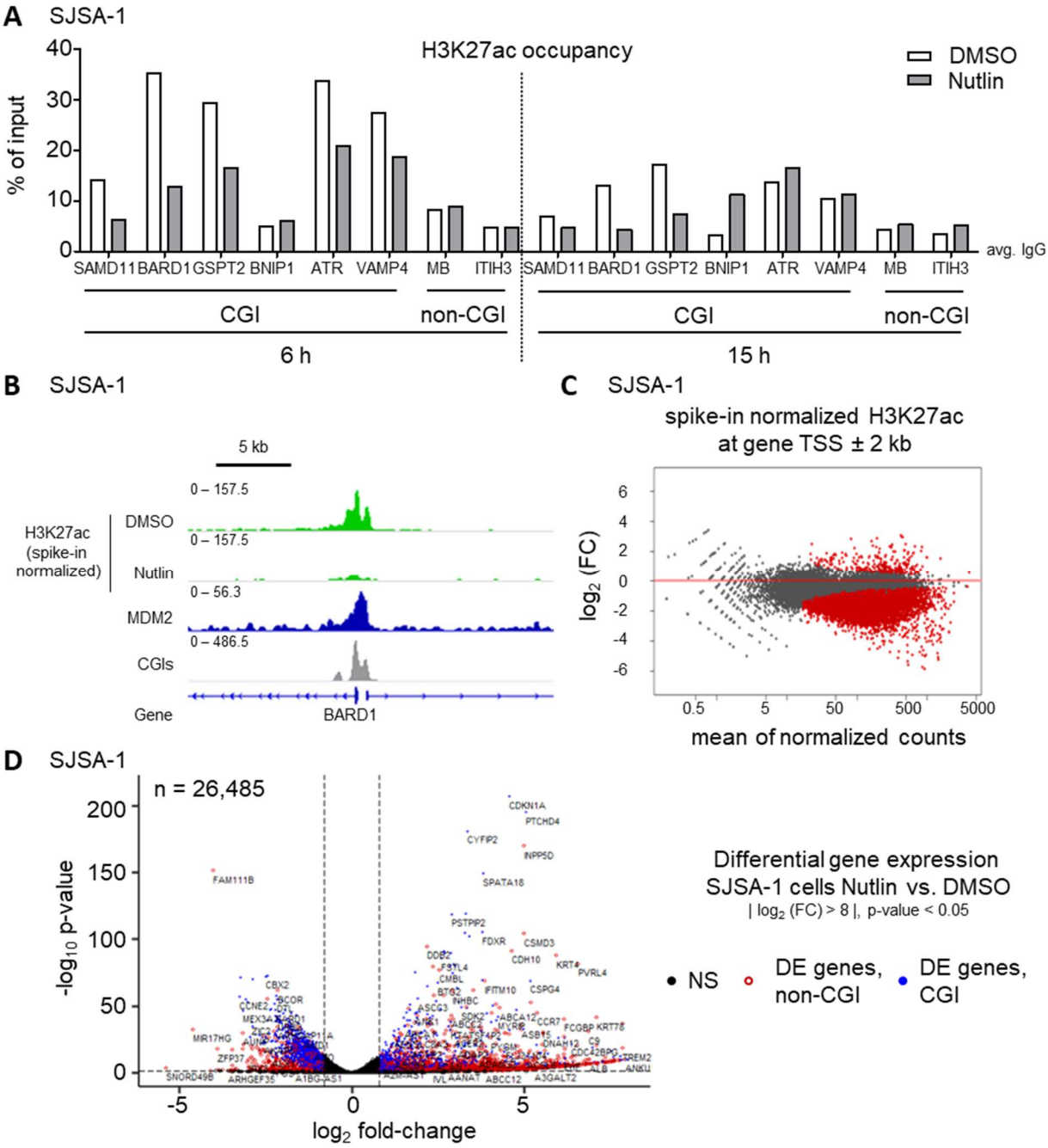

Fig. 4.13: MDM2 represses genes with CGI-associated promoters. (A) H3K27ac occupancy at CGI-associated MDM2 binding sites determined in SJSA-1 cells treated with 20 µM Nutlin-3a for 6 h (left side) and 15 h (right side) using ChIP-qPCR. Non-CGI sites served as negative controls. Asterisks indicate primer binding sites that are not associated with the gene's TSS. Background precipitation (avg. IgG) is indicated as a dotted line. Bar diagrams illustrate the mean ± SEM (n=1). (B) Visualization of spike-in normalized H3K27ac tracks in SJSA-1 cells upon treatment with 20 µM Nutlin-3a or the respective DMSO control for 15 h. H3K27ac signals (green) correlated with previously identified MDM2 peaks (blue) and persistent human CGIs (grey). (C) Differential binding analysis of spike-in normalized H3K27ac signals at hg38 TSSs extended for ± 2000b bp, visualized as MA plot. Red dots highlight differentially bound sites (padj ≤ 0.05). (D) Volcano plot of gene expression analysis conducted in SJSA-1 cells treated with 20 µM Nutlin-3a for 6 h (Sriraman et al., 2018). Genes exhibiting a | $\log_2$ (FC) > 0.8 | and a p-value < 0.05 were shown in red. CGI-associated genes of this subset were highlighted in blue. Genes that did not match these criteria were shown in black (NS).

Differential gene expression analysis was performed using DESeq2 and the results were visualized in a volcano plot (Fig. 4.13 D). Genes exhibiting an absolute log_2 fold-change > 0.8 and a p-value < 0.05 were defined as differentially expressed (DE) genes and displayed as red circles. All genes that did not match these criteria were labeled as “not significant” (NS) and shown in black. Differentially expressed genes were further classified into CGI and non-CGI-associated genes, of which the CGI-associated ones were shown as blue dots while the non-CGI ones remained in red. Analysis of differentially expressed genes matching the selected criteria revealed that genes were more strongly upregulated as indicated by overall higher log_2 fold-changes and $-log_{10}$ p-value values (Fig. 4.13 D, right side). These upregulated genes were comprised of multiple p53 targets such as *CDKN1A*, *SPATA18*, *FDXR*, *ABCA12* and others (Fischer, 2017; International Agency for Research on Cancer, 2020). This indicates that this significant upregulation of genes is largely based on an active p53 response instead of CGI-related gene regulation. In contrast, a strikingly large proportion of downregulated genes was associated with CGIs at their TSS as indicated by an enrichment of blue dots in this subset of genes (Fig. 4.13 D, left side). This completes and further confirms the hypothesis that Nutlin treatment decreases the expression of CGI-associated genes, most likely through MDM2 specifically binding to CGI sites. Taken together, the results shown in this section confirm that Nutlin treatment and subsequent MDM2 chromatin recruitment result in a repression of CGI-associated genes, thus supporting previous preliminary data. However, the function of this global gene repression still needs to be elucidated.

4.9. MDM2 functions as a repressor of inducible gene expression

To identify physiological consequences of the MDM2-mediated repression of CGI-associated genes, gene set enrichment analysis (GSEA) was performed. GSEA is a powerful tool to identify gene signatures enriched in a given gene set by comparing it with publicly available gene sets related to certain physiological processes. This may serve as a first filter to identify processes linked to the present gene expression pattern. To guarantee that the genes submitted to the GSEA analyses are indeed expressed in cells, the gene expression data obtained from DESeq2 was pre-filtered based on the normalized count files generated. This will exclude genes that are only slightly changed upon treatment and thus generate more robust and reliable results. For this purpose, only genes exhibiting a normalized count ≥ 30 in at least one of the samples tested were included into this analysis.

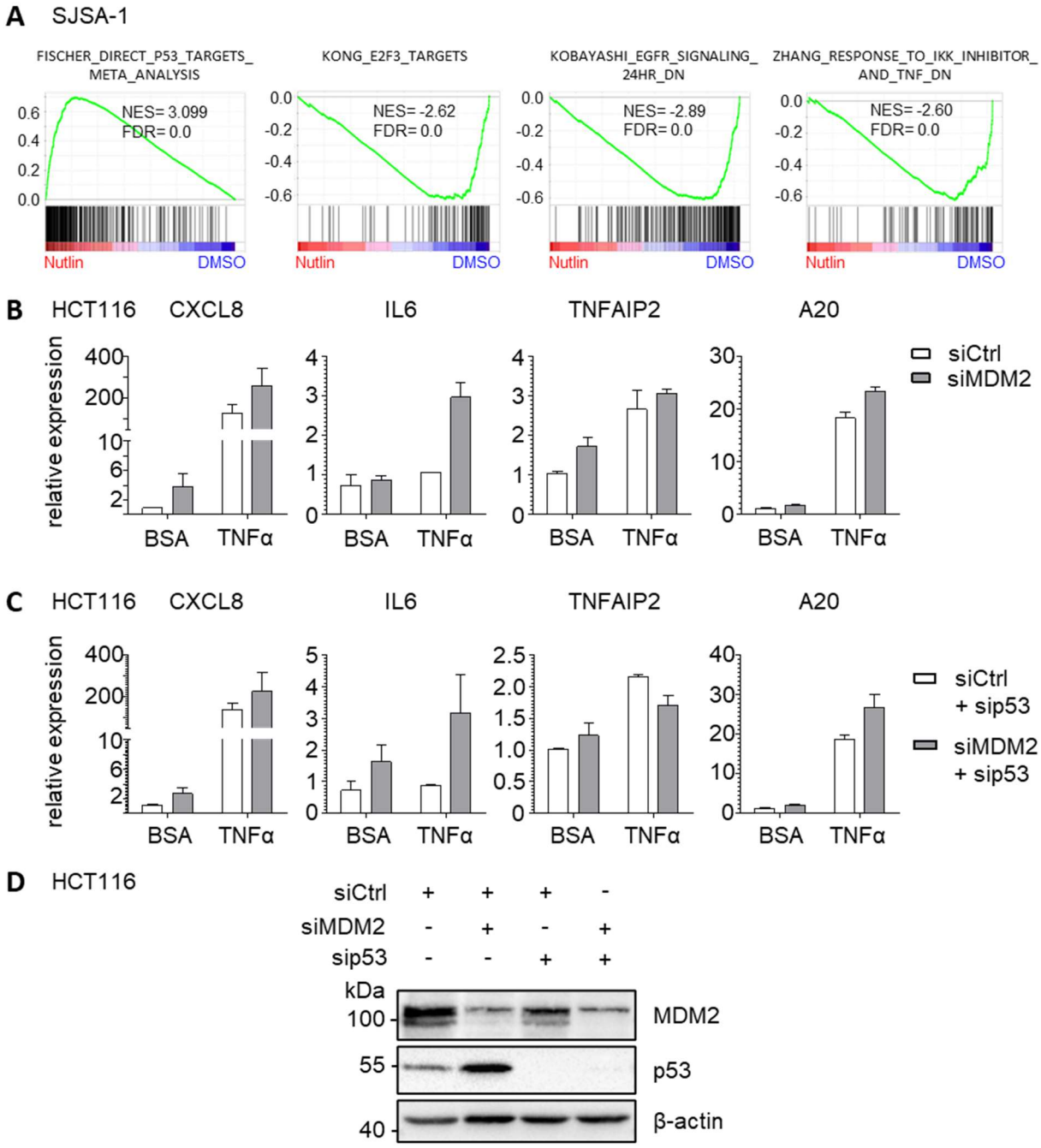

Fig. 4.14: MDM2 represses TNFα-induced genes. (A) Gene set enrichment analysis (GSEA) of genes expressed in SJSA-1 cells upon treatment with 20 µM Nutlin-3a for 6 h. Truly expressed genes were identified prior to GSEA through filtering for genes exhibiting a normalized count ≥ 30 in at least one sample across all conditions and replicates tested. (B) Relative expression of TNFα-responsive genes in HCT116 cells with and without additional MDM2 depletion upon treatment with 10 ng/ml human recombinant TNFα for 1 h. Treatment of cells with BSA served as solvent control. Gene expression was normalized to the expression of the housekeeping gene β-actin and to the ΔCt value of the "Ctrl KD+BSA" condition of the first biological replicate. Data is shown as $\log_2$ fold-change of $2^{-\Delta\Delta Ct}$ and was illustrated as bar diagrams of the mean expression ± SEM (n=2). (C) Repetition of the experiments from (B) with additional p53 depletion in all conditions to exclude p53-dependent effects (n=2). (D) Immunoblot analysis confirming the efficiency of MDM2 and p53 depletion in (B) and (C).

GSEA analysis revealed two major effects. On the one hand, it attested a strong and robust p53 response in SJSA-1 cells upon Nutlin treatment as shown by the enrichment of gene sets related to p53 targets and the diminishment of gene sets describing E2F3 targets (Fig. 4.14 A). On the other hand, the induction of MDM2 through Nutlin treatment strongly reduced gene sets associated with inducible gene expression pathways such as EGF and inflammatory signaling (Fig. 4.14 A). For this purpose, it was tested whether MDM2 fulfills a repressive function in inducible gene expression as well. For these studies, the inflammatory signaling pathway that is inducible by tumor necrosis factor α (TNFα) was chosen as model system. Binding of TNFα to TNF receptor 1 activates a signaling cascade releasing NF-κB transcription factors from their antagonists that results in their nuclear translocation and subsequent target gene induction (Oeckinghaus et al., 2011). To check whether MDM2 represses this TNFα-induced gene expression, MDM2 was depleted from HCT116 cells that were subsequently treated with 10 ng/ml TNFα for 1h. Gene expression analysis of TNFα-induced NF-κB target genes confirmed the results obtained from GSEA. Indeed, MDM2 depletion de-repressed the NF-κB targets *CXCL8* and *TNFAIP2*, even without additional triggering of the signaling cascade (Fig. 4.14 B). This effect was even more pronounced upon additional stimulation of cells by TNFα treatment. In this condition, MDM2 depletion increased the expression of all NF-κB target genes tested, indicating that MDM2 indeed works as a repressor of gene expression in this inducible system.

However as shown by immunoblot analyses, MDM2 depletion also leads to a stabilization of endogenous p53 (Fig. 4.14 D). Indeed, p53 has already been shown to inhibit NF-κB responses through competition for the co-transcriptional factor p300/CBP (Webster and Perkins, 1999). Hence it had to be tested whether the observed effects are MDM2-specific or simply a side-effect of p53 activation due to MDM2 depletion. For this purpose, gene expression studies shown in Fig. 4.14 B were repeated in combination with an additional p53 knockdown in all conditions. In line with previous results, MDM2 depletion still led to a de-repression of NF-κB target genes in both, TNFα and control treated cells, proving that this is an MDM2-specific effect (Fig. 4.14 C).

At next, it should be tested whether this observed MDM2-mediated repression of TNFα-inducible genes depends on KDM2B as well. To avoid potential bias due to the activation of p53 upon MDM2 depletion, the following studies were carried out in PANC-1 cells expressing the R273H a gain-of-function mutant of p53. Since efficient siRNA-mediated knockdown of KDM2B has not worked in our hands so far, the PRC1 enzymatic subunit RNF2 was depleted instead.

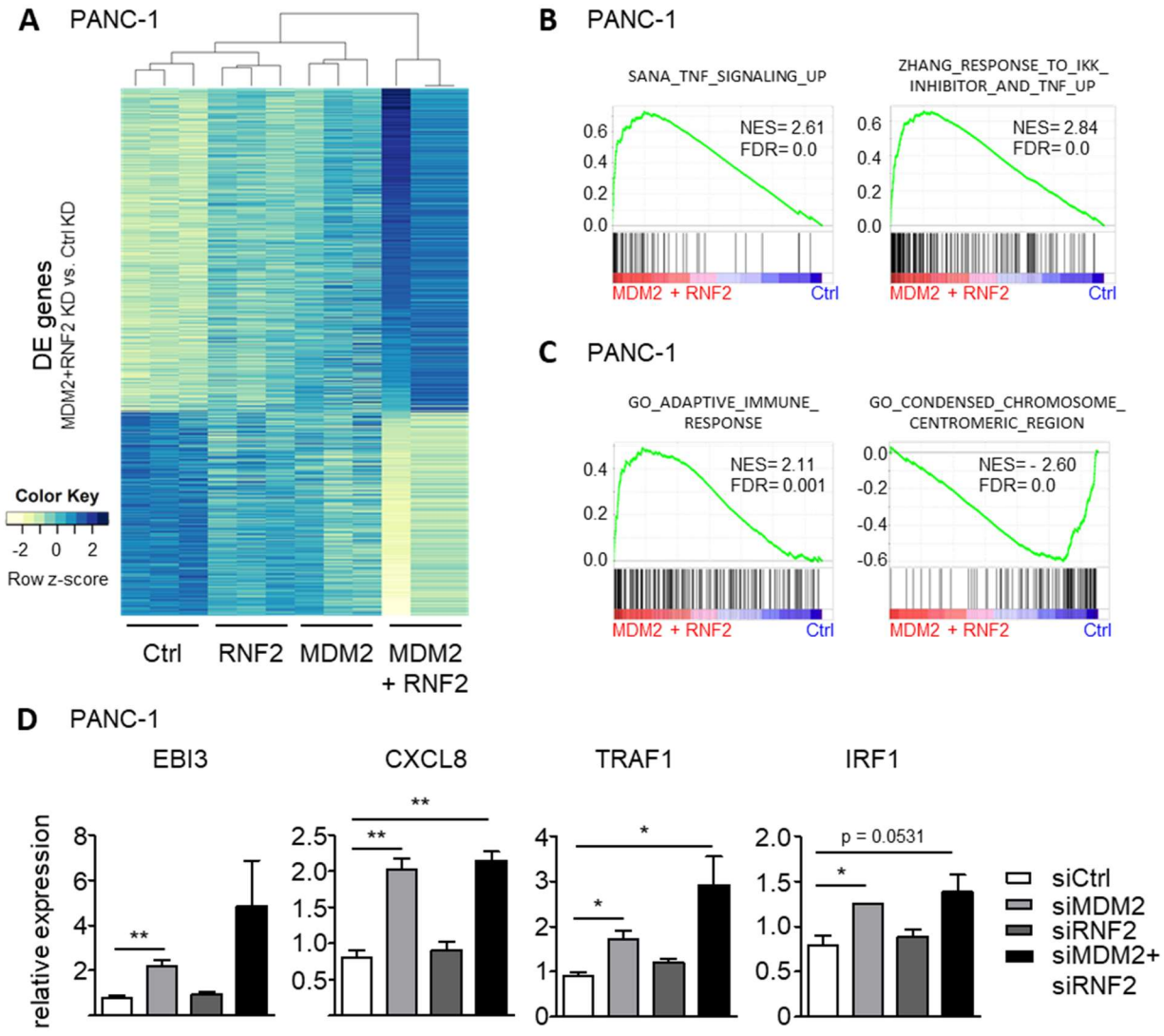

Fig. 4.15: MDM2 and PRC1 regulate NF-κB-responsive genes in PANC-1 cells. (A) Heatmap showing the expression of genes that were differentially expressed in MDM2+RNF2 double knockdown conditions versus control cells (selection criteria: gene base mean > 20, $|\log_2$ (FC) > 0.8, padj. < 0.05). Gene expression of each gene is represented by the individual z-score determined in PANC-1 cells depleted from MDM2, RNF2, both in combination for 72 h and in control cells. (B+C) Gene set enrichment (B) and gene ontology term analysis (C) of pathways and processes enriched in MDM2+RNF2 KD cells in comparison to control cells. (D) Relative expression of NF-κB target genes in PANC-1 cells depleted from MDM2, RNF2 and both in combination for 72 h. Gene expression was normalized to the expression of the housekeeping gene β-actin and to the ΔCt value of the control condition of the first biological replicate. Data is shown as $\log_2$ fold-change of $2^{-\Delta\Delta Ct}$ and was illustrated as bar diagrams of the mean expression ± SEM (n=3). Statistical analyses of samples were performed using two-tailed, unpaired Student's t-tests with a confidence interval of 95 %; * p ≤ 0.05.

Considering that MDM2 colocalizes with KDM2B and RNF2 at CGIs (Fig. 4.5 A) and that KDM2B is a known member of a variant PRC1 complex (Gao et al., 2012), it is quite possible that MDM2 cooperates with PRC1 complexes at CGIs as well. For this purpose, MDM2 and RNF2 were depleted from PANC-1 cells both, alone and in combination, for 72 h prior to further analyses. Total mRNA sequencing conducted in PANC-1 cells confirmed the results of previous publications showing a cooperation of MDM2 and PRC function (Wienken et al., 2016). While depletion of RNF2 or MDM2 alone only slightly affected gene expression, the simultaneous depletion of both synergistically intensified the respective effect on gene expression (Fig. 4.15 A).

Further analysis of differentially expressed genes using GSEA showed an enrichment of gene sets related to inflammatory signaling again (Fig. 4.15 B). This is in line with previous results and confirms a repressive function for MDM2 in inducible gene expression irrespective of the p53 status of cells. Gene ontology (GO) term analysis further verified the repressive function of MDM2 in TNFα-induced gene expression (Fig. 4.15 C). Interestingly GO term analysis also indicated a loss of gene sets associated with pericentromeric chromosome condensation upon depletion of MDM2 and RNF2.

To confirm the RNA-seq results, the expression of TNFα-inducible genes was tested in PANC-1 cells depleted from MDM2, RNF2 and both in combination for 72 h. In accordance to the RNA-seq results from PANC-1 as well as gene expression data from HCT116 cells, the loss of MDM2 significantly de-repressed all genes tested (Fig. 4.15 D). The additional depletion of RNF2 partially fortified this de-repression of genes, like for *EBI3* and *TRAF1*, albeit never to a significant extend. This proves the hypothesis that MDM2 is the crucial factor mediating gene repression.

Collectively, the hypothesis that MDM2 functions as a repressor of inducible gene expression was confirmed using wet lab gene expression analyses in different systems as well as RNA-seq data in PANC-1 cells. The fact that this function is partially supported by PRC1 complexes in PANC-1 cells additionally suggests that the effects are mediated through the interaction of MDM2 and KDM2B. However, it still needs to be evaluated whether additional physiological consequences may arise from this gene regulatory function of MDM2.

4.10. Loss of MDM2 sensitizes cells towards extrinsic apoptosis

In addition to the induction of NF-κB target genes, TNFα-signaling may also result in the induction of extrinsic apoptosis. This is mediated through the formation of a death-inducing signaling complex composed of components of the TNF-signaling pathway and the initiator caspases 8 and 10 (Oeckinghaus et al., 2011). Once activated, these initiator caspases cleave the effector caspases 3 and 7 that cleave further downstream substrates, thus inducing apoptosis (Li and Yuan, 2008). In this regard, the loss of KDM2B has already been reported to sensitize GBM cells towards extrinsic apoptosis induced by TNF-related apoptosis-inducing ligand (TRAIL), supposedly through epigenetic regulation of several antiapoptotic genes (Kurt et al., 2017). Assuming that MDM2 represses TNFα-inducible genes and that MDM2 chromatin recruitment is mediated by KDM2B, it would be possible that MDM2 fulfills a similar protective function towards extrinsic apoptosis as KDM2B. To test this hypothesis, PANC-1 cells were depleted for MDM2, RNF2 or both in combination for 72h and then treated with 10 ng/ml TNFα for 2.5 h. To silence the anti-apoptotic branch of the TNF-signaling cascade, the cells were additionally treated with 2.5 µg/ml cycloheximide (CHX) to inhibit *de novo* translation of anti-apoptotic proteins. Visual evaluation of PANC-1 cells revealed that CHX treatment alone equally affected the cells of all conditions while its combination with TNFα induced more cell death in cells depleted from MDM2+RNF2 compared to others (Fig. 4.16 A).

To further investigate this phenomenon, apoptosis induction was quantified in the same system using the ViaStain™ Live Caspase-3/7 Detection Kit (Nexcelom). This assay is based on the ability of active, pro-apoptotic caspase 3/7 to cleave a small peptide sequence linked to a DNA binding dye with a fluorescent probe, thus enabling this dye to bind to DNA and to emit a fluorescent signal. To determine the fold-induction of apoptosis in each condition, the number of fluorescent cells was normalized to the initial number of apoptotic cells before treatment start (“0 h”) and was plotted as a function over time. In line with the gene expression data, MDM2 and MDM2+RNF2 depletion sensitized PANC-1 cells towards extrinsic apoptosis induced by TNFα in comparison to RNF2 or control knockdowns (Fig. 4.16 B, left panel). Furthermore, parallel treatment of PANC-1 cells with CHX alone revealed no differences between the conditions, confirming the previous visual evaluation (Fig. 4.16 A). The repetition of this experiment using the alternative death ligand TRAIL led to highly comparable results (Fig. 4.16 B, right panel), suggesting that MDM2 protects cells towards extrinsic apoptosis irrespectively of the death ligand used.

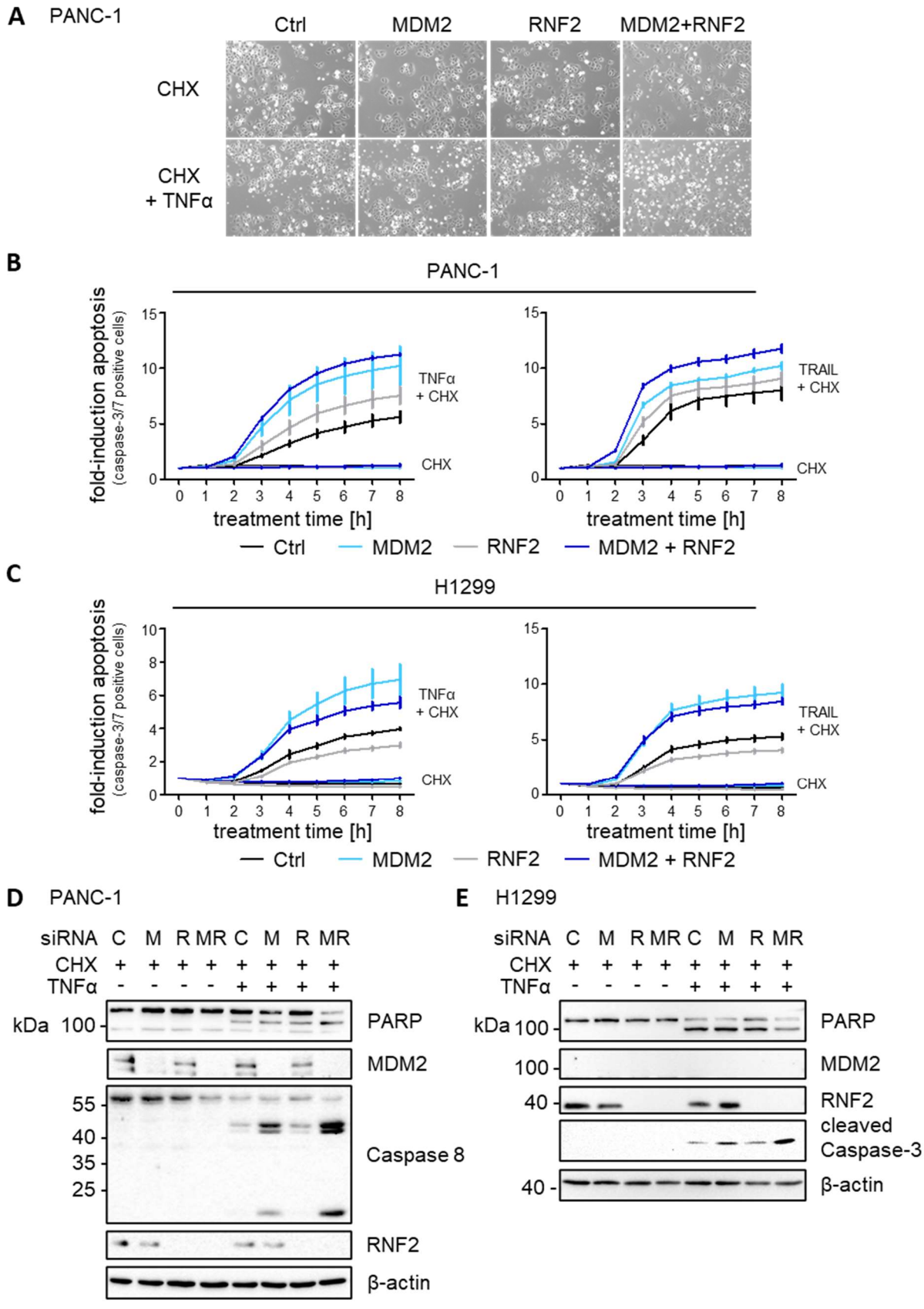

(Figure legend on next page)

Fig. 4.16: Loss of MDM2 sensitizes p53-deficient cells towards extrinsic apoptosis. (A) Brightfield images of PANC-1 cells treated with 2.5 µg/ml CHX alone (upper panel) and in combination with 10 ng/ml TNFα (lower panel) upon depletion of MDM2, RNF2 or both in combination for 72 h. (B+C) Extrinsic apoptosis induction in PANC-1 (B) and H1299 (C) cells depleted for MDM2, RNF2 or both in combination, treated with either 2.5 µg/ml CHX + 10 ng/ml TNFα (left panel) or 2.5 µg/ml CHX + 20 ng/ml TRAIL (right panel). Data is shown as a function of the fold-induction of apoptosis over treatment time (n=1; three technical replicates per condition). (D+E) Immunoblot analyses of whole-cell lysates harvested from PANC-1 (D) and H1299 (E) treated with 2.5 µg/ml CHX + 10 ng/ml TNFα for 2.5 h (D) and 4 h (E) respectively. Knockdown conditions were labeled as followed: Ctrl (C), MDM2 (M), RNF2 (R), MDM2+RNF2 (MR).

To test whether this effect was conferrable to other cellular systems, the same experiment was conducted in the p53-deficient H1299 cell line. Indeed, H1299 cells showed the same sensitization towards extrinsic apoptosis as PANC-1 cells did. This was indicated by nearly doubled apoptosis inductions upon MDM2 and MDM2+RNF2 depletion, irrespective of the death ligand used (Fig. 4.16 C).

The results obtained from the fluorescent-based assays were further confirmed by immunoblot analyses detecting the cleavage of caspase 8 and 3 in PANC-1 and H1299 cells respectively (Fig. 4.16 D+E). In accordance with previous results, treatment of PANC-1 cells with TNFα and CHX led to an increased cleavage of the initiator caspase 8 upon depletion of MDM2 or MDM2+RNF2 in comparison to RNF2 and control knockdowns (Fig. 4.16 D). This was associated by a decrease of full-length PARP in these conditions (Fig. 4.16 D, PARP staining upper band) which is a substrate of activated caspase 3. Similar patterns were observed in immunoblot analyses of whole-cell lysates derived from TNFα + CHX-treated H1299 cells. In this system, elevated cleavage of the effector caspase 3 was monitored upon depletion of MDM2 and MDM2+RNF2 compared to RNF2 and control knockdown associated with reduced levels of full-length PARP (Fig. 4.16 E, lane 5-8). Taken together, MDM2 alone and in combination with PRC1 complexes mediates a resistance towards extrinsic apoptosis, thus providing another potential physiological role of MDM2-mediated gene regulation. However, since the depicted experiments were performed only once, further experiments are required to clarify whether this is indeed a reliable function of MDM2.

5. Discussion

In this thesis, we identified and compared chromatin binding sites of endogenous MDM2 in various cell systems. Analysis and characterization of the determined binding pattern suggest that there are two mechanisms mediating MDM2 chromatin recruitment. Concordant with previous reports, MDM2 binding to p53 target genes is p53-dependent. In contrast, recruitment to other genomic regions occurs in a p53-independent fashion. Detailed analysis of MDM2 chromatin binding sites discovered that MDM2 is recruited to CpG islands via its interaction with the CGI binding histone demethylase KDM2B that also colocalizes with PRC1 complexes. Once recruited, MDM2 seems to repress CGI-associated genes as indicated by reduced H3K27ac occupancy and gene expression data. However, the exact mechanism driving this gene repression and its physiological consequences are still elusive. Preliminary data suggests that MDM2 recruitment could lead to a destabilization of the transcriptional pre-initiation complex, hence reducing Pol II recruitment to genes. Furthermore, the repression of inflammation-related genes and the inhibition of extrinsic apoptosis could represent two potential consequences of MDM2-mediated gene repression. However, these are only suggestions based on preliminary data, hence the exact mechanism of the MDM2-mediated gene repression and its physiological consequences will be subject of further investigations.

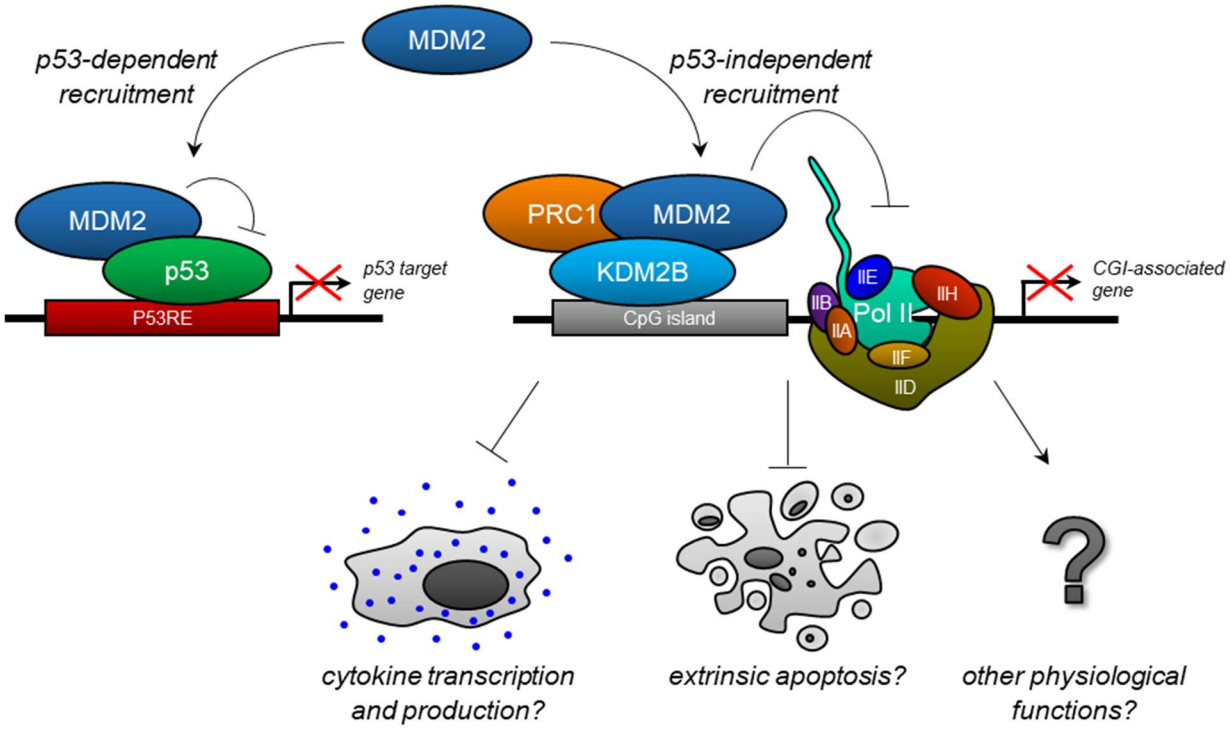

Fig. 5.1: Proposed mechanism of MDM2 chromatin recruitment and its physiological consequences. MDM2 chromatin recruitment is achieved in two ways. While binding to p53 target genes is p53-dependent (left), recruitment of MDM2 to CGIs is mediated through its interaction with KDM2B (right). This leads to a repression of CGI-associated genes that could be involved in the regulation of central physiological processes such as cytokine production, extrinsic apoptosis and potentially other functions that have not been identified yet.

5.1. MDM2 and KDM2B - One interaction, multiple outcomes?

Of all results shown, the interaction of MDM2 and the histone demethylase KDM2B represents one of the key findings of this thesis. Although both proteins have already been studied separately in the context of cancer and other cellular systems (Karni-Schmidt et al., 2016; Vacík et al., 2018; Yan et al., 2018), a connection of both has not been reported yet. However, comparison of their postulated functions in different cell systems reveals high similarities, supporting the finding of an interaction and synergistic function of MDM2 and KDM2B. Hereinafter, the roles of both proteins in different physiological processes and disease are discussed to underline their close relationship.

5.1.1. KDM2B increases MDM2 protein levels

One strong indication that MDM2 is a valuable interaction partner of KDM2B is the fact that the presence of KDM2B increases MDM2 protein levels upon exogenous expression (Fig. 4.9 B). Although the underlying mechanism of this effect remains elusive, there are several hypotheses on how this might be mediated. Beside other substrates such as p53, MDM2 auto-ubiquitinates itself through its C-terminal RING finger, thus affecting its own stability and activity (Fang et al., 2000; Ranaweera and Yang, 2013; Stommel and Wahl, 2004). In this regard, the heterodimerization of MDM2 with its homolog MDMX has already been shown to increase MDM2 protein stability by serving as an alternative ubiquitination substrate and hence buffering the MDM2 auto-ubiquitination (Linke et al., 2008). Accordingly, the interaction of KDM2B with MDM2 could potentially result in a reduced auto-ubiquitination as well, thus stabilizing MDM2 protein levels. To test this hypothesis, experiments overexpressing MDM2 and KDM2B alone and in combination could be conducted in H1299 cells and MDM2 and KDM2B protein stability could be determined using a subsequent CHX chase.

Another possibility how KDM2B could sustain MDM2 protein levels in cells is through regulation of the MDM2 antagonist $p14^{ARF}$. *In vitro* as well as overexpression experiments conducted in HeLa cells revealed that $p14^{ARF}$ binds to the C-terminal domain of MDM2, resulting in decreased MDM2 protein stability and an inhibition of nuclear-cytoplasmic shuttling (Tao and Levine, 1999; Zhang et al., 1998). KDM2B was shown to restrain $p14^{ARF}$ expression by increasing PRC1 and PRC2-mediated repression of the *INK4A/ARF* locus along with removing of the activating histone mark H3K36me2 through the KDM2B JmjC-domain (Tzatsos et al., 2008). To test this idea, one could again make use of the mentioned overexpression system in H1299 cells and determine endogenous $p14^{ARF}$ levels upon KDM2B overexpression. Furthermore, an additional depletion of $p14^{ARF}$ prior to overexpression of MDM2 and KDM2B could help to answer the question whether the downregulation of endogenous $p14^{ARF}$ through

KDM2B causes elevated MDM2 protein stability. Considering these two mechanisms, KDM2B would have several options to sustain the levels of its interaction partner MDM2, thus supporting its own function.

5.1.2. Cellular functions common to MDM2 and KDM2B

5.1.2.1. MDM2 and KDM2B are regulators of gene expression

In addition to effects on MDM2 protein stability, the close relationship of MDM2 and KDM2B is also proven by similar functions carried out in different cell systems. Of the numerous functions reported for KDM2B, transcriptional repression is the most important one being the underlying cause of multiple different physiological outcomes (Vacík et al., 2018; Yan et al., 2018). KDM2B has been shown to fulfill this function through H3K36me2 and H3K4me3 demethylation (Kang et al., 2018; Tzatsos et al., 2008; Zheng et al., 2018) as well as independently of its JmjC-demethylase domain (Andricovich et al., 2016; Turberfield et al., 2019).

Although its involvement in global, CGI-associated gene repression is a novelty first described in the present study, MDM2 has already been reported to regulate gene expression in other ways. Similar to KDM2B, MDM2 has been shown to affect the formation of both, activating and repressive histone marks *in vivo* and *in vitro* and to suppress gene transcription in a p53-independent manner (Minsky and Oren, 2004). This finding has been extended by the discovery of MDM2 being a direct interaction partner of Polycomb repressor complexes that supports the formation of repressive H3K27me3 and H2AK119ub1 (Wienken et al., 2016). However, MDM2 has also been reported to regulate transcription in histone-independent ways, for instance through direct interactions with transcription factors or their associated factors as well as promotion of mRNA stabilization and translation (Biderman et al., 2012; Riscal et al., 2016). The fact that both proteins regulate gene expression in a histone-dependent and -independent manner represents their first, and probably most important, common feature that can now be expanded for the synergistic regulation of CGI-associated genes by MDM2 and KDM2B.

5.1.2.2. MDM2 and KDM2B as promoters of cellular stemness

As a consequence of gene regulation, MDM2 and KDM2B have both been shown to maintain cellular stemness through their cooperation with Polycomb repressor complexes. In this context, KDM2B has been reported to repress early lineage-specific genes in murine embryonic stem cells, thus suppressing their differentiation into tissue-specific cell types. This depends on the site-specific binding of KDM2B through its CxxC-domain and subsequent

recruitment of PRC1 complexes leading to gene repression (He et al., 2013). Strikingly, this effect is not restricted to pluripotent cells. Experiments conducted in the pre-adipocyte cell line 3T3-L1 revealed that the KDM2B-PRC1 axis represses their differentiation into adipocytes as well (Inagaki et al., 2015). Hence, the recruitment of PRC1 complexes to differentiation-associated genes via the KDM2B CxxC-domain seems to be a major driver of stemness in all cell systems. Concordant with these findings, KDM2B supports the reprogramming of MEFs into induced pluripotent stem cells by binding to mesoderm-specific genes via its CxxC-domain and recruiting variant PRC1 complexes (Zhou et al., 2017). Importantly, the JmjC-demethylase domain of KDM2B supports its role in cellular reprogramming by removing H3K36me2 at the promoters of early reprogramming genes that is supposed to facilitate the binding of pluripotency factors (Liang et al., 2012). The importance of KDM2B in the maintenance of cellular stemness is also reflected in transgenic KDM2B mouse models. While the total ablation of KDM2B from germline cells is embryonic lethal (Andricovich et al., 2016), the restricted deletion of its CxxC-domain results in malformations of the spine and severe delays in embryonic development (Blackledge et al., 2014).

Similar phenotypes were also reported for transgenic mouse models targeting MDM2. While heterozygous mice develop normally, the homozygous deletion of MDM2 results in an embryonic lethality occurring between the implantation and E6.5 upon fertilization (Jones et al., 1995; Montes de Oca Luna et al., 1995). Since this phenotype is completely resolved by simultaneous p53 deletion, it was postulated that this effect bases on the p53 antagonism mediated by MDM2. However, recent studies prove that MDM2 itself promotes stemness as shown by an increased pluripotent stem cell induction in the presence of MDM2 and an elevated differentiation of mesenchymal stem cells into osteoblasts upon MDM2 depletion (Wienken et al., 2016). Unlike postulated, this function is p53-independent and relies on the interaction of MDM2 and PRC2 complexes, thus proving that MDM2 and KDM2B promote cellular stemness in a highly similar fashion.

5.1.2.3. MDM2 and KDM2B maintain redox homeostasis

Another common function that relies on MDM2 and KDM2B-regulated gene expression is the detoxification of cells through the reduction of cellular H_2O_2 levels. H_2O_2 is a reactive oxygen species (ROS) that is mainly generated through the conversion of superoxide, a byproduct of the respiratory chain of cells, by superoxide dismutases (Lennicke et al., 2015). Although the conversion of superoxide to the less reactive H_2O_2 represents a major mechanism to prevent oxidative damage in cells, H_2O_2 may also harm cells and trigger tumorigenesis. Elevated H_2O_2 levels may function as a secondary messenger inducing pro-proliferative signaling pathways and oxidize guanine to 8-oxo-guanine (Lennicke et al., 2015; Nakabeppu, 2014). This alternative guanine form is incorporated into the DNA and pairs with adenine and cytosine

which may result in stable G-to-T transversions and increased mutation rates in cells (Nakabeppu, 2014). For this purpose, tight regulation and maintenance of the redox homeostasis in cells through the antioxidant system is essential to keep their mutagenic rate minimal. MDM2 as well as KDM2B have both been shown to regulate the expression of various genes encoding members of the antioxidant system (Polytarchou et al., 2008; Riscal et al., 2016). But in contrast to developmental genes, MDM2 and KDM2B promote their expression instead of suppressing it and different regulatory mechanisms have been reported for both proteins to achieve this. While MDM2 regulates genes involved in the synthesis and recycling of the antioxidant glutathione through its interaction with ATF3/4, KDM2B regulates genes of other antioxidative responses through the removal of H3K36me2 via its JmjC-domain (Polytarchou et al., 2008; Riscal et al., 2016). However, despite the seemingly different mechanisms of MDM2 and KDM2B-mediated gene expression in this context, there are still some conformities between both studies suggesting the presence of a common, underlying process. Looking at the genes responsive to MDM2 and KDM2B expression, the gene *NQO1* was shown to be regulated by both proteins (Polytarchou et al., 2008; Riscal et al., 2016). Furthermore, closer examination of the qPCR assay published by Tsichlis and colleagues revealed that several genes related to glutathione synthesis and recycling, such as *Gpx3-7*, *Gstk1* and *Gsr*, were 0.67-fold and 1.33-fold upregulated upon KDM2B OE respectively (Polytarchou et al., 2008). Collectively, comparison of these results points to a common role of MDM2 and KDM2B in the maintenance of the redox homeostasis through the regulation of glutathione levels. This might be based on their interaction at target gene promoters; however, further studies are required to prove this hypothesis.

5.1.2.4. MDM2 and KDM2B function as oncogenic factors

In addition to their depicted roles in normal tissue homeostasis, MDM2 and KDM2B function as oncogenic factors driving tumor maintenance and spreading. During tumorigenesis, cells acquire certain characteristics enabling them to form continuously growing primary tumors that may spread into surrounding tissues. One of these so called “Hallmarks of Cancer” (Hanahan and Weinberg, 2011) that is, at least partially, regulated by MDM2 and KDM2B is the resistance to cell death.

Cells may die from various different processes such as apoptosis, pryoptosis, necrosis, necroptosis or autophagy (D’Arcy, 2019), of which apoptosis is the most common one. It describes a “programmed” cell death relying on the action of caspases, a family of cysteine-aspartic proteases. They get activated upon cleavage and induce cell death through proteolytic processes resulting in e.g. DNA fragmentation, protein crosslinking or the proteolysis of nuclear and cytosolic proteins (D’Arcy, 2019; Li and Yuan, 2008). There are two signaling cascades initiating apoptosis: the extrinsic and the intrinsic pathway. Extrinsic apoptosis is

mediated through binding of death ligands, such as tumor necrosis factors, to their respective receptors. This triggers the oligomerization of death receptors and the recruitment of a death-inducing signaling complex that induces the self-cleavage of the initiator caspases 8 and 10. In turn, caspase 8 and 10 cleave the effector caspases 3 and 7 which induce cell death through proteolysis (D'Arcy, 2019; Elmore, 2007). In contrast, intrinsic apoptosis pathways induce changes within the mitochondrial transmembrane potential and an opening of the mitochondrial permeability transition pore. This releases pro-apoptotic factors, such as cytochrome c, from the mitochondrial intermembrane space into the cytoplasm, resulting in the formation of an apoptosome, and subsequent activation of the initiator caspase 9 (Elmore, 2007; Haupt et al., 2003).

Interestingly, p53 regulates target genes involved in both apoptosis pathways. It induces the expression of the death receptors Fas and DR5 and regulates cytochrome c-release from mitochondria through its target genes *BAX*, *BBC3*, *NOXA* and *BID* (Haupt et al., 2003). Accordingly, MDM2 has frequently been shown to inhibit apoptosis by antagonizing p53 function (Ciardullo et al., 2019; Feng et al., 2016; De Rozieres et al., 2000; Yu et al., 2019), and even in the context of death ligand-induced apoptosis, MDM2 inhibition is mainly regarded as a way to activate p53 to fortify apoptosis induction (Hori et al., 2010; Singh et al., 2016; Urso et al., 2017). Therefore, it is even more surprising that MDM2 seems to promote the resistance towards TNFα and TRAIL-induced extrinsic apoptosis in p53-deficient cells (Fig. 4.16). One potential mechanism mediating this function would be the regulation of XIAP. XIAP is an inhibitor of the effector caspases 3 and 7, whose protein levels are mainly regulated on the translational level. MDM2 has been shown to bind to the internal ribosome entry segment within the 5' UTR of XIAP mRNA, thus facilitating its translation (Gu et al., 2009). Therefore, indirect regulation of apoptosis through upregulation of a caspase inhibitor would represent a suitable mechanism for MDM2 to mediate the resistance towards extrinsic apoptosis.

However, considering that the observed anti-apoptotic effect of MDM2 was supported by PRC1 complexes in PANC-1 and H1299 cells, it would also be possible that this physiological role is again mediated through the interaction with KDM2B. Indeed, KDM2B has also been reported to suppress extrinsic apoptosis, thus contributing to the resistance towards TRAIL-induced apoptosis in various cancer entities (Ge et al., 2011; Kurt et al., 2017). Although the proposed mechanisms mediating this resistance were focusing on different components of the apoptotic signaling cascade, both studies have proven that KDM2B-regulated gene expression is the driving force of it. Therefore, assuming that MDM2 and KDM2B cooperate in regulating gene transcription, it would also be possible that this physiological role of MDM2 is based on the MDM2-KDM2B interaction that has been identified in this work.

In addition to cell death resistance, the activation of cell invasion and metastasis is another "Hallmark of Cancer" that is affected by MDM2 and KDM2B. Invasion of cancer cells into surrounding tissues and subsequent metastasis formation are facilitated by epithelial-mesenchymal transition (EMT). EMT is a reversible process through which epithelial cells convert to a mesenchymal-like state that contributes to tumor initiation, spreading and the resistance towards chemotherapeutic and immunologic therapies. It bases on the downregulation of epithelial genes and the concomitant upregulation of genes expressed in mesenchymal cells. This results in the loss of epithelial-like characteristics such as lateral cell-cell contacts or connections to the underlying basal membrane, thus increasing cell motility and cancer cell dissemination (Dongre and Weinberg, 2019).

KDM2B has been shown to be an oncogenic factor driving EMT in cancer cells. Studies showing that KDM2B mRNA expression is regulated through fibroblast growth factor-B in different cancer entities (Kottakis et al., 2011; Zacharopoulou et al., 2018) and that KDM2B accumulates in high-grade malignant tissues already point to a tumor-promoting role (Kottakis et al., 2011; Kuang et al., 2017; Quan et al., 2020; Tzatsos et al., 2013). This is further supported by investigations showing that KDM2B expression increases cell proliferation, migration and invasion of mouse embryonic fibroblasts as well as pancreatic, ovarian (OvCar) and prostate cancer cells (Kottakis et al., 2011; Kuang et al., 2017; Quan et al., 2020; Tzatsos et al., 2013; Zacharopoulou et al., 2018). In line, xenograft experiments revealed that implanted cancer cells lacking KDM2B are less potent to form tumors in mice (Kuang et al., 2017; Tzatsos et al., 2013), thus proving that KDM2B also promotes tumorigenesis *in vivo*. Although the detailed underlying mechanisms varied between the different cancer entities, all publications prove that the tumor-promoting function of KDM2B relies on gene regulation assisted by PRC2 complexes. Accordingly, EZH2 has also been reported to be significantly higher expressed in high-grade pancreatic ductal adenocarcinoma (PDAC) cells and in ovarian cancers (Kuang et al., 2017; Ougolkov et al., 2008).

Since MDM2 colocalizes with KDM2B and Polycomb repressor complexes at CGI-associated genes to regulate their expression, it would be plausible if MDM2 fulfills similar functions in tumor progression as KDM2B. Indeed, MDM2 also accumulates in OvCar tissues in an ascending fashion depending on the severity grade of the tumor while normal tissues exhibit low MDM2 levels (Chen et al., 2017). Furthermore, MDM2 supports the proliferation of PDAC and hepatocellular carcinoma cells (HCC) (Li et al., 2017; Wang et al., 2019). Additional wound healing and transwell assays revealed that MDM2 also contributes to the migration and invasion of PDAC, OvCar and HCC cells (Chen et al., 2017; Li et al., 2017; Wang et al., 2019). Again, this oncogenic potential of MDM2 was confirmed in mouse xenograft and patient-derived xenograft studies showing that MDM2 inhibition diminishes HCC tumor formation *in*

vivo (Wang et al., 2019). Detailed mechanisms on how MDM2 facilitates tumor progression are not described except for the fact that MDM2 inhibition associates with a downregulation of the epithelial marker E-cadherin and a concomitant upregulation of the mesenchymal markers N-cadherin and vimentin (Wang et al., 2019). But considering that the depicted published data highlight identical roles for MDM2 and KDM2B in tumor progression, it is indeed possible that this is another commonality that relies on the cooperation of MDM2 and KDM2B in gene regulation.

Taken together, the comparison of published MDM2 and KDM2B functions in various systems and context revealed highly similar roles for both proteins in normal cells as well as in malignant tissues. This strongly supports our finding that MDM2 and KDM2B cooperate with each other in regulating gene expression and that this interaction is a fundamental mechanism of multiple different processes shaping a cell's phenotype.

5.2. KDM2A - A backup for KDM2B?

Assuming that the cooperation of MDM2 and KDM2B builds the basis of various physiological functions in cells, it would be interesting to investigate whether a similar interaction exists between MDM2 and the KDM2B-paralog KDM2A. An own protein sequence analysis using Blastp (NCBI) revealed that KDM2A and B exhibit a sequence homology of 70-85 % depending on the respective domain (data not shown). Hence it would be possible that MDM2 interacts with KDM2A as well.

Based on their high sequence homology, KDM2A and KDM2B share several characteristics. Studies conducted in mouse embryonic stem cells and MEFs revealed that KDM2A co-occupies CGIs along with KDM2B and that this specific CGI-binding is mediated through its structurally highly similar CxxC-domain (Blackledge et al., 2010; Turberfield et al., 2019). Notably, KDM2A binding to CGIs does not directly depend on the presence of multiple CpG dinucleotides but rather correlates with the methylation status of annotated CGIs (Blackledge et al., 2010). According to this, "strong" CGIs exhibiting large stretches of non-methylated DNA are supposed to register higher KDM2A occupancies than weak ones. This is in line with our conclusions drawn from the comparison of MDM2, KDM2B and RNF2 chromatin-binding at annotated CGIs (Fig. 4.5 A+B). Motif analysis of the CGIs showing the highest MDM2 occupancy revealed that MDM2 and KDM2B preferably bind to CGIs exhibiting several CpG dinucleotides and high GC content. Although this is no direct factor driving KDM2A recruitment (Blackledge et al., 2010), it is still another characteristic of CGIs that may be used as an indicator of the "strength" of the respective CGI. Therefore, it is valid to say that MDM2 and

KDM2A both preferably associate with “strong” CGIs, hence strengthening the hypothesis that they might interact with each other.

In addition to common binding sites, KDM2A and KDM2B also share several functions that, partially, also agree with accounted roles for MDM2. Like KDM2B, KDM2A is a regulator of cellular differentiation as shown by increased differentiation of mesenchymal stem cells into cells of the adipogenic, chondrogenic, osteogenic and dentinogenic lineage upon KDM2A depletion (Dong et al., 2013; Yu et al., 2016). At least in case of the osteo- and dentinogenic differentiation, this effect depends on KDM2A and BCOR-mediated gene repression and the associated removal of H3K36me2 and H3K4me3, hence showing high conformity to KDM2B (Yu et al., 2016). Concordant with these findings, results published by Zeng and colleagues revealed that KDM2A elevates the somatic reprogramming of MEFs in the presence of vitamin-C (Wang et al., 2011a). However, this function strongly depends on its cooperation with KDM2B, with KDM2B being the predominant factor promoting cellular stemness while KDM2A only played a supportive role. Similar effects have recently been published by Klose and colleagues in the context of gene expression. Chromatin-binding studies of KDM2A and KDM2B along with corresponding gene expression analyses conducted in mouse embryonic stem cells revealed that both proteins contribute to the repression of CGI-associated genes. But again, KDM2B was the predominant factor mediating the repression of the vast majority of differentially regulated genes while KDM2A only contributed to the repression of a small proportion of genes (Turberfield et al., 2019). Taken together, KDM2A and KDM2B fulfill similar functions but, despite expressing highly homologous functional domains, KDM2B seems to be the main factor affecting general CGI-associated gene expression. This could argue against a potential interaction and cooperation of MDM2 and KDM2A on CGIs.

KDM2A additionally functions as a promoter of genome stability through the maintenance of pericentromeric heterochromatin in a KDM2B-independent fashion. Pericentromeric heterochromatin is part of the persistent, constitutive heterochromatin and is transcriptionally silenced by DNA methylation and large stretches of repressive H3K9me3 that is bound by heterochromatin protein 1 (HP1). Functionally, constitutive heterochromatin is essential to fundamental cellular processes such as chromosome segregation or the silencing of repetitive sequences (Janssen et al., 2018). In this context, KDM2A has been shown to directly interact with HP1 through an HP1-binding motif that is not expressed in KDM2B (Borgel et al., 2017). Based on this domain, KDM2A can be recruited to pericentromeric heterochromatin and subsequently repress satellite DNA within these regions in a demethylase-dependent manner (Frescas et al., 2008). Furthermore, it can bind to non-methylated CGIs within pericentromeric regions, thus promoting HP1 recruitment and contributing to the formation and maintenance of heterochromatin compaction.

Interestingly, GO term analysis of gene expression data raised in PANC-1 cells depleted from MDM2 and MDM2+RNF2 revealed a downregulation of gene sets related to condensed chromosomes and the condensation of centromeric regions (Fig. 4.15 C, data not shown for MDM2 depletion alone). This suggests that MDM2 might support the protective role of KDM2A in genome stability. Another interesting aspect is that the additional loss of RNF2 fortifies the enrichment of GO terms associated with condensed chromosomes and chromosomal segregation in comparison to MDM2 knockdown alone (data not shown). Although KDM2A is no known PcG component, canonical PRC1 complexes have already been shown to associate with constitutive heterochromatin that has lost DNA methylation-mediated repression in malignant systems. The formation of these so called “PcG bodies” supposedly functions as a buffering system to compensate for the loss of heterochromatin compaction, thus maintaining genome stability (Brückmann et al., 2018; Johansen, 2020). Since MDM2 is known to physically interact with Polycomb complexes (Wienken et al., 2016), it would be possible that MDM2 serves as a link facilitating PRC1 recruitment to non-methylated pericentromeric regions bound by KDM2A, hence fulfilling a role in genome stability as well. At first glance, this hypothesis contradicts previous publications showing that MDM2 promotes genomic instability through the delay of the DNA damage signaling cascade and inhibition of the transcriptional repressor HBP-1 (Bouska et al., 2008; Cao et al., 2019). However, these studies were mainly performed using MDM2 overexpression hence it would be possible that MDM2 fulfills different functions in cells exhibiting physiological MDM2 levels compared to MDM2 overexpressing systems. Furthermore, the H1299 system was used to study the impact of MDM2 depletion in genomic instability and MDM2 has previously been shown to fulfill anti-tumorigenic functions by supporting DNA replication in these cells (Klusmann et al., 2018). Hence it is not excluded that this function contributes to the establishment of the genomic instability phenotype. Therefore, it is still possible that MDM2 functions as a double-edged sword, promoting heterogeneity preferably in cancer cells expressing high MDM2 levels while protecting non-transformed cells from genome instability through its potential interaction with KDM2A.

5.3. The MDM2-KDM2 axis as a prolonged arm of p53?

The idea that MDM2 fulfills p53-independent functions preventing tumorigenesis in normal cells is tempting considering that MDM2 is rapidly induced upon p53 activation. Indeed, there are already several hints indicating a tumor suppressive role of MDM2 in several systems as reviewed by Manfredi in 2010 (Manfredi, 2010). Therefore, it will be subsequently discussed whether this newly discovered MDM2-KDM2 axis may be implemented into physiological p53 responses and thus work as a prolonged arm of the “guardian of the genome” (Lane, 1992).

P53 is known to prevent tumor development by promoting cell cycle arrest, apoptosis, DNA repair or cellular senescence through inducing the expression of a wide variety of target genes in response to genotoxic stresses and DNA damage (Kastenhuber and Lowe, 2017). In this regard, the MDM2-KDM2 axis could potentially sustain p53 responses in cells trough fortifying the induction of p53 target genes. Our study has proven that MDM2 is recruited to CGIs upon Nutlin treatment and that its binding correlates with a global repression of CGI-associated genes as well as a reduction of chromatin-associated Pol II without changing the overall Pol II protein levels (Fig. 4.11-13). Assuming that this dissociated Pol II is still capable to initiate transcription, MDM2-dependent gene repression could potentially result in a redistribution of Pol II from CGI-associated to p53 target genes. Thus, MDM2 would fortify the expression of p53 target genes in the context of cellular stress. Of course, this is just a hypothesis that requires further confirmation. To address this question, Nutlin-induced p53 target gene expression as well as Pol II chromatin binding could be determined in the presence and absence of MDM2. This would show whether MDM2 depletion prevents Pol II reduction at CGI-associated genes and inhibits its recruitment to p53 target sites. Furthermore, the physiological consequences of p53 target gene induction could be measured using propidium-iodine-based cell cycle analysis or immunofluorescence-based quantification of the DNA damage marker γH2AX.

In addition to the depicted well-known p53 functions, recent publications highlight that p53 may not only react on existing DNA damage, but even prevent its occurrence through regulating DNA replication (Gottifredi and Wiesmüller, 2018). There are several mechanisms proposed through which p53 should fulfill this regulatory function. On the one hand, p53 directly associates with DNA replication forks and facilitates replication-coupled DNA repair based on its exonuclease activity and on interactions with proteins involved in DNA repair mechanisms (Hampp et al., 2016; Roy et al., 2018). On the other hand, p53 was also reported to increase the fidelity of DNA replication forks through orchestrating DNA replication and ongoing transcription (Yeo et al., 2016). In line with these findings, our group has proven that p53 resolves the interference between DNA replication and transcription indirectly through MDM2 expression (Klusmann et al., 2016, 2018). MDM2 supports DNA replication in primary and malignant cells, supposedly by preventing the excessive formation of R-loops. R-loops are formed through the hybridization of RNA with its template DNA and the subsequent exposure of the complementary, single DNA strand. Although they may occur as natural byproducts of ongoing transcription, increased R-loop formation also represents an obstacle for DNA replication forks (Crossley et al., 2019). MDM2 has been demonstrated to inhibit excessive R-loop formation by maintaining the repressive epigenetic landscape through its interaction with PRC1 complexes and the formation of H2AK119ub1 (Klusmann et al., 2018; Wienken et al., 2016).

However, additional mechanisms on how MDM2 might facilitate DNA replication are conceivable, considering its interaction with KDM2B and Polycomb repressor complexes. In addition to the CxxC-domain facilitating CGI binding, the PHD finger located in the center of KDM2 proteins as well as their JmjC-demethylase domain could enable them to additionally associate with sites of H3K36 methylation (Sanchez and Zhou, 2011; Yan et al., 2018). Strikingly, H3K36 methylations do not only decorate actively transcribed genes but have also been shown to facilitate a wide range of DNA repair mechanisms. Experiments using a system to induce site-specific DNA double strand breaks revealed that ambient H3K36me3 serves as docking platform for proteins mediating the resection of damaged DNA, thus promoting homologous recombination repair (Pfister et al., 2014). Furthermore, increased H3K36me3 levels that were established during G1 and S phase of the cell cycle are directly bound by the mismatch repair complex MutSα to ensure rapid DNA repair during replication (Li et al., 2013). Similar effects were also published for the di-methylation of histone 3 at this site. H3K36me2 has been shown to be rapidly induced in response to DNA double strand breaks and to mediate non-homologous end-joining of damaged sites through interactions with MRN complex members and the Ku70 protein (Fnu et al., 2011). In line with these findings, KDM2A has recently been reported to accumulate at induced DNA double-strand breaks due to its JmjC and CxxC-domains and to facilitate the recruitment, ubiquitination and subsequent stabilization of 53BP1, another factor promoting non-homologous end-joining (Bueno et al., 2018). In addition to H3K36 methylation, the DNA damage-sensitizing protein PARP1 represents another way to recruit KDM2 proteins to DNA damage sites. A variant PRC1 complex comprising KDM2B, PCGF1 and RNF2 was shown to represses transcription around DNA damage sites through the formation of H2AK119ub1 and to promote the exchange of H2A by the H2A.Z variant within damaged sites. This renders the chromatin right at these site more accessible to repair factors, resulting in an increased homologous recombination in the presence of KDM2B (Rona et al., 2018). Further evidence of this DNA repair-promoting role of KDM2B has been provided by Hamerlik and colleagues showing that KDM2B depletion in glioblastoma cells results in increased DNA damage foci and diminished DNA repair capacities (Staberg et al., 2018). Comparable to KDM2B, PRC2 complexes are recruited to DNA damage sites in a PARP-dependent manner and support the repair of double-strand breaks (Campbell et al., 2013). Taking together, the depicted published data already demonstrates a close involvement of KDM2 proteins and PRC complexes in DNA repair mechanisms. Considering that MDM2 interacts with both, it would be feasible that these interactions drive MDM2 recruitment to DNA damage sites as well and that MDM2 facilitates DNA repair in the context of physiological p53 responses in a yet unknown fashion.

In addition to DNA repair, the regulation of replication initiation from replication origins represents another way to sustain DNA replication in cells. The human genome comprises

about 100,000 replication origins that are licensed by loading of MCM helicases during the G1 phase of the cell cycle. This ensures a rapid replication initiation at about 20-30 % of all primed origins upon entering the S-phase (Courtot et al., 2018). Similar to transcription, replication initiation requires the recruitment of pre-recognition and pre-initiation complexes, hence accessible genomic regions are prone to harbor replication origins. Accordingly, CpG islands frequently correlate with both, transcription as well as replication initiation sites (Delgado et al., 1998). Considering that MDM2 is recruited to CGIs upon induction (Fig. 4.4+5) and that CGI-associated replication origins are activated in the early S-phase (Delgado et al., 1998), MDM2 might play an important role in licensing replication origins prior to S-phase. This seemingly contradicts published data showing that MDM2 expression accelerates the S-phase entry, resulting in the activation of the DNA damage response and the suppression of origin firing in early S-phase (Frum et al., 2014). However, since these experiments were conducted in p53 null systems, these effects rely on the absence of a p53-mediated cell cycle arrest that is normally induced by active DNA damage responses. Therefore, these results are, most likely, not applicable to p53-proficient systems and hence, it would still be possible that MDM2 contributes to physiological p53 responses through the regulation of CGI-associated origin firing. A potential mechanism how MDM2 may fulfill this function is already indicated by our preliminary results showing decreased Pol II occupancies at CGIs upon Nutlin-treatment (Fig. 4.11). MDM2 and KDM2B-driven removal of the transcriptional machinery from CGIs might make room for the recruitment of replicative pre-initiation complexes and subsequent replication initiation, thus supporting DNA replication.

Considering the depicted published data, there are several possibilities how the MDM2-KDM2 axis might contribute to p53 responses and fulfill tumor-suppressive functions (Fig. 5.2). P53 responses might be fortified through the simultaneous repression of CGI-associated genes by MDM2 and KDM2B. Furthermore, MDM2 might support DNA repair through its recruitment to DNA damage sites via interaction with KDM2 proteins and/or PRC complexes and support DNA repair. In addition to these general mechanisms that might take place during all p53 responses, there are additional scenarios possible depending on when p53 is activated during the cell cycle. P53 is activated upon DNA damage and might induce both, a G1/S and a G2/M arrest of cell cycle (Kastenhuber and Lowe, 2017). In case of a G1/S arrest, the removal of Pol II machineries at CGIs due to KDM2B-dependent MDM2 recruitment could additionally facilitate origin licensing at those sites, thus ensuring the rapid progression into S-phase upon termination of p53 responses (Fig. 5.2, left panel). In contrast, p53-induced G2/M cell cycle arrest could provide a time window for MDM2 to interact with KDM2A bound to pericentromeric heterochromatin and to promote chromosome condensation during M-phase.

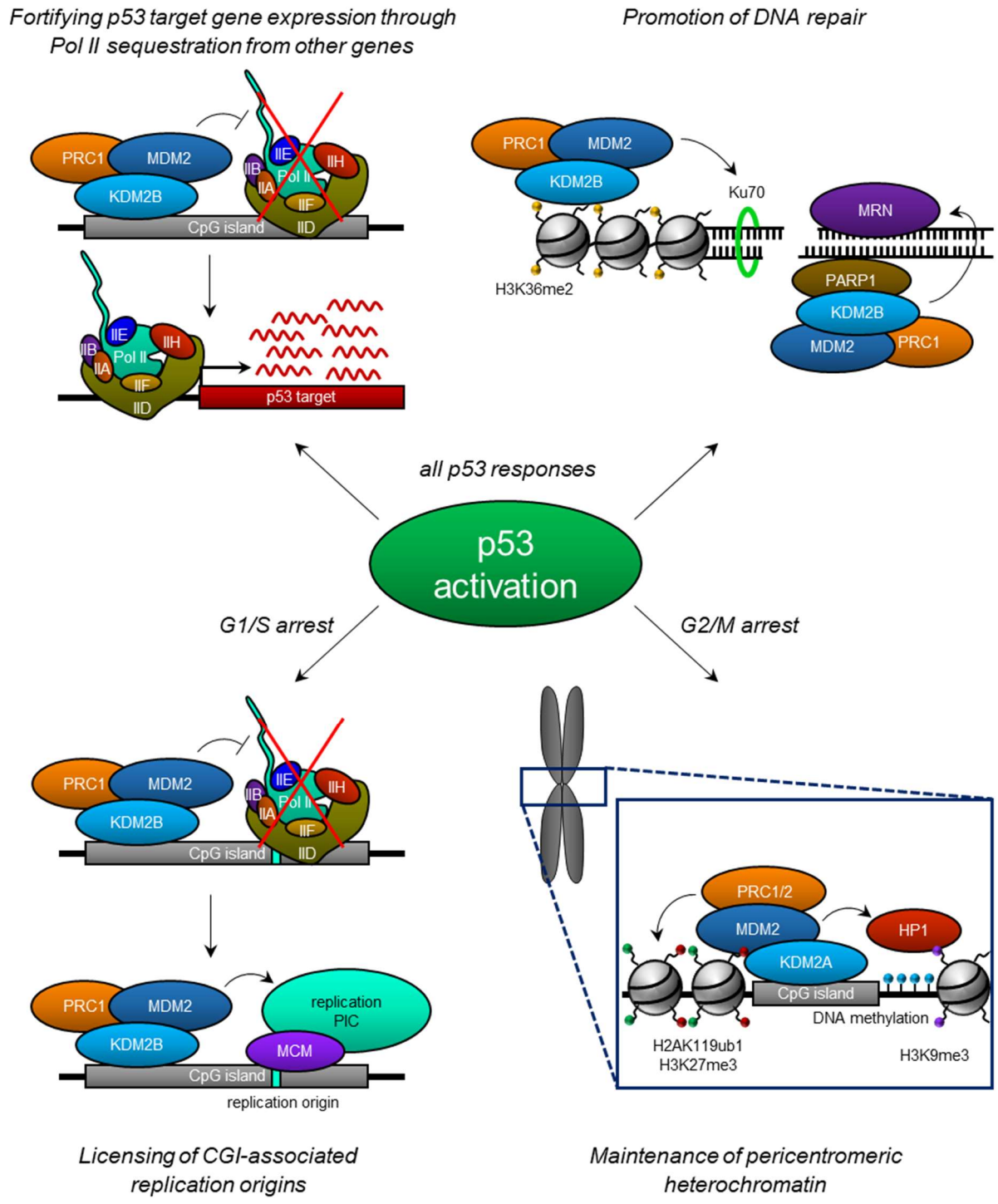

Fig. 5.2: Hypothetical model illustrating the potential involvement of the MDM2-KDM2 axis in p53 responses. The MDM2-KDM2 axis might contribute to physiological p53 responses in several manners. Generally, it might fortify p53 target gene expression through sequestration of Pol II transcription machineries from CGI-associated genes to p53 targets (upper left) and support DNA repair mechanisms (upper right). Notably, DNA repair through homologous recombination (MRN) or non-homologous end-joining (Ku70) could both be promoted by MDM2 and KDM2 proteins. Additionally, the MDM2-KDM2 axis might promote the assembly of pre-replicative complexes at CGI-associated origins through the removal of Pol II machineries (lower left) prior to S-phase and support chromosomal segregation through the maintenance of pericentromeric heterochromatin prior to M-phase (lower right).

Worth noticing, this is a purely hypothetical model on how the MDM2-KDM2 axis might be implemented in physiological p53 responses, hence intensive studies are required to test for all hypotheses depicted above.

5.4. Clinical relevance

Considering that the MDM2-KDM2 axis is involved in such a large variety of physiological relevant processes even in the absence of functional p53, MDM2 and KDM2B in combination with PRC complexes might serve as attractive therapeutic targets to treat cancer patients.

One potential therapeutic approach would be the selective treatment of malignancies exhibiting elevated levels of KDM2B, PRC complexes or MDM2. Pre-clinical studies targeting PDAC cells with accumulated nuclear EZH2 have already proven that the depletion of EZH2 increases the sensitivity of cells towards Gemcitabine treatment (Ougolkov et al., 2008). Similarly, MDM2 inhibition reduces the resistance of HCC and triple-negative breast cancer cells towards chemotherapeutics (Fan et al., 2019; Wang et al., 2019). Additionally, the depletion and inhibition of KDM2B diminishes the stemness of stem-like glioblastoma cells and sensitizes them towards chemotherapeutic treatment (Staberg et al., 2018). The fact that high MDM2 and KDM2B levels promote tumor formation in xenograft experiments (Tzatsos et al., 2013; Wang et al., 2019) discloses another potential field of application for MDM2 and KDM2B inhibition, namely the prevention of tumor metastases. As a prerequisite of such pre-clinical studies, specific inhibitors targeting the respective substrate are required. Surprisingly, this could still be a bottleneck restricting such preclinical studies since there is currently no inhibitor available that specifically targets KDM2B without additional affecting of other lysine demethylases (Staberg et al., 2018; Yan et al., 2018). However, a functional cooperation of MDM2 and KDM2B could help to overcome this problem. In contrast to KDM2B, there are numerous MDM2 inhibitors available targeting both, the N-terminal p53-binding domain as well as its C-terminal RING finger (Burgess et al., 2016). Considering that MDM2 and KDM2B physically interact with each other and support their cellular functions, it would be possible that targeting MDM2 could serve as an alternative treatment to kill KDM2B-dependent cancers. However, this requires further testing and evaluation through extensive pre-clinical studies in both, cell culture as well as xenograft systems.

5.5. Concluding remarks and future prospects

In conclusion, this study has proven that two mechanisms mediate the association of MDM2 with chromatin. On the one hand and in accordance with previous publications, MDM2 is recruited to p53 target genes in a p53-dependent fashion. On the other hand, additional p53-independent chromatin recruitment was detected even in the presence of wild-type p53.

Furthermore, this study provides the first identification and characterization of genome-wide MDM2 chromatin-binding sites in multiple cell lines with different p53 status. Comparison of MDM2 peaks called in the different systems revealed that MDM2 preferably associates with CpG islands and it strongly suggests that this binding is driven through its interaction with the lysine demethylase KDM2B. Furthermore, first functional analyses of MDM2-associated CGIs suggest that MDM2 recruitment affects basal transcription by reducing Pol II occupancy at those sites, leading to a global repression of CGI-associated genes.

This gene regulatory function of the MDM2-KDM2B axis was not only restricted to basal transcription but was also present in inducible systems. For instance, pilot experiments presented in this study revealed a clear repressive function of MDM2 on TNF-inducible gene expression and extrinsic apoptosis that was supported by PRC1 complexes. However, the exact mechanism underlying this phenomenon is still elusive and literature research regarding the different functions of MDM2 and KDM2B in cells revealed that many more processes might rely on the identified MDM2-KDM2B axis. Therefore, as diverse the physiological roles of this interaction might be, as numerous are the future studies that would need to be conducted to evaluate all hypothetical mechanisms. At first, experiments confirming the gene regulatory functions of the MDM2-KDM2B axis need to be repeated and complemented by further investigations addressing the question how MDM2 and KDM2B induce the removal of Pol II from CGI-associated genes. Furthermore, it needs to be tested whether MDM2 interacts with KDM2A. Upon clarifying that, the depicted hypotheses on the potential physiological roles of the MDM2-KDM2 axis might serve as basis for numerous further studies. Hence, this thesis represents the cornerstone of many potential follow-up studies that might add an entirely new layer of p53-driven tumor suppression through the MDM2-KDM2 axis and might contribute to new therapeutic approaches for cancer patients through combined targeting of MDM2 and KDM2B.

6. References

Ahn, S.H., Kim, M., and Buratowski, S. (2004). Phosphorylation of Serine 2 within the RNA Polymerase II C-Terminal Domain Couples Transcription and 3′ End Processing. Mol. Cell *13*, 67–76.

Allen, B.L., and Taatjes, D.J. (2015). The Mediator complex: A central integrator of transcription. Nat. Rev. Mol. Cell Biol. *16*, 155–166.

Anders, S., Pyl, P.T., and Huber, W. (2015). HTSeq-A Python framework to work with high-throughput sequencing data. Bioinformatics *31*, 166–169.

Andrews, S., Krueger, F., Seconds-Pichon, A., Biggins, F., and Wingett, S. (2015). FastQC. A quality control tool for high throughput sequence data. Babraham Bioinformatics. Babraham Inst. *1*, 1.

Andricovich, J., Kai, Y., Peng, W., Foudi, A., and Tzatsos, A. (2016). Epigenetic regulation of lineage commitment in normal and malignant hematopoiesis by histone demethylase KDM2B. J *126*, 905–920.

Baek, H.J., Kang, Y.K., and Roeder, R.G. (2006). Human mediator enhances basal transcription by facilitating recruitment of transcription factor IIB during preinitiation complex assembly. J. Biol. Chem. *281*, 15172–15181.

Bálint, E., Bates, S., and Vousden, K.H. (1999). Mdm2 binds p73α without targeting degradation. Oncogene *18*, 3923–3929.

Barak, Y., Gottlieb, E., Juven-Gershon, T., and Oren, M. (1994). Regulation of mdm2 expression by p53: Alternative promoters produce transcripts with nonidentical translation potential. Genes Dev. *8*, 1739–1749.

Barski, A., Cuddapah, S., Cui, K., Roh, T.Y., Schones, D.E., Wang, Z., Wei, G., Chepelev, I., and Zhao, K. (2007). High-Resolution Profiling of Histone Methylations in the Human Genome. Cell *129*, 823–837.

Bernstein, B.E., Kamal, M., Lindblad-Toh, K., Bekiranov, S., Bailey, D.K., Huebert, D.J., McMahon, S., Karlsson, E.K., Kulbokas, E.J., Gingeras, T.R., et al. (2005). Genomic maps and comparative analysis of histone modifications in human and mouse. Cell *120*, 169–181.

Biderman, L., Manley, J.L., and Prives, C. (2012). Mdm2 and MdmX as Regulators of Gene Expression. Genes and Cancer *3*, 264–273.

Bird, A. (2002). Epigentic Memory. Genes Dev. *16*, 16–21.

Bird, A., Taggart, M., Frommer, M., Miller, O.J., and Macleod, D. (1985). A fraction of the mouse genome that is derived from islands of nonmethylated, CpG-rich DNA. Cell *40*, 91–99.

Blackledge, N.P., and Klose, R.J. (2011). CpG island chromatin: A platform for gene regulation. Epigenetics *6*, 147–152.

Blackledge, N.P., Zhou, J.C., Tolstorukov, M.Y., Farcas, A.M., Park, P.J., and Klose, R.J. (2010). CpG Islands Recruit a Histone H3 Lysine 36 Demethylase. Mol. Cell *38*, 179–190.

Blackledge, N.P., Farcas, A.M., Kondo, T., King, H.W., McGouran, J.F., Hanssen, L.L.P., Ito, S., Cooper, S., Kondo, K., Koseki, Y., et al. (2014). Variant PRC1 complex-dependent H2A ubiquitylation drives PRC2 recruitment and polycomb domain formation. Cell *157*, 1445–1459.

Blighe, K., Rana, S., and Lewis, M. (2019). EnhancedVolcano: Publication-ready volcano plots with enhanced colouring and labeling. R package version 1.4.0. Https://Github.Com/Kevinblighe/EnhancedVolcano.

Borgel, J., Tyl, M., Schiller, K., Pusztai, Z., Dooley, C.M., Deng, W., Wooding, C., White, R.J., Warnecke, T., Leonhardt, H., et al. (2017). KDM2A integrates DNA and histone modification signals through a CXXC/PHD module and direct interaction with HP1. Nucleic Acids Res. *45*, 1114–1129.

Bouska, A., Lushnikova, T., Plaza, S., and Eischen, C.M. (2008). Mdm2 Promotes Genetic Instability and Transformation Independent of p53. Mol. Cell. Biol. *28*, 4862–4874.

Boyd, S.D., Tsai, K.Y., and Jacks, T. (2000). An intact HDM2 RING-finger domain is required for nuclear exclusion of p53. Nat. Cell Biol. *2*, 563–568.

Bradner, J.E., Hnisz, D., and Young, R.A. (2017). Transcriptional Addiction in Cancer. Cell *168*, 629–643.

Brooks, C.L., Li, M., Hu, M., Shi, Y., and Gu, W. (2007). The p53-Mdm2-HAUSP complex is involved in p53 stabilization by HAUSP. Oncogene *26*, 7262–7266.

Brückmann, N.H., Pedersen, C.B., Ditzel, H.J., and Gjerstorff, M.F. (2018). Epigenetic reprogramming of pericentromeric satellite DNA in premalignant and malignant lesions. Mol. Cancer Res. *16*, 417–427.

Bueno, M.T.D., Baldascini, M., Richard, S., and Lowndes, N.F. (2018). Recruitment of lysine demethylase 2A to DNA double strand breaks and its interaction with 53BP1 ensures genome stability. Oncotarget *9*, 15915–15930.

Burgess, A., Chia, K.M., Haupt, S., Thomas, D., Haupt, Y., and Lim, E. (2016). Clinical overview of MDM2/X-targeted therapies. Front. Oncol. *6*, 1–7.

Busuttil, V., Droin, N., McCormick, L., Bernassol, F., Candi, E., Melino, G., and Green, D.R. (2010). NF-κB inhibits T-cell activation-induced, p73-dependent cell death by induction of MDM2. Proc. Natl. Acad. Sci. U. S. A. *107*, 18061–18066.

Campanero, M.R., Armstrong, M.I., and Flemington, E.K. (2000). CpG methylation as a mechanism for the regulation of E2F activity. Proc. Natl. Acad. Sci. U. S. A. *97*, 6481–6486.

Campbell, S., Ismail, I.H., Young, L.C., Poirier, G.G., and Hendzel, M.J. (2013). Polycomb repressive complex 2 contributes to DNA double-strand break repair. Cell Cycle *12*, 2675–2683.

Cao, Z., Xue, J., Cheng, Y., Wang, J., Liu, Y., Li, H., Jiang, W., Li, G., Gui, Y., and Zhang, X. (2019). MDM2 promotes genome instability by ubiquitinating the transcription factor HBP1. Oncogene *38*, 4835–4855.

Carter, S., Bischof, O., Dejean, A., and Vousden, K.H. (2007). C-terminal modifications regulate MDM2 dissociation and nuclear export of p53. Nat. Cell Biol. *9*, 428–435.

Cerami, E., Gao, J., Dogrusoz, U., Gross, B.E., Sumer, S.O., Aksoy, B.A., Jacobsen, A., Byrne, C.J., Heuer, M.L., Larsson, E., et al. (2012). The cBio Cancer Genomics Portal: An open platform for exploring multidimensional cancer genomics data. Cancer Discov. *2*, 401–404.

Chen, E.Y., Tan, C.M., Kou, Y., Duan, Q., Wang, Z., Meirelles, G. V., Clark, N.R., and Ma'ayan, A. (2013). Enrichr: Interactive and collaborative HTML5 gene list enrichment analysis tool. BMC Bioinformatics *14*.

Chen, J., Marechal, V., and Levine, A.J. (1993). Mapping of the p53 and mdm-2 interaction domains. Mol. Cell. Biol. *13*, 4107–4114.

Chen, Y., Wang, D.D., Wu, Y.P., Su, D., Zhou, T.Y., Gai, R.H., Fu, Y.Y., Zheng, L., He, Q.J., Zhu, H., et al. (2017). MDM2 promotes epithelial-mesenchymal transition and metastasis of ovarian cancer SKOV3 cells. Br. J. Cancer *117*, 1192–1201.

Chittock, E.C., Latwiel, S., Miller, T.C.R., and Müller, C.W. (2017). Molecular architecture of polycomb repressive complexes. Biochem. Soc. Trans. *45*, 193–205.

Chomczynski, P., and Sacchi, N. (1987). Single-step method of RNA isolation by acid guanidinium thiocyanate-phenol-chloroform extraction. Anal. Biochem. *162*, 156–159.

Choy, J.S., Wei, S., Lee, J.Y., Tan, S., Chu, S., and Lee, T.H. (2010). DNA methylation increases nucleosome compaction and rigidity. J. Am. Chem. Soc. *132*, 1782–1783.

Ciardullo, C., Aptullahoglu, E., Woodhouse, L., Lin, W.Y., Wallis, J.P., Marr, H., Marshall, S., Bown, N., Willmore, E., and Lunec, J. (2019). Non-genotoxic MDM2 inhibition selectively

induces a pro-apoptotic p53 gene signature in chronic lymphocytic leukemia cells. Haematologica *104*, 2429–2442.

Cojocaru, M., Jeronimo, C., Forget, D., Bouchard, A., Bergeron, D., Côte, P., Poirier, G.G., Greenblatt, J., and Coulombe, B. (2008). Genomic location of the human RNA polymerase II general machinery: Evidence for a role of TFIIF and Rpb7 at both early and late stages of transcription. Biochem. J. *409*, 139–147.

Cosgrove, M.S., Boeke, J.D., and Wolberger, C. (2004). Regulated nucleosome mobility and the histone code. Nat. Struct. Mol. Biol. *11*, 1037–1043.

Courtot, L., Hoffmann, J.S., and Bergoglio, V. (2018). The protective role of dormant origins in response to replicative stress. Int. J. Mol. Sci. *19*.

Cramer, P., Armache, K.-J., Baumli, S., Benkert, S., Brueckner, F., Buchen, C., Damsma, G.E., Dengl, S., Geiger, S.R., Jasiak, A.J., et al. (2008). Structure of Eukaryotic RNA Polymerases. Annu. Rev. Biophys. *37*, 337–352.

Creyghton, M.P., Cheng, A.W., Welstead, G.G., Kooistra, T., Carey, B.W., Steine, E.J., Hanna, J., Lodato, M.A., Frampton, G.M., Sharp, P.A., et al. (2010). Histone H3K27ac separates active from poised enhancers and predicts developmental state. Proc. Natl. Acad. Sci. U. S. A. *107*, 21931–21936.

Cross, B., Chen, L., Cheng, Q., Li, B., Yuan, Z.M., and Chen, J. (2011). Inhibition of p53 DNA binding function by the MDM2 protein acidic domain. J. Biol. Chem. *286*, 16018–16029.

Crossley, M.P., Bocek, M., and Cimprich, K.A. (2019). R-Loops as Cellular Regulators and Genomic Threats. Mol. Cell *73*, 398–411.

D'Arcy, M.S. (2019). Cell death: a review of the major forms of apoptosis, necrosis and autophagy. Cell Biol. Int. *43*, 582–592.

D'Oto, A., Tian, Q., Davidoff, A.M., and Yang, J. (2016). Histone Demethylases and Their Roles in Cancer Epigenetics. J. Med. Oncol. Ther. *01*, 34–40.

Dana, H., Chalbatani, G.M., Mahmoodzadeh, H., Karimloo, R., Rezaiean, O., Moradzadeh, A., Mehmandoost, N., Moazzen, F., Mazraeh, A., Marmari, V., et al. (2017). Molecular Mechanisms and Biological Functions of siRNA. Int. J. Biomed. Sci. *13*, 48–57.

Davis, C.A., Hitz, B.C., Sloan, C.A., Chan, E.T., Davidson, J.M., Gabdank, I., Hilton, J.A., Jain, K., Baymuradov, U.K., Narayanan, A.K., et al. (2018). The Encyclopedia of DNA elements (ENCODE): Data portal update. Nucleic Acids Res. *46*, D794–D801.

Deaton, A.M., and Bird, A. (2011). CpG islands and the regulation of transcription. Genes Dev.

25, 1010–1022.

Delgado, S., Gómez, M., Bird, A., and Antequera, F. (1998). Initiation of DNA replication at CpG islands in mammalian chromosomes. EMBO J. *17*, 2426–2435.

Denissov, S., Van Driel, M., Voit, R., Hekkelman, M., Hulsen, T., Hernandez, N., Grummt, I., Wehrens, R., and Stunnenberg, H. (2007). Identification of novel functional TBP-binding sites and general factor repertoires. EMBO J. *26*, 944–954.

Ding, Q., Zhang, Z., Liu, J.J., Jiang, N., Zhang, J., Ross, T.M., Chu, X.J., Bartkovitz, D., Podlaski, F., Janson, C., et al. (2013). Discovery of RG7388, a potent and selective p53-MDM2 inhibitor in clinical development. J. Med. Chem. *56*, 5979–5983.

Dobbelstein, M., Wienzek, S., König, C., and Roth, J. (1999). Inactivation of the p53-homologue p73 by the mdm2-oncoprotein. Oncogene *18*, 2101–2106.

Dobin, A., Davis, C.A., Schlesinger, F., Drenkow, J., Zaleski, C., Jha, S., Batut, P., Chaisson, M., and Gingeras, T.R. (2013). STAR: Ultrafast universal RNA-seq aligner. Bioinformatics *29*, 15–21.

Dong, R., Yao, R., Du, J., Wang, S., and Fan, Z. (2013). Depletion of histone demethylase KDM2A enhanced the adipogenic and chondrogenic differentiation potentials of stem cells from apical papilla. Exp. Cell Res. *319*, 2874–2882.

Dongre, A., and Weinberg, R.A. (2019). New insights into the mechanisms of epithelial–mesenchymal transition and implications for cancer. Nat. Rev. Mol. Cell Biol. *20*, 69–84.

Duncan, I.M. (1982). Polycomblike: A gene that appears to be required for the normal expression of the bithorax and antennapedia gene complexes of Drosophila melanogaster. Genetics *102*, 49–70.

Dunham, I., Kundaje, A., Aldred, S.F., Collins, P.J., Davis, C.A., Doyle, F., Epstein, C.B., Frietze, S., Harrow, J., Kaul, R., et al. (2012). An integrated encyclopedia of DNA elements in the human genome. Nature *489*, 57–74.

Dvir, A. (2002). Promoter escape by RNA polymerase II. Biochim. Biophys. Acta - Gene Struct. Expr. *1577*, 208–223.

Ebmeier, C.C., Erickson, B., Allen, B.L., Allen, M.A., Kim, H., Fong, N., Jacobsen, J.R., Liang, K., Shilatifard, A., Dowell, R.D., et al. (2017). Human TFIIH Kinase CDK7 Regulates Transcription-Associated Chromatin Modifications. Cell Rep. *20*, 1173–1186.

Elmore, S. (2007). Apoptosis: A Review of Programmed Cell Death. Toxicol. Pathol. *35*, 495–516.

Esnault, C., Ghavi-Helm, Y., Brun, S., Soutourina, J., Van Berkum, N., Boschiero, C., Holstege, F., and Werner, M. (2008). Mediator-Dependent Recruitment of TFIIH Modules in Preinitiation Complex. Mol. Cell *31*, 337–346.

Espinosa, J.M., and Emerson, B.M. (2001). Transcriptional regulation by p53 through intrinsic DNA/chromatin binding and site-directed cofactor recruitment. Mol. Cell *8*, 57–69.

Fåhraeus, R., and Olivares-Illana, V. (2014). MDM2's social network. Oncogene *33*, 4365–4376.

Fakharzadeh, S.S., Trusko, S.P., and George, D.L. (1991). Tumorigenic potential associated with enhanced expression of a gene that is amplified in a mouse tumor cell line. EMBO J. *10*, 1565–1569.

Fan, Y., Li, M., Ma, K., Hu, Y., Jing, J., Shi, Y., Li, E., and Dong, D. (2019). Dual-target MDM2/MDMX inhibitor increases the sensitization of doxorubicin and inhibits migration and invasion abilities of triple-negative breast cancer cells through activation of TAB1/TAK1/p38 MAPK pathway. Cancer Biol. Ther. *20*, 617–632.

Fang, S., Jensen, J.P., Ludwig, R.L., Vousden, K.H., and Weissman, A.M. (2000). Mdm2 is a RING finger-dependent ubiquitin protein ligase for itself and p53. J. Biol. Chem. *275*, 8945–8951.

Farcas, A.M., Blackledge, N.P., Sudbery, I., Long, H.K., McGouran, J.F., Rose, N.R., Lee, S., Sims, D., Cerase, A., Sheahan, T.W., et al. (2012). KDM2B links the polycomb repressive complex 1 (PRC1) to recognition of CpG islands. Elife *2012*, 1–26.

Feng, F.Y., Zhang, Y., Kothari, V., Evans, J.R., Jackson, W.C., Chen, W., Johnson, S.B., Luczak, C., Wang, S., and Hamstra, D.A. (2016). MDM2 Inhibition Sensitizes Prostate Cancer Cells to Androgen Ablation and Radiotherapy in a p53-Dependent Manner. Neoplasia (United States) *18*, 213–222.

Feng, J., Liu, T., Qin, B., Zhang, Y., and Liu, X.S. (2012). Identifying ChIP-seq enrichment using MACS. Nat. Protoc. *7*, 1728–1740.

Fischer, M. (2017). Census and evaluation of p53 target genes. Oncogene *36*, 3943–3956.

Fnu, S., Williamson, E.A., De Haro, L.P., Brenneman, M., Wray, J., Shaheen, M., Radhakrishnan, K., Lee, S.H., Nickoloff, J.A., and Hromas, R. (2011). Methylation of histone H3 lysine 36 enhances DNA repair by nonhomologous end-joining. Proc. Natl. Acad. Sci. U. S. A. *108*, 540–545.

Francis, N.J., Kingston, R.E., and Woodcock, C.L. (2004). Chromatin compaction by a polycomb group protein complex. Science (80-.). *306*, 1574–1577.

Frescas, D., Guardavaccaro, D., Kuchay, S.M., Kato, H., Poleshko, A., Basrur, V., Elenitoba-Johnson, K.S., Katz, R.A., and Pagano, M. (2008). KDM2A represses transcription of centromeric satellite repeats and maintains the heterochromatic state. Cell Cycle *7*, 3539–3547.

Frum, R.A., Singh, S., Vaughan, C., Mukhopadhyay, N.D., Grossman, S.R., Windle, B., Deb, S., and Deb, S.P. (2014). The human oncoprotein MDM2 induces replication stress eliciting early intra-S-phase checkpoint response and inhibition of DNA replication origin firing. Nucleic Acids Res. *42*, 926–940.

Fu, W., Ma, Q., Chen, L., Li, P., Zhang, M., Ramamoorthy, S., Nawaz, Z., Shimojima, T., Wang, H., Yang, Y., et al. (2009). MDM2 acts downstream of p53 as an E3 ligase to promote FOXO ubiquitination and degradation. J. Biol. Chem. *284*, 13987–14000.

Fursova, N.A., Blackledge, N.P., Nakayama, M., Ito, S., Koseki, Y., Farcas, A.M., King, H.W., Koseki, H., and Klose, R.J. (2019). Synergy between Variant PRC1 Complexes Defines Polycomb-Mediated Gene Repression. Mol. Cell *74*, 1020-1036.e8.

Gao, J., Aksoy, B.A., Dogrusoz, U., Dresdner, G., Gross, B., Sumer, S.O., Sun, Y., Jacobsen, A., Sinha, R., Larsson, E., et al. (2013). Integrative analysis of complex cancer genomics and clinical profiles using the cBioPortal. Sci. Signal. *6*, 1–20.

Gao, Z., Zhang, J., Bonasio, R., Strino, F., Sawai, A., Parisi, F., Kluger, Y., and Reinberg, D. (2012). PCGF Homologs, CBX Proteins, and RYBP Define Functionally Distinct PRC1 Family Complexes. Mol. Cell *45*, 344–356.

Ge, R., Wang, Z., Zeng, Q., Xu, X., and Olumi, A.F. (2011). F-box protein 10, an NF-B-κdependent anti-apoptotic protein, regulates TRAIL-induced apoptosis through modulating c-Fos/c-FLIP pathway. Cell Death Differ. *18*, 1184–1195.

Gelfman, S., Cohen, N., Yearim, A., and Ast, G. (2013). DNA-methylation effect on cotranscriptional splicing is dependent on GC architecture of the exon-intron structure. Genome Res. *23*, 789–799.

Giaccia, A.J., and Kastan, M.B. (1998). The complexity of p53 modulation: Emerging patterns from divergent signals. Genes Dev. *12*, 2973–2983.

Gottifredi, V., and Wiesmüller, L. (2018). The tip of an iceberg: Replication-associated functions of the tumor suppressor p53. Cancers (Basel). *10*.

Greenberg, M.V.C., and Bourc'his, D. (2019). The diverse roles of DNA methylation in mammalian development and disease. Nat. Rev. Mol. Cell Biol. *20*, 590–607.

Grossman, S.R., Perez, M., Kung, A.L., Joseph, M., Mansur, C., Xiao, Z.X., Kumar, S., Howley,

P.M., and Livingston, D.M. (1998). p300/MDM2 complexes participate in MDM2-mediated p53 degradation. Mol. Cell *2*, 405–415.

Gu, B., and Zhu, W.G. (2012). Surf the Post-translational Modification Network of p53 Regulation. Int. J. Biol. Sci. *8*, 672–684.

Gu, L., Zhu, N., Zhang, H., Durden, D.L., Feng, Y., and Zhou, M. (2009). Regulation of XIAP Translation and Induction by MDM2 following Irradiation. Cancer Cell *15*, 363–375.

Haberle, V., and Stark, A. (2018). Eukaryotic core promoters and the functional basis of transcription initiation. Nat. Rev. Mol. Cell Biol. *19*, 621–637.

Hampp, S., Kiessling, T., Buechle, K., Mansilla, S.F., Thomale, J., Rall, M., Ahn, J., Pospiech, H., Gottifredi, V., and Wiesmüller, L. (2016). DNA damage tolerance pathway involving DNA polymerase ι and the tumor suppressor p53 regulates DNA replication fork progression. Proc. Natl. Acad. Sci. U. S. A. *113*, E4311–E4319.

Hanahan, D., and Weinberg, R.A. (2011). Hallmarks of cancer: The next generation. Cell *144*, 646–674.

Hannon, G.J. (2010). FASTX-Toolkit. http://hannonlab.cshl.edu/fastx_toolkit.

Haupt, S., Berger, M., Goldberg, Z., and Haupt, Y. (2003). Apoptosis - The p53 network. J. Cell Sci. *116*, 4077–4085.

Haupt, Y., Maya, R., Kazaz, A., and Oren, M. (1997). Mdm2 promotes the rapid degradation of p53. Nature *387*, 296–299.

He, J., Shen, L., Wan, M., Taranova, O., Wu, H., and Zhang, Y. (2013). Kdm2b maintains murine embryonic stem cell status by recruiting PRC1 complex to CpG islands of developmental genes. Nat. Cell Biol. *15*, 373–384.

Heinz, S., Benner, C., Spann, N., Bertolino, E., Lin, Y.C., Laslo, P., Cheng, J.X., Murre, C., Singh, H., and Glass, C.K. (2010). Simple Combinations of Lineage-Determining Transcription Factors Prime cis-Regulatory Elements Required for Macrophage and B Cell Identities. Mol. Cell *38*, 576–589.

Hergeth, S.P., and Schneider, R. (2015). The H1 linker histones: multifunctional proteins beyond the nucleosomal core particle. EMBO Rep. *16*, 1439–1453.

Higuchi, R., Fockler, C., Dollinger, G., and Watson, R. (1993). Kinetic PCR Analysis: Real-time Monitoring of DNA Amplification Reactions.

Hilton, I.B., D'Ippolito, A.M., Vockley, C.M., Thakore, P.I., Crawford, G.E., Reddy, T.E., and Gersbach, C.A. (2015). Epigenome editing by a CRISPR-Cas9-based acetyltransferase

activates genes from promoters and enhancers. Nat. Biotechnol. *33*, 510–517.

Ho, C.K., Sriskanda, V., McCracken, S., Bentley, D., Schwer, B., and Shuman, S. (1998). The guanylyltransferase domain of mammalian mRNA capping enzyme binds to the phosphorylated carboxyl-terminal domain of RNA polymerase II. J. Biol. Chem. *273*, 9577–9585.

Hong, L., Schroth, G.P., Matthews, H.R., Yau, P., and Bradbury, E.M. (1993). Studies of the DNA binding properties of histone H4 amino terminus. Thermal denaturation studies reveal that acetylation markedly reduces the binding constant of the H4 “tail” to DNA. J. Biol. Chem. *268*, 305–314.

Hori, T., Kondo, T., Kanamori, M., Tabuchi, Y., Ogawa, R., Zhao, Q.L., Ahmed, K., Yasuda, T., Seki, S., Suzuki, K., et al. (2010). Nutlin-3 enhances tumor necrosis factor-related apoptosis-inducing ligand (TRAIL)-induced apoptosis through up-regulation of death receptor 5 (DR5) in human sarcoma HOS cells and human colon cancer HCT116 cells. Cancer Lett. *287*, 98–108.

Horn, H.F., and Vousden, K.H. (2007). Coping with stress: Multiple ways to activate p53. Oncogene *26*, 1306–1316.

Huang, C., and Zhu, B. (2018). Roles of H3K36-specific histone methyltransferases in transcription: antagonizing silencing and safeguarding transcription fidelity. Biophys. Reports *4*, 170–177.

Illingworth, R.S. (2019). Chromatin folding and nuclear architecture: PRC1 function in 3D. Curr. Opin. Genet. Dev. *55*, 82–90.

Illingworth, R.S., Gruenewald-Schneider, U., Webb, S., Kerr, A.R.W., James, K.D., Turner, D.J., Smith, C., Harrison, D.J., Andrews, R., and Bird, A.P. (2010). Orphan CpG Islands Identify numerous conserved promoters in the mammalian genome. PLoS Genet. *6*.

Inagaki, T., Iwasaki, S., Matsumura, Y., Kawamura, T., Tanaka, T., Abe, Y., Yamasaki, A., Tsurutani, Y., Yoshida, A., Chikaoka, Y., et al. (2015). The FBXL10/KDM2B scaffolding protein associates with novel polycomb repressive complex-1 to regulate adipogenesis. J. Biol. Chem. *290*, 4163–4177.

International Agency for Research on Cancer (2020). IARC TP53 Database.

Iwakuma, T., and Lozano, G. (2003). MDM2 , An Introduction. Mol. Cancer Res. *1*, 993–1000.

Janssen, A., Colmenares, S.U., and Karpen, G.H. (2018). Heterochromatin: Guardian of the Genome. Annu. Rev. Cell Dev. Biol. *34*, 265–288.

Joerger, A.C., and Fersht, A.R. (2010). The tumor suppressor p53: from structures to drug

discovery. Cold Spring Harb. Perspect. Biol. *2*, 1–21.

Johansen, S. (2020). Pericentromeric Heterochromatin Function and Its Implication in Cancer. *2*, 9–11.

Jones, P.L., Veenstra, G.J.C., Wade, P.A., Vermaak, D., Kass, S.U., Landsberger, N., Strouboulis, J., and Wolffe, A.P. (1998). Methylated DNA and MeCP2 recruit histone deacetylase to repress transcription. Nat. Genet. *19*, 187–191.

Jones, S.N., Roe, A.E., Donehower, L.A., and Bradley, A. (1995). Rescue of embryonic lethality in Mdm2-deficient mice by absence of p53. Nature *378*, 206–208.

Kaimori, J.Y., Maehara, K., Hayashi-Takanaka, Y., Harada, A., Fukuda, M., Yamamoto, S., Ichimaru, N., Umehara, T., Yokoyama, S., Matsuda, R., et al. (2016). Histone H4 lysine 20 acetylation is associated with gene repression in human cells. Sci. Rep. *6*, 1–10.

Kang, J.Y., Kim, J.Y., Kim, K.B., Park, J.W., Cho, H., Hahm, J.Y., Chae, Y.C., Kim, D., Kook, H., Rhee, S., et al. (2018). KDM2B is a histone H3K79 demethylase and induces transcriptional repression via sirtuin-1–mediated chromatin silencing. FASEB J. *32*, 5737–5750.

Karni-Schmidt, O., Lokshin, M., and Prives, C. (2016). The Roles of MDM2 and MDMX in Cancer. Annu. Rev. Pathol. Mech. Dis. *11*, 617–644.

Kastenhuber, E.R., and Lowe, S.W. (2017). Putting p53 in Context. Cell *170*, 1062–1078.

Kawai, H., Wiederschain, D., and Yuan, Z.-M. (2003). Critical Contribution of the MDM2 Acidic Domain to p53 Ubiquitination. Mol. Cell. Biol. *23*, 4939–4947.

Kim, J.B., and Sharp, P.A. (2001). Positive Transcription Elongation Factor b Phosphorylates hSPT5 and RNA Polymerase II Carboxyl-terminal Domain Independently of Cyclin-dependent Kinase-activating Kinase. J. Biol. Chem. *276*, 12317–12323.

Kireeva, M.L., Kashlev, M., and Burton, Z.F. (2013). RNA polymerase structure, function, regulation, dynamics, fidelity, and roles in GENE EXPRESSION. Chem. Rev. *113*, 8325–8330.

Klusmann, I., Rodewald, S., Müller, L., Friedrich, M., Wienken, M., Li, Y., Schulz-Heddergott, R., and Dobbelstein, M. (2016). p53 Activity Results in DNA Replication Fork Processivity. Cell Rep. *17*, 1845–1857.

Klusmann, I., Wohlberedt, K., Magerhans, A., Teloni, F., Korbel, J.O., Altmeyer, M., and Dobbelstein, M. (2018). Chromatin modifiers Mdm2 and RNF2 prevent RNA:DNA hybrids that impair DNA replication. Proc. Natl. Acad. Sci. U. S. A. *115*, E11311–E11320.

Komarnitsky, P., Cho, E.J., and Buratowski, S. (2000). Different phosphorylated forms of RNA polymerase II and associated mRNA processing factors during transcription. Genes Dev. *14*,

2452–2460.

Kottakis, F., Polytarchou, C., Foltopoulou, P., Sanidas, I., Kampranis, S.C., and Tsichlis, P.N. (2011). FGF-2 Regulates Cell Proliferation, Migration, and Angiogenesis through an NDY1/KDM2B-miR-101-EZH2 Pathway. Mol. Cell *43*, 285–298.

Kouzarides, T. (2007). Chromatin Modifications and Their Function. Cell *128*, 693–705.

Kuang, Y., Lu, F., Guo, J., Xu, H., Wang, Q., Xu, C., Zeng, L., and Yi, S. (2017). Histone demethylase KDM2B upregulates histone methyltransferase EZH2 expression and contributes to the progression of ovarian cancer in vitro and in vivo. Onco. Targets. Ther. *10*, 3131–3144.

Kubbutat, M.H.G., Jones, S.N., and Vousden, K.H. (1997). Regulation of p53 stability by Mdm2. Nature *387*, 299–303.

Kuehner, J.N., Pearson, E.L., and Moore, C. (2011). Unravelling the means to an end: RNA polymerase II transcription termination. Nat. Rev. Mol. Cell Biol. *12*, 283–294.

Kuleshov, M. V., Jones, M.R., Rouillard, A.D., Fernandez, N.F., Duan, Q., Wang, Z., Koplev, S., Jenkins, S.L., Jagodnik, K.M., Lachmann, A., et al. (2016). Enrichr: a comprehensive gene set enrichment analysis web server 2016 update. Nucleic Acids Res. *44*, W90–W97.

Kurt, I.C., Sur, I., Kaya, E., Cingoz, A., Kazancioglu, S., Kahya, Z., Toparlak, O.D., Senbabaoglu, F., Kaya, Z., Ozyerli, E., et al. (2017). KDM2B, an H3K36-specific demethylase, regulates apoptotic response of GBM cells to TRAIL. Cell Death Dis. *8*, e2897.

Kussie, P.H., Gorina, S., Marechal, V., Elenbaas, B., Moreau, J., Levine, A.J., and Pavletich, N.P. (1996). Structure of the MDM2 oncoprotein bound to the p53 tumor suppressor transactivation domain. Science (80-.). *274*, 948–953.

Lachmann, A., Xu, H., Krishnan, J., Berger, S.I., Mazloom, A.R., and Ma'ayan, A. (2010). ChEA: Transcription factor regulation inferred from integrating genome-wide ChIP-X experiments. Bioinformatics *26*, 2438–2444.

Lane, D.P. (1992). p53, guardian of the genome. Nature *358*, 15–16.

Lane, D.P., and Crawford, L. V. (1979). T antigen is bound to a host protein in SV40-transformed cells. Nature *278*, 261–263.

Langmead, B., and Salzberg, S.L. (2012). Fast gapped-read alignment with Bowtie 2. Nat. Methods *9*, 357–359.

Laptenko, O., and Prives, C. (2006). Transcriptional regulation by p53: One protein, many possibilities. Cell Death Differ. *13*, 951–961.

Laugesen, A., Højfeldt, J.W., and Helin, K. (2019). Molecular Mechanisms Directing PRC2 Recruitment and H3K27 Methylation. Mol. Cell *74*, 8–18.

Lawrence, M., Daujat, S., and Schneider, R. (2016). Lateral Thinking: How Histone Modifications Regulate Gene Expression. Trends Genet. *32*, 42–56.

Leinonen, R., Sugawara, H., and Shumway, M. (2011). The sequence read archive. Nucleic Acids Res. *39*, 2010–2012.

Lennicke, C., Rahn, J., Lichtenfels, R., Wessjohann, L.A., and Seliger, B. (2015). Hydrogen peroxide - Production, fate and role in redox signaling of tumor cells. Cell Commun. Signal. *13*, 1–19.

Leslie, P.L., Ke, H., and Zhang, Y. (2015). The MDM2 RING domain and central acidic domain play distinct roles in MDM2 protein homodimerization and MDM2-MDMX protein heterodimerization. J. Biol. Chem. *290*, 12941–12950.

Léveillard, T., and Wasylyk, B. (1997). The MDM2 C-terminal region binds to TAF(II)250 and is required for MDM2 regulation of the cyclin a promoter. J. Biol. Chem. *272*, 30651–30661.

Lewis, E.B. (1978). A gene complex controlling segmentation in Drosophila. Nature *276*, 565–570.

Li, J., and Yuan, J. (2008). Caspases in apoptosis and beyond. Oncogene *27*, 6194–6206.

Li, F., Mao, G., Tong, D., Huang, J., Gu, L., Yang, W., and Li, G.M. (2013). The histone mark H3K36me3 regulates human DNA mismatch repair through its interaction with MutSα. Cell *153*, 590–600.

Li, H., Handsaker, B., Wysoker, A., Fennell, T., Ruan, J., Homer, N., Marth, G., Abecasis, G., and Durbin, R. (2009). The Sequence Alignment/Map format and SAMtools. Bioinformatics *25*, 2078–2079.

Li, M., Brooks, C.L., Wu-Baer, F., Chen, D., Baer, R., and Gu, W. (2003). Mono- Versus Polyubiquitination: Differential Control of p53 Fate by Mdm2. Science (80-.). *302*, 1972–1975.

Li, X., Li, Y., Wan, L., Chen, R., and Chen, F. (2017). MiR-509-5p inhibits cellular proliferation and migration via targeting MDM2 in pancreatic cancer cells. Onco. Targets. Ther. *10*, 4455–4464.

Liang, G., He, J., and Zhang, Y. (2012). Kdm2b promotes induced pluripotent stem cell generation by facilitating gene activation early in reprogramming. Nat. Cell Biol. *14*, 457–466.

Liberzon, A., Subramanian, A., Pinchback, R., Thorvaldsdóttir, H., Tamayo, P., and Mesirov, J.P. (2011). Molecular signatures database (MSigDB) 3.0. Bioinformatics *27*, 1739–1740.

Linares, L.K., Kiernan, R., Triboulet, R., Chable-Bessia, C., Latreille, D., Cuvier, O., Lacroix, M., Le Cam, L., Coux, O., and Benkirane, M. (2007). Intrinsic ubiquitination activity of PCAF controls the stability of the oncoprotein Hdm2. Nat. Cell Biol. *9*, 331–338.

Linke, K., Mace, P.D., Smith, C.A., Vaux, D.L., Silke, J., and Day, C.L. (2008). Structure of the MDM2/MDMX RING domain heterodimer reveals dimerization is required for their ubiquitylation in trans. Cell Death Differ. *15*, 841–848.

Linzer, D.I.H., and Levine, a. J. (1979). Characterization Tumor Antigen and Uninfected of a 54K Dalton Cellular SV40 Present in SV40-Transformed Cells. Cell *17*, 43–52.

Lister, R., Pelizzola, M., Dowen, R.H., Hawkins, R.D., Hon, G., Tonti-Filippini, J., Nery, J.R., Lee, L., Ye, Z., Ngo, Q.M., et al. (2009). Human DNA methylomes at base resolution show widespread epigenomic differences. Nature *462*, 315–322.

Liu, X., Kraus, W.L., and Bai, X. (2015). Ready, pause, go: Regulation of RNA polymerase II pausing and release by cellular signaling pathways. Trends Biochem. Sci. *40*, 516–525.

Liu, X., Tan, Y., Zhang, C., Zhang, Y., Zhang, L., Ren, P., Deng, H., Luo, J., Ke, Y., and Du, X. (2016). NAT10 regulates p53 activation through acetylating p53 at K120 and ubiquitinating Mdm2. EMBO Rep. *17*, 349–366.

Liu, Y., Kung, C., Fishburn, J., Ansari, A.Z., Shokat, K.M., and Hahn, S. (2004). Two Cyclin-Dependent Kinases Promote RNA Polymerase II Transcription and Formation of the Scaffold Complex. Mol. Cell. Biol. *24*, 1721–1735.

Livak, K.J., and Schmittgen, T.D. (2001). Analysis of relative gene expression data using real-time quantitative PCR and the 2-ΔΔCT method. Methods *25*, 402–408.

Long, H.K., Blackledge, N.P., and Klose, R.J. (2013). ZF-CxxC domain-containing proteins, CpG islands and the chromatin connection. Biochem. Soc. Trans. *41*, 727–740.

Love, M.I., Huber, W., and Anders, S. (2014). Moderated estimation of fold change and dispersion for RNA-seq data with DESeq2. Genome Biol. *15*, 1–21.

Lovén, J., Hoke, H.A., Lin, C.Y., Lau, A., Orlando, D.A., Vakoc, C.R., Bradner, J.E., Lee, T.I., and Young, R.A. (2013). Selective inhibition of tumor oncogenes by disruption of super-enhancers. Cell *153*, 320–334.

Ma, J., Martin, J.D., Zhang, H., Auger, K.R., Ho, T.F., Kirkpatrick, R.B., Grooms, M.H., Johanson, K.O., Tummino, P.J., Copeland, R.A., et al. (2006). A second p53 binding site in the central domain of Mdm2 is essential for p53 ubiquitination. Biochemistry *45*, 9238–9245.

Manfredi, J.J. (2010). p53-MDM2 Review The Mdm2–p53 relationship evolves.pdf. *53*, 1580–

1589.

Marshall, N.F., Peng, J., Xie, Z., and Price, D.H. (1996). Control of RNA polymerase II elongation potential by a novel carboxyl- terminal domain kinase. J. Biol. Chem. *271*, 27176–27183.

Martin, K., Trouche, D., Hagemeier, C., Sorensent, T.S., Thanguet, N.B. La, and Kouzaridest, T. (1995). Stimulation of E2F1/DP1 transcriptional activity by MDM2 oncoprotein. Nature *375*, 691–694.

Mashima, J., Kodama, Y., Fujisawa, T., Katayama, T., Okuda, Y., Kaminuma, E., Ogasawara, O., Okubo, K., Nakamura, Y., and Takagi, T. (2017). DNA Data Bank of Japan. Nucleic Acids Res. *45*, D25–D31.

Meek, D.W., and Anderson, C.W. (2009). Post-translational modification of p53. Cold Spring Harb. Perspect. Biol. 1–16.

Mehrotra, S., Galdieri, L., Zhang, T., Zhang, M., Pemberton, L.F., and Vancura, A. (2014). Histone hypoacetylation-activated genes are repressed by acetyl-CoA- and chromatin-mediated mechanisms. Biochim. Biophys. Acta *1839*, 751–763.

Minsky, N., and Oren, M. (2004). The RING domain of Mdm2 mediates histone ubiquitylation and transcriptional repression. Mol. Cell *16*, 631–639.

Missra, A., and Gilmour, D.S. (2010). Interactions between DSIF (DRB sensitivity inducing factor), NELF (negative elongation factor), and the Drosophila RNA polymerase II transcription elongation complex. Proc. Natl. Acad. Sci. U. S. A. *107*, 11301–11306.

Mohammad, H.P., Barbash, O., and Creasy, C.L. (2019). Targeting epigenetic modifications in cancer therapy: erasing the roadmap to cancer. Nat. Med. *25*, 403–418.

Momand, J., Zambetti, G.P., Olson, D.C., George, D., and Levine, A.J. (1992). The mdm-2 oncogene product forms a complex with the p53 protein and inhibits p53-mediated transactivation. Cell *69*, 1237–1245.

Montes de Oca Luna, R., Wagner, D.S., and Lozano, G. (1995). Rescue of early embryonic lethality in mdm2-deficient mice by deletion of p53. Nature *378*, 206–208.

Najafova, Z., Tirado-Magallanes, R., Subramaniam, M., Hossan, T., Schmidt, G., Nagarajan, S., Baumgart, S.J., Mishra, V.K., Bedi, U., Hesse, E., et al. (2017). BRD4 localization to lineage-specific enhancers is associated with a distinct transcription factor repertoire. Nucleic Acids Res. *45*, 127–141.

Nakabeppu, Y. (2014). Cellular levels of 8-oxoguanine in either DNA or the nucleotide pool

play pivotal roles in carcinogenesis and survival of cancer cells. Int. J. Mol. Sci. *15*, 12543–12557.

National Center for Biotechnology Information (2020). KDM2B gene information.

National Diagnostics (2010). Multiphasic Buffer Systems.

NCBI SRA Toolkit Development Team (2020). The SRA Toolkit. http://ncbi.github.io/sra-tools/.

Nechaev, S., and Adelman, K. (2012). Transcription Initiation Into Productive Elongation. Biochim. Biophys. Acta *1809*, 34–45.

Neri, F., Rapelli, S., Krepelova, A., Incarnato, D., Parlato, C., Basile, G., Maldotti, M., Anselmi, F., and Oliviero, S. (2017). Intragenic DNA methylation prevents spurious transcription initiation. Nature *543*, 72–77.

Neuwirth, E. (2014). RColorBrewer: ColorBrewer Palettes. R package version 1.1-2. https://CRAN.R-project.org/package=RColorBrewer.

Ng, H.H., Zhang, Y., Hendrich, B., Johnson, C.A., Turner, B.M., Erdjument-Bromage, H., Tempst, P., Reinberg, D., and Bird, A. (1999). MBD2 is a transcriptional repressor belonging to the MeCP1 histone deacetylase complex. Nat. Genet. *23*, 58–61.

O'Brien, J., Hayder, H., Zayed, Y., and Peng, C. (2018). Overview of microRNA biogenesis, mechanisms of actions, and circulation. Front. Endocrinol. (Lausanne). *9*, 1–12.

Oeckinghaus, A., Hayden, M.S., and Ghosh, S. (2011). Crosstalk in NF-κB signaling pathways. Nat. Immunol. *12*, 695–708.

Ofir-Rosenfeld, Y., Boggs, K., Michael, D., Kastan, M.B., and Oren, M. (2008). Mdm2 Regulates p53 mRNA Translation through Inhibitory Interactions with Ribosomal Protein L26. Mol. Cell *32*, 180–189.

Oliner, J.D., Kinzler, K.W., Meltzer, P.S., George, D.L., and Vogelstein, B. (1992). Amplification of a gene encoding a p53-associated protein in human sarcomas. Nature *358*, 80–83.

Oliner, J.D., Pietenpol, J.A., Thiagalingam, S., Gyuris, J., Kinzler, K.W., and Vogelstein, B. (1993). Oncoprotein MDM2 conceals the activation domain of tumour suppressor p53. Nature *362*, 857–860.

Orozco, I.J., Kim, S.J., and Martinson, H.G. (2002). The poly(A) signal, without the assistance of any downstream element, directs RNA polymerase II to pause in vivo and then to release stochastically from the template. J. Biol. Chem. *277*, 42899–42911.

Ougolkov, A. V, Bilim, V.N., and Billadeau, D.D. (2008). Regulation of Pancreatic Tumor

Proliferation and Chemoresistance by the Histone Methyltransferase EZH2. Clin. Cancer Res. *14*, 6790–6796.

Perry, M.E., Mendrysa, S.M., Saucedo, L.J., Tannous, P., and Holubar, M. (2000). p76(MDM2) inhibits the ability of p90(MDM2) to destabilize p53. J. Biol. Chem. *275*, 5733–5738.

Petty, E., and Pillus, L. (2013). Balancing chromatin remodeling and histone modifications in transcription. Trends Genet *29*, 621–629.

Pfister, S.X., Ahrabi, S., Zalmas, L.P., Sarkar, S., Aymard, F., Bachrati, C.Z., Helleday, T., Legube, G., LaThangue, N.B., Porter, A.C.G., et al. (2014). SETD2-Dependent Histone H3K36 Trimethylation Is Required for Homologous Recombination Repair and Genome Stability. Cell Rep. *7*, 2006–2018.

Phatnani, H.P., and Greenleaf, A.L. (2006). Phosphorylation and functions of the RNA polymerase II CTD. Genes Dev. *20*, 2922–2936.

Polytarchou, C., Pfau, R., Hatziapostolou, M., and Tsichlis, P.N. (2008). The JmjC Domain Histone Demethylase Ndy1 Regulates Redox Homeostasis and Protects Cells from Oxidative Stress. Mol. Cell. Biol. *28*, 7451–7464.

Popowicz, G.M., Czarna, A., and Holak, T.A. (2008). Structure of the human Mdmx protein bound to the p53 tumor suppressor transactivation domain. Cell Cycle *7*, 2441–2443.

Pott, S., and Lieb, J.D. (2015). What are super-enhancers? Nat. Genet. *47*, 8–12.

Poyurovsky, M. V., Katz, C., Laptenko, O., Beckerman, R., Lokshin, M., Ahn, J., Byeon, I.J.L., Gabizon, R., Mattia, M., Zupnick, A., et al. (2010). The C terminus of p53 binds the N-terminal domain of MDM2. Nat. Struct. Mol. Biol. *17*, 982–989.

Proudfoot, N.J. (2016). Transcriptional termination in mammals: Stopping the RNA polymerase II juggernaut. Science (80-.). *352*.

Quan, M., Chen, Z., Jiao, F., Xiao, X., Xia, Q., Chen, J., Chao, Q., Li, Y., Gao, Y., Yang, H., et al. (2020). Lysine demethylase 2 (KDM2B) regulates hippo pathway via MOB1 to promote pancreatic ductal adenocarcinoma (PDAC) progression. J. Exp. Clin. Cancer Res. *39*, 1–15.

Quinlan, A.R., and Hall, I.M. (2010). BEDTools: A flexible suite of utilities for comparing genomic features. Bioinformatics *26*, 841–842.

R Development Core Team 3.0.1. (2013). A Language and Environment for Statistical Computing.

Raj, N., and Attardi, L.D. (2017). The transactivation domains of the p53 protein. Cold Spring Harb. Perspect. Med. *7*, 1–18.

Ramírez, F., Ryan, D.P., Grüning, B., Bhardwaj, V., Kilpert, F., Richter, A.S., Heyne, S., Dündar, F., and Manke, T. (2016). deepTools2: a next generation web server for deep-sequencing data analysis. Nucleic Acids Res. *44*, W160–W165.

Ranaweera, R.S., and Yang, X. (2013). Auto-ubiquitination of Mdm2 enhances its substrate ubiquitin ligase activity. J. Biol. Chem. *288*, 18939–18946.

Rasmussen, E.B., and Lis, J.T. (1993). In vivo transcriptional pausing and cap formation on three Drosophila heat shock genes. Proc. Natl. Acad. Sci. U. S. A. *90*, 7923–7927.

Riley, M.F., and Lozano, G. (2012). The Many Faces of MDM2 Binding Partners. Genes and Cancer *3*, 226–239.

Riscal, R., Schrepfer, E., Arena, G., Cissé, M.Y., Bellvert, F., Heuillet, M., Rambow, F., Bonneil, E., Sabourdy, F., Vincent, C., et al. (2016). Chromatin-Bound MDM2 Regulates Serine Metabolism and Redox Homeostasis Independently of p53. Mol. Cell *62*, 890–902.

Robinson, J.T., Thorvaldsdóttir, H., Winckler, W., Guttman, M., Lander, E.S., Getz, G., and Mesirov, J.P. (2011). Integrative genomics viewer. Nat. Biotechnol. *29*, 24–26.

Robinson, J.T., Thorvaldsdóttir, H., Wenger, A.M., Zehir, A., and Mesirov, J.P. (2017). Variant review with the integrative genomics viewer. Cancer Res. *77*, e31–e34.

Rodriguez, M.S., Desterro, J.M.P., Lain, S., Lane, D.P., and Hay, R.T. (2000). Multiple C-Terminal Lysine Residues Target p53 for Ubiquitin-Proteasome-Mediated Degradation. Mol. Cell. Biol. *20*, 8458–8467.

Rona, G., Roberti, D., Yin, Y., Pagan, J.K., Homer, H., Sassani, E., Zeke, A., Busino, L., Rothenberg, E., and Pagano, M. (2018). PARP1-dependent recruitment of the FBXL10-RNF68-RNF2 ubiquitin ligase to sites of DNA damage controls H2A.Z loading. Elife *7*, 1–31.

Roth, J., Dobbelstein, M., Freedman, D.A., Shenk, T., and Levine, A.J. (1998). Nucleo-cytoplasmic shuttling of the hdm2 oncoprotein regulates the levels of the p53 protein via a pathway used by the human immunodeficiency virus rev protein. EMBO J. *17*, 554–564.

Roy, S., Tomaszowski, K.H., Luzwick, J.W., Park, S., Li, J., Murphy, M., and Schlacher, K. (2018). p53 orchestrates DNA replication restart homeostasis by suppressing mutagenic RAD52 and POLθ pathways. Elife *7*, 1–3.

De Rozieres, S., Maya, R., Oren, M., and Lozano, G. (2000). The loss of mdm2 induces p53 mediated apoptosis. Oncogene *19*, 1691–1697.

RStudio Inc., Boston, M. (2019). RStudio: Integrated Development for R. http://www.rstudio.com/.

Sainsbury, S., Bernecky, C., and Cramer, P. (2015). Structural basis of transcription initiation by RNA polymerase II. Nat. Rev. Mol. Cell Biol. *16*, 129–143.

Sanchez, R., and Zhou, M.M. (2011). The PHD finger: A versatile epigenome reader. Trends Biochem. Sci. *36*, 364–372.

Saxonov, S., Berg, P., and Brutlag, D.L. (2006). A genome-wide analysis of CpG dinucleotides in the human genome distinguishes two distinct classes of promoters. Proc. Natl. Acad. Sci. U. S. A. *103*, 1412–1417.

Schuettengruber, B., Bourbon, H.M., Di Croce, L., and Cavalli, G. (2017). Genome Regulation by Polycomb and Trithorax: 70 Years and Counting. Cell *171*, 34–57.

Sen, M., Wang, X., Hamdan, F.H., Rapp, J., Eggert, J., Kosinsky, R.L., Wegwitz, F., Kutschat, A.P., Younesi, F.S., Gaedcke, J., et al. (2019). ARID1A facilitates KRAS signaling-regulated enhancer activity in an AP1-dependent manner in colorectal cancer cells. Clin. Epigenetics *11*, 1–16.

Shao, Z., Raible, F., Mollaaghababa, R., Guyon, J.R., Wu, C.T., Bender, W., and Kingston, R.E. (1999). Stabilization of chromatin structure by PRC1, a polycomb complex. Cell *98*, 37–46.

Shapiro, A.L., Viñuela, E., and V. Maizel Jr., J. (1967). Molecular weight estimation of polypeptide chains by electrophoresis in SDS-polyacrylamide gels. Biochem. Biophys. Res. Commun. *28*, 815–820.

Shi, D., and Gu, W. (2012). Dual Roles of MDM2 in the Regulation of p53: Ubiquitination Dependent and Ubiquitination Independent Mechanisms of MDM2 Repression of p53 Activity. Genes and Cancer *3*, 240–248.

Shi, J., and Vakoc, C.R. (2014). The Mechanisms behind the Therapeutic Activity of BET Bromodomain Inhibition. Mol. Cell *54*, 728–736.

Shvarts, A., Steegenga, W.T., Riteco, N., van Laar, T., Dekker, P., Bazuine, M., van Ham, R.C., van der Houven van Oordt, W., Hateboer, G., van der Eb, A.J., et al. (1996). MDMX: a novel p53-binding protein with some functional properties of MDM2. EMBO J. *15*, 5349–5357.

Singh, A.K., Chauhan, S.S., Singh, S.K., Verma, V.V., Singh, A., Arya, R.K., Maheshwari, S., Akhtar, M.S., Sarkar, J., Rangnekar, V.M., et al. (2016). Dual targeting of MDM2 with a novel small-molecule inhibitor overcomes TRAIL resistance in cancer. Carcinogenesis *37*, 1027–1040.

Smith, P.K., Krohn, R.I., Hermanson, G.T., Mallia, A.K., Gartner, F.H., Provenzano, M.D., Fujimoto, E.K., Goeke, N.M., Olson, B.J., and Klenk, D.C. (1985). Measurement of protein

using bicinchoninic acid. Anal. Biochem. *150*, 76–85.

Søgaard, T.M.M., and Svejstrup, J.Q. (2007). Hyperphosphorylation of the C-terminal repeat domain of RNA polymerase II facilitates dissociation of its complex with mediator. J. Biol. Chem. *282*, 14113–14120.

Soshnev, A.A., Josefowicz, S.Z., and Allis, C.D. (2016). Greater Than the Sum of Parts: Complexity of the Dynamic Epigenome. Mol. Cell *62*, 681–694.

Sriraman, A., Dickmanns, A., Najafova, Z., Johnsen, S.A., and Dobbelstein, M. (2018). CDK4 inhibition diminishes p53 activation by MDM2 antagonists. Cell Death Dis. *9*.

Staberg, M., Rasmussen, R.D., Michaelsen, S.R., Pedersen, H., Jensen, K.E., Villingshøj, M., Skjoth-Rasmussen, J., Brennum, J., Vitting-Seerup, K., Poulsen, H.S., et al. (2018). Targeting glioma stem-like cell survival and chemoresistance through inhibition of lysine-specific histone demethylase KDM2B. Mol. Oncol. *12*, 406–420.

Stommel, J.M., and Wahl, G.M. (2004). Accelerated MDM2 auto-degradation induced by DNA-damage kinases is required for p53 activation. EMBO J. *23*, 1547–1556.

Strahl, B.D., and Allis, C.D. (2000). The language of covalent histone modifications. Nature *403*, 41–45.

Su, W., Han, H.H., Wang, Y., Zhang, B., Zhou, B., Cheng, Y., Rumandla, A., Gurrapu, S., Chakraborty, G., Su, J., et al. (2019). The Polycomb Repressor Complex 1 Drives Double-Negative Prostate Cancer Metastasis by Coordinating Stemness and Immune Suppression. Cancer Cell *36*, 139-155.e10.

Subramanian, A., Tamayo, P., Mootha, V.K., Mukherjee, S., Ebert, B.L., Gillette, M.A., Paulovich, A., Pomeroy, S.L., Golub, T.R., Lander, E.S., et al. (2005). Gene set enrichment analysis: A knowledge-based approach for interpreting genome-wide expression profiles. Proc. Natl. Acad. Sci. U. S. A. *102*, 15545–15550.

Sui, G., Affar, E.B., Shi, Y., Brignone, C., Wall, N.R., Yin, P., Donohoe, M., Luke, M.P., Calvo, D., Grossman, S.R., et al. (2004). Yin Yang 1 is a negative regulator of p53. Cell *117*, 859–872.

Sullivan, K.D., Galbraith, M.D., Andrysik, Z., and Espinosa, J.M. (2018). Mechanisms of transcriptional regulation by p53. Cell Death Differ. *25*, 133–143.

Suzuki, A., Makinoshima, H., Wakaguri, H., Esumi, H., Sugano, S., Kohno, T., Tsuchihara, K., and Suzuki, Y. (2014). Aberrant transcriptional regulations in cancers: Genome, transcriptome and epigenome analysis of lung adenocarcinoma cell lines. Nucleic Acids Res. *42*, 13557–13572.

Tao, W., and Levine, A.J. (1999). P19ARF stabilizes p53 by blocking nucleo-cytoplasmic shuttling of Mdm2. Proc. Natl. Acad. Sci. U. S. A. *96*, 6937–6941.

Thomson, J.P., Skene, P.J., Selfridge, J., Clouaire, T., Guy, J., Webb, S., Kerr, A.R.W., Deaton, A., Andrews, R., James, K.D., et al. (2010). CpG islands influence chromatin structure via the CpG-binding protein Cfp1. Nature *464*, 1082–1086.

Thorvaldsdóttir, H., Robinson, J.T., and Mesirov, J.P. (2013). Integrative Genomics Viewer (IGV): High-performance genomics data visualization and exploration. Brief. Bioinform. *14*, 178–192.

Thut, C.J., Goodrich, J.A., and Tjian, R. (1997). Repression of p53-mediated transcription by MDM2: A dual mechanism. Genes Dev. *11*, 1974–1986.

Turberfield, A.H., Kondo, T., Nakayama, M., Koseki, Y., King, H.W., Koseki, H., and Klose, R.J. (2019). KDM2 proteins constrain transcription from CpG island gene promoters independently of their histone demethylase activity. Nucleic Acids Res. *47*, 9005–9023.

Tzatsos, A., Pfau, R., Kampranis, S.C., and Tsichlis, P.N. (2008). Ndy1 / KDM2B immortalizes mouse embryonic fibroblasts by repressing the Ink4a / Arf locus. Sci. York *2008*, 1–6.

Tzatsos, A., Paskaleva, P., Ferrari, F., Deshpande, V., Stoykova, S., Contino, G., Wong, K.K., Lan, F., Trojer, P., Park, P.J., et al. (2013). KDM2B promotes pancreatic cancer via Polycomb-dependent and -independent transcriptional programs. J. Clin. Invest. *123*, 727–739.

U.S. National Library of Medicine (2020). ClinicalTrials.gov, https://clinicaltrials.gov/ct2/show/NCT04029688.

Urso, L., Cavallari, I., Silic-Benussi, M., Biasini, L., Zago, G., Calabrese, F., Conte, P.F., Ciminale, V., and Pasello, G. (2017). Synergistic targeting of malignant pleural mesothelioma cells by MDM2 inhibitors and TRAIL agonists. Oncotarget *8*, 44232–44241.

Vacík, T., Lađinović, D., and Raška, I. (2018). Kdm2a/b lysine demethylases and their alternative isoforms in development and disease. Nucleus *9*, 431–441.

Vassilev, L.T., Vu, B.T., Graves, B., Carvajal, D., Podlaski, F., Filipovic, Z., Kong, N., Kammlott, U., Lukacs, C., Klein, C., et al. (2004). In Vivo Activation of the p53 Pathway by Small-Molecule Antagonists of MDM2. Science (80-.). *303*, 844–848.

Vermeulen, M., Mulder, K.W., Denissov, S., Pijnappel, W.W.M.P., van Schaik, F.M.A., Varier, R.A., Baltissen, M.P.A., Stunnenberg, H.G., Mann, M., and Timmers, H.T.M. (2007). Selective Anchoring of TFIID to Nucleosomes by Trimethylation of Histone H3 Lysine 4. Cell *131*, 58–69.

Wade, M., Li, Y.C., and Wahl, G.M. (2013). MDM2, MDMX and p53 in oncogenesis and cancer therapy. Nat. Rev. Cancer *13*, 83–96.

Wang, T., Chen, K., Zeng, X., Yang, J., Wu, Y., Shi, X., Qin, B., Zeng, L., Esteban, M.A., Pan, G., et al. (2011a). The histone demethylases Jhdm1a/1b enhance somatic cell reprogramming in a vitamin-C-dependent manner. Cell Stem Cell *9*, 575–587.

Wang, W., Hu, B., Qin, J.J., Cheng, J.W., Li, X., Rajaei, M., Fan, J., Yang, X.R., and Zhang, R. (2019). A novel inhibitor of MDM2 oncogene blocks metastasis of hepatocellular carcinoma and overcomes chemoresistance. Genes Dis. *6*, 419–430.

Wang, X., Wang, J., and Jiang, X. (2011b). MdmX protein is essential for Mdm2 protein-mediated p53 polyubiquitination. J. Biol. Chem. *286*, 23725–23734.

Warnes, G.R., Bolker, B., Bonebakker, L., Gentlemen, R., Huber, W., Liaw, A., Lumley, T., Maechler, M., Magnusson, A., Moeller, S., et al. (2020). gplots: Various R Programming Tools for Plotting Data. R package version 3.0.3. https://CRAN.R-project.org/package=gplots.

Webster, G.A., and Perkins, N.D. (1999). Transcriptional Cross Talk between NF-κB and p53. Mol. Cell. Biol. *19*, 3485–3495.

West, S., Gromak, N., and Proudfoot, N.J. (2004). Human 5′ → 3′ exonuclease Xm2 promotes transcription termination at co-transcriptional cleavage sites. Nature *432*, 522–525.

Whyte, W.A., Orlando, D.A., Hnisz, D., Abraham, B.J., Lin, C.Y., Kagey, M.H., Rahl, P.B., Lee, T.I., and Young, R.A. (2013). Master transcription factors and mediator establish super-enhancers at key cell identity genes. Cell *153*, 307–319.

Wickham, H. (2016). ggplot2: Elegant Graphicsfor Data Analysis. (Springer-Verlag New York).

Wienken, M., Dickmanns, A., Nemajerova, A., Kramer, D., Najafova, Z., Weiss, M., Karpiuk, O., Kassem, M., Zhang, Y., Lozano, G., et al. (2016). MDM2 Associates with Polycomb Repressor Complex 2 and Enhances Stemness-Promoting Chromatin Modifications Independent of p53. Mol. Cell *61*, 68–83.

Wong, K.H., Jin, Y., and Struhl, K. (2014). TFIIH Phosphorylation of the Pol II CTD Stimulates Mediator Dissociation from the Preinitiation Complex and Promoter Escape. Mol. Cell *54*, 601–612.

Wu, H., and Leng, R.P. (2015). MDM2 mediates p73 ubiquitination: A new molecular mechanism for suppression of p73 function. Oncotarget *6*, 21479–21492.

Wu, X., Johansen, J.V., and Helin, K. (2013). Fbxl10/Kdm2b Recruits Polycomb Repressive Complex 1 to CpG Islands and Regulates H2A Ubiquitylation. Mol. Cell *49*, 1134–1146.

Yamaguchi, Y., Wada, T., Watanabe, D., Takagi, T., Hasegawa, J., and Handa, H. (1999a). Structure and function of the human transcription elongation factor DSIF. J. Biol. Chem. *274*, 8085–8092.

Yamaguchi, Y., Takagi, T., Wada, T., Yano, K., Furuya, A., Sugimoto, S., Hasegawa, J., and Handa, H. (1999b). NELF, a multisubunit complex containing RD, cooperates with DSIF to repress RNA polymerase II elongation. Cell *97*, 41–51.

Yan, M., Yang, X., Wang, H., and Shao, Q. (2018). The critical role of histone lysine demethylase KDM2B in cancer. Am. J. Transl. Res. *10*, 2222–2233.

Yeo, C.Q.X., Alexander, I., Lin, Z., Lim, S., Aning, O.A., Kumar, R., Sangthongpitag, K., Pendharkar, V., Ho, V.H.B., and Cheok, C.F. (2016). P53 Maintains Genomic Stability by Preventing Interference between Transcription and Replication. Cell Rep. *15*, 132–146.

Yin, Y., Morgunova, E., Jolma, A., Kaasinen, E., Sahu, B., Khund-Sayeed, S., Das, P.K., Kivioja, T., Dave, K., Zhong, F., et al. (2017). Impact of cytosine methylation on DNA binding specificities of human transcription factors. Science (80-.). *356*.

Young, M.D., Wakefield, M.J., Smyth, G.K., and Oshlack, A. (2010). Gene ontology analysis for RNA-seq: accounting for selection bias. Genome Biol. *11*.

Yu, G.W. (2006). Solution structure of the C4 zinc finger domain of HDM2. Protein Sci. *15*, 384–389.

Yu, G., Wang, J., Lin, X., Diao, S., Cao, Y., Dong, R., Wang, L., Wang, S., and Fan, Z. (2016). Demethylation of SFRP2 by histone demethylase KDM2A regulated osteo-/dentinogenic differentiation of stem cells of the apical papilla. Cell Prolif. *49*, 330–340.

Yu, J.G., Ji, C.H., and Shi, M.H. (2019). Nitroxoline induces cell apoptosis by inducing MDM2 degradation in small-cell lung cancer. Kaohsiung J. Med. Sci. *35*, 202–208.

Yudkovsky, N., Ranish, J.A., and Hahn, S. (2000). A transcription reinitiation intermediate that is stabilized by activator. Nature *408*, 225–229.

Zacharopoulou, N., Tsapara, A., Kallergi, G., Schmid, E., Tsichlis, P.N., Kampranis, S.C., and Stournaras, C. (2018). The epigenetic factor KDM2B regulates cell adhesion, small rho GTPases, actin cytoskeleton and migration in prostate cancer cells. Biochim. Biophys. Acta - Mol. Cell Res. *1865*, 587–597.

Zauberman, A., Flusberg, D., Haupt, Y., Barak, Y., and Oren, M. (1995). A functional p53-responsive intronic promoter is contained within the human mdm2 gene. Nucleic Acids Res. *23*, 2584–2592.

Zhang, H., Rigo, F., and Martinson, H.G. (2015). Poly(A) Signal-Dependent Transcription Termination Occurs through a Conformational Change Mechanism that Does Not Require Cleavage at the Poly(A) Site. Mol. Cell *59*, 437–448.

Zhang, Y., Xiong, Y., and Yarbrough, W.G. (1998). ARF promotes MDM2 degradation and stabilizes p53: ARF-INK4a locus deletion impairs both the Rb and p53 tumor suppression pathways. Cell *92*, 725–734.

Zhang, Y., Liu, T., Meyer, C.A., Eeckhoute, J., Johnson, D.S., Bernstein, B.E., Nussbaum, C., Myers, R.M., Brown, M., Li, W., et al. (2008). Model-based analysis of ChIP-Seq (MACS). Genome Biol. *9*.

Zhang, Z., Wang, H., Li, M., Rayburn, E.R., Agrawal, S., and Zhang, R. (2005). Stabilization of E2F1 protein by MDM2 through the E2F1 ubiquitination pathway. Oncogene *24*, 7238–7247.

Zhao, Y., and Garcia, B.A. (2015). Comprehensive catalog of currently documented histone modifications. Cold Spring Harb. Perspect. Biol. *7*, 1–21.

Zhao, Y., Yu, H., and Hu, W. (2014). The regulation of MDM2 oncogene and its impact on human cancers Regulation of MDM2 at the Transcriptional Level. Acta Biochim Biophys Sin *46*, 180–189.

Zheng, Q., Fan, H., Meng, Z., Yuan, L., Liu, C., Peng, Y., Zhao, W., Wang, L., Li, J., and Feng, J. (2018). Histone demethylase KDM2B promotes triple negative breast cancer proliferation by suppressing p15INK4B, p16INK4A, and p57KIP2 transcription. Acta Biochim. Biophys. Sin. (Shanghai). *50*, 897–904.

Zhou, Z., Yang, X., He, J., Liu, J., Wu, F., Yu, S., Liu, Y., Lin, R., Liu, H., Cui, Y., et al. (2017). Kdm2b Regulates Somatic Reprogramming through Variant PRC1 Complex-Dependent Function. Cell Rep. *21*, 2160–2170.